NASA Technical Memorandum 105185

COLD-SAT Dynamic Model

Neil S. Adams
Analex Corporation
Brook Park, Ohio

and

Gary Bollenbacher
Lewis Research Center
Cleveland, Ohio

December 1992

NASA

Contents

COLD–SAT Dynamic Model

Neil S. Adams
Analex Corporation
Brook Park, Ohio 44142

and

Gary Bollenbacher
National Aeronautics and Space Administration
Lewis Research Center
Cleveland, Ohio 44135

1.0 Introduction

The COLD–SAT dynamic model is a six-degree-of-freedom, rigid-body computer simulation of a spacecraft in orbit around the Earth. The model was developed as part of a conceptual design review at the NASA Lewis Research Center to study the feasibility of a proposed spacecraft known as COLD–SAT. COLD–SAT is an acronym for cryogenic on-orbit liquid depot—storage, acquisition, and transfer. The purpose of the COLD–SAT spacecraft is the investigation of the fluid dynamics and thermodynamics of subcritical cryogenic fluids in a microgravity environment. In order to carry out these investigations, a series of experiments will be performed onboard the spacecraft during its proposed 60-day operational life.

As envisioned during the study, the COLD–SAT spacecraft will be placed in a circular low Earth orbit at an initial altitude of 550 nautical miles and an inclination of 18°. The spacecraft will incorporate three hydrogen tanks: one large tank (the supply tank), which will be filled with liquid hydrogen at lift-off, and two smaller tanks (the large receiver tank and the small receiver tank), which will be filled with and drained of liquid hydrogen during the course of various onboard experiments. In order to provide a controlled microgravity environment during the execution of some of the experiments, axial thrusters that provide three levels of microgravity acceleration will be mouted on the spacecraft. The cumulative time of this thrust over the 60-day mission will be approximately 60 hours; for the remaining time the spacecraft will be in a zero-gravity condition. During the course of some onboard experiments unwanted disturbances (resulting primarily from attitude control system activity) must be minimized. Otherwise these disturbances could be transferred to the cryogenic fluids and degrade the quality of the resulting experimental data. This effect is of greatest concern during experiments involving the application of axial thrust. The design life of the spacecraft was specified as six months.

At the outset of the design study the baseline attitude control system was an all-thruster system consisting of six pairs of hydrazine thrusters. A single-axis reaction wheel was explored for meeting the requirements for low microgravity disturbances. A two-axis gimbal of one axial thruster was also provided to augment the fixed thrusters. As the study progressed, the paired control thrusters on two of the spacecraft axes were replaced with single thrusters to reduce system cost and complexity.

The design of the COLD–SAT dynamic model (fig. 1.1) was shaped largely by the requirements of the COLD–SAT design study. The model was a major tool that was used throughout the study, primarily to evaluate and compare the performance of several attitude control system design options. Other areas of investigation for which the model was extensively employed were the following:

(1) The analysis of the microgravity environment within the liquid hydrogen tanks, which was largely produced by the activity of the attitude control system

(2) The evaluation of the effects of prolonged periods of constant, low-level thrust on the spacecraft orbit over the 60-day mission life

(3) An assessment of the effects of liquid hydrogen sloshing in each of the three tanks on the spacecraft dynamic behavior

Although throughout its development the design of the COLD–SAT dynamic model was guided by the requirements of the design study, an attempt was made to keep the model as general as possible so that its usefulness would extend to future projects as well as to COLD–SAT. To achieve this goal, approximations and simplifications were avoided to the maximum extent feasible.

The resultant model consists of three parts: a translation model, a rotation model, and a slosh model (figs. 1.2 to 1.4). Each of the three parts is described in detail in subsequent sections of this report. The translation model simulates the motion of the spacecraft center of gravity about the Earth under the influence of gravitational force, atmospheric drag, and the thrust produced by the axial thrusters and by uncoupled control thrusters. The rotation model simulates the attitudinal motion of the spacecraft about its center of gravity under the influence of various disturbance torques and control torques acting on the spacecraft. The slosh model computes the torque on the spacecraft produced by the motion of the liquid hydrogen in any or all of the three tanks. In addition to the primary function of each part of the model, other computations are included as required. Thus, the translation model also computes the desired spacecraft attitude for a large number of attitude options, and it computes the torque resulting from axial thrust misalignment acting on the spacecraft. The rotation model simulates the attitude control system and computes the microgravity environment within the spacecraft body.

Some of the features included in the model are

(1) The capability to simulate a large number of possible spacecraft attitudes

(2) An Earth gravity model that includes the fundamental component and zonal harmonics up to the fourth and accurately represents nodal regression and apsidal progression

(3) Accurate simulation of gravity-gradient torque and atmospheric density

(4) A tilted-dipole model of the Earth's magnetic field, which provides sufficient accuracy over the range of orbital altitudes used for COLD–SAT

(5) A Sun model that gives the position of the Sun as a function of time and date and determines if the Sun is blocked by the Earth

(6) A two-axis slosh model that can simulate slosh in one tank or in more than one tank simultaneously

(7) An axial thrust model that includes thrust decay due to the unregulated (blowdown) system

(8) Simulation of control thruster (reaction control system, or RCS) startup and shutdown transients, as well as minimum on-time constraints

(9) A reaction wheel model that includes viscous and static friction

(10) A microgravity acceleration computation that includes gravity-gradient-induced acceleration, as well as accelerations caused by spacecraft lateral and rotational motion and angular acceleration

(11) Quaternions that are used throughout the model to represent spacecraft attitude, which result in a representation that is valid for all rotations, is devoid of singularities and small-angle approximations, and requires a minimum number of numerical integrations per time step

Other computations that are included in the model but are modeled in a simplified or approximated form or are only modeled for certain attitude options are

(1) Solar pressure torque, which is approximated so that it is only valid for the attitude selected for the COLD–SAT spacecraft with small attitude errors

(2) Aerodynamic drag torque, the accuracy of which is limited by the modeling of the spacecraft surfaces as simple geometric shapes

(3) Magnetic torque, the accuracy of which is limited by the modeling of the Earth's magnetic field as a simple dipole

However, these torques are very small relative to the dominant disturbance torques so that accurate simulation was not required. Furthermore, highly accurate computation of these torques would result in a model that required excessive computer run time.

Another limitation of the model is the computation of slosh torque, which cannot be simulated for certain attitude options because the slosh model in its present form will allow no more than a 180° spacecraft rotation with respect to inertial space. Thus, the slosh model will only function properly with attitude options that are nearly inertially fixed.

Often during the design phase of the COLD–SAT study, alternative systems were evaluated to determine which system best met COLD–SAT's requirements in the most cost-effective manner. Consequently, the COLD–SAT dynamic model was constructed to have the capability to simulate all possible alternative systems. Examples of this include the following items:

(1) Both regulated and blowdown thrust systems were considered for COLD–SAT, and both can be simulated by using the COLD–SAT dynamic model.

(2) A single-axis reaction wheel was considered during the design phase to improve the microgravity environment during periods of no axial thrust. Although the reaction wheel was eliminated from the final design, it is included in the model.

(3) Both coupled and uncoupled RCS thruster systems were considered for COLD–SAT. An uncoupled scheme was chosen for COLD–SAT to satisfy cost and complexity considerations, but the model can simulate either system.

The model is implemented by using the EASY5 modeling and analysis package and will run on a variety of computing platforms, including the Cray X/MP supercomputer. Execution time is a strong function of the thrust level simulated. Simulation of the full-up model for one complete orbit on the

Cray, using the most efficient numerical integration method available, varies from about 1 min for no thrust to about 12 to 15 min for the highest thrust level. Execution time for the translation model alone, simulating the entire 60-day mission, is on the order of 2 to 3 hours of Cray time.

The remainder of this report provides detailed descriptions of all aspects of the model. Included are the mathematical formulations and definitions of variables. The constants, quaternion algebra, and coordinate systems used are discussed in the appropriate appendixes. The code listings are available through the Computer Software Management and Information Center, Athens, Georgia, 30602.

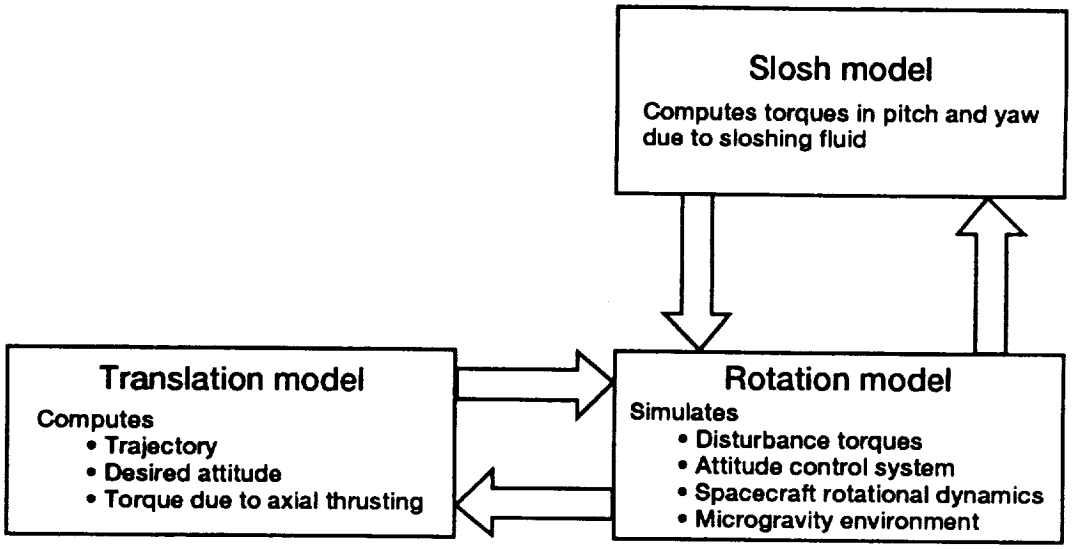

Figure 1.1.—Overview of COLD-SAT model.

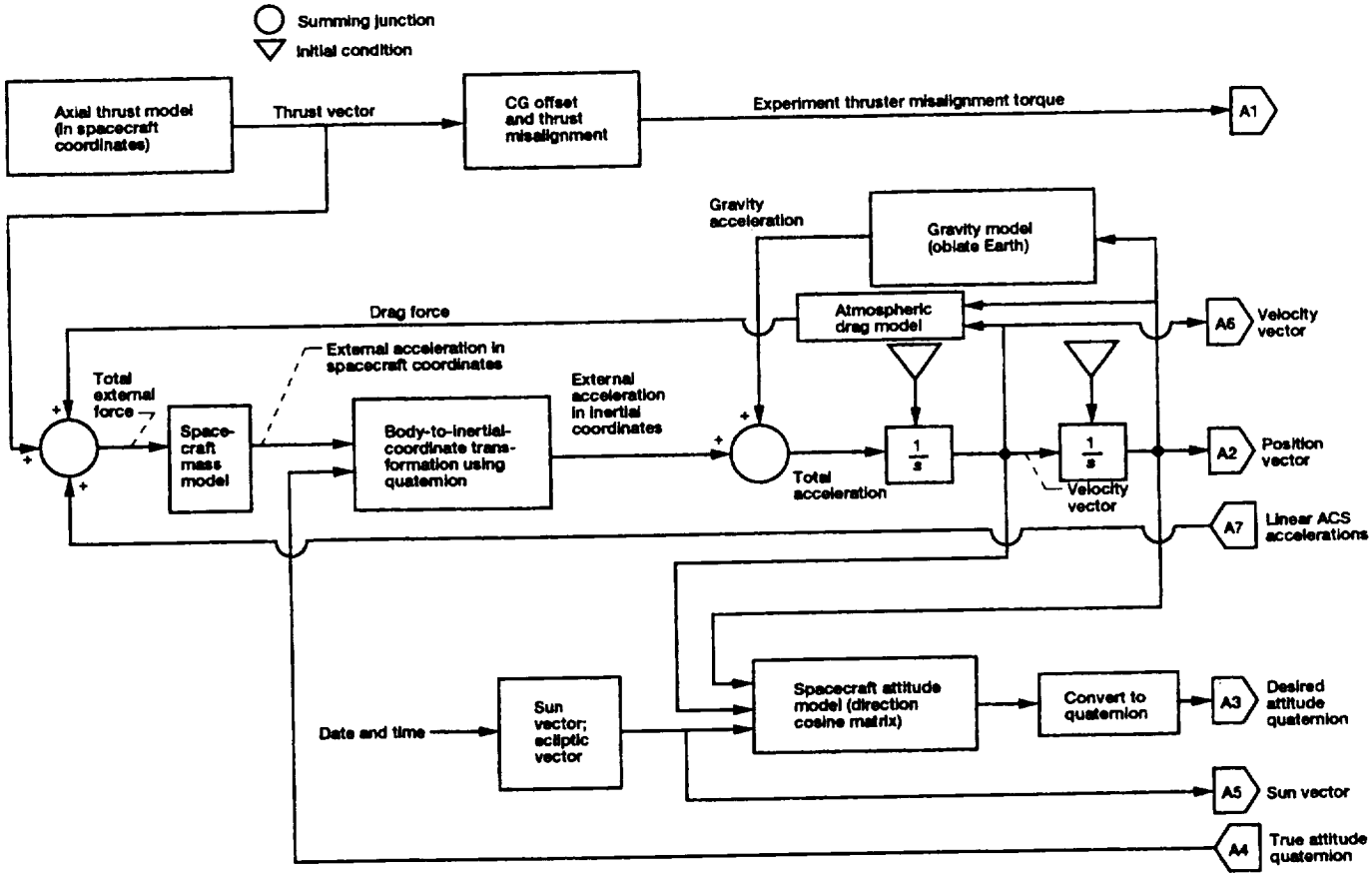

Figure 1.2.—Translation model.

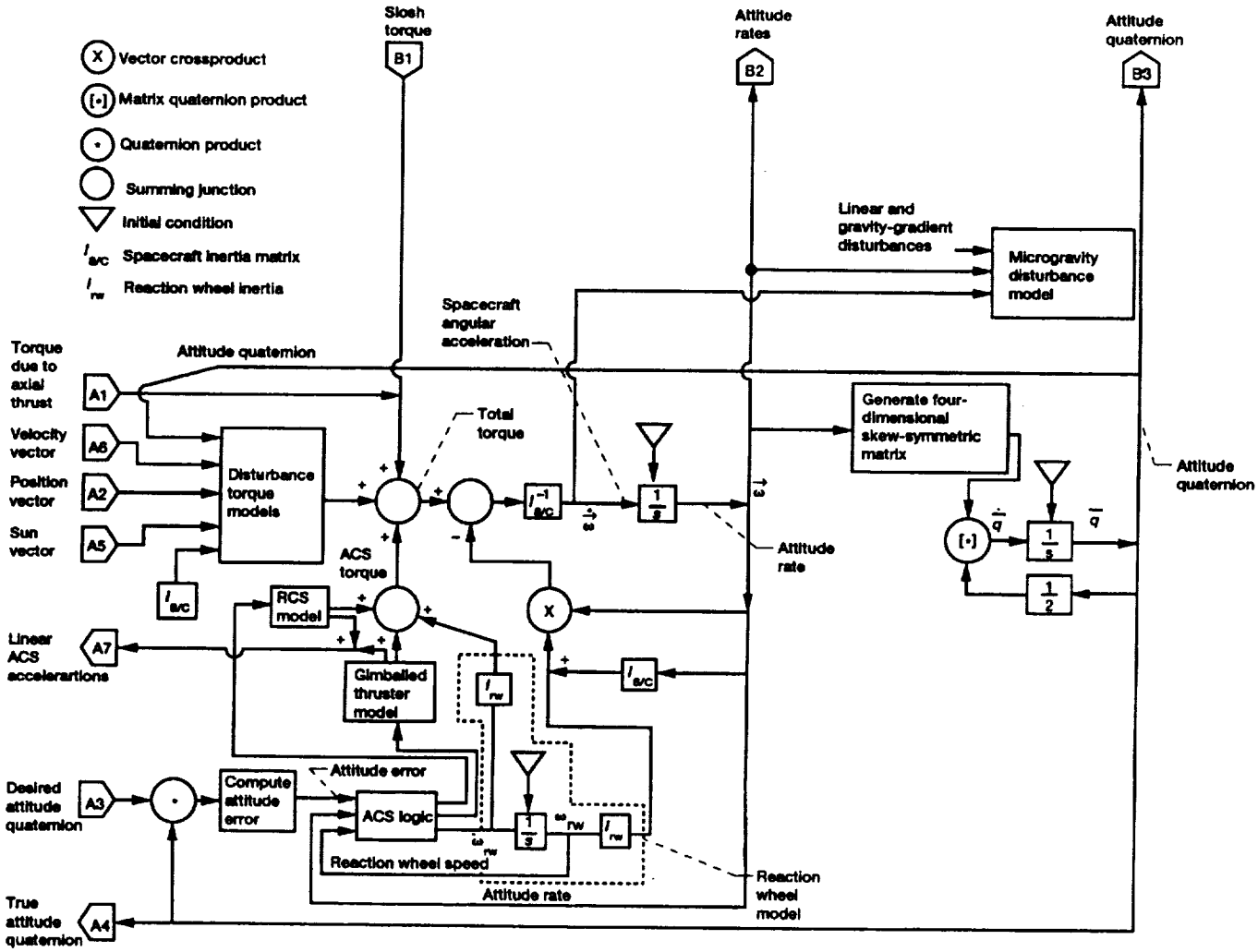

Figure 1.3.—Rotation model.

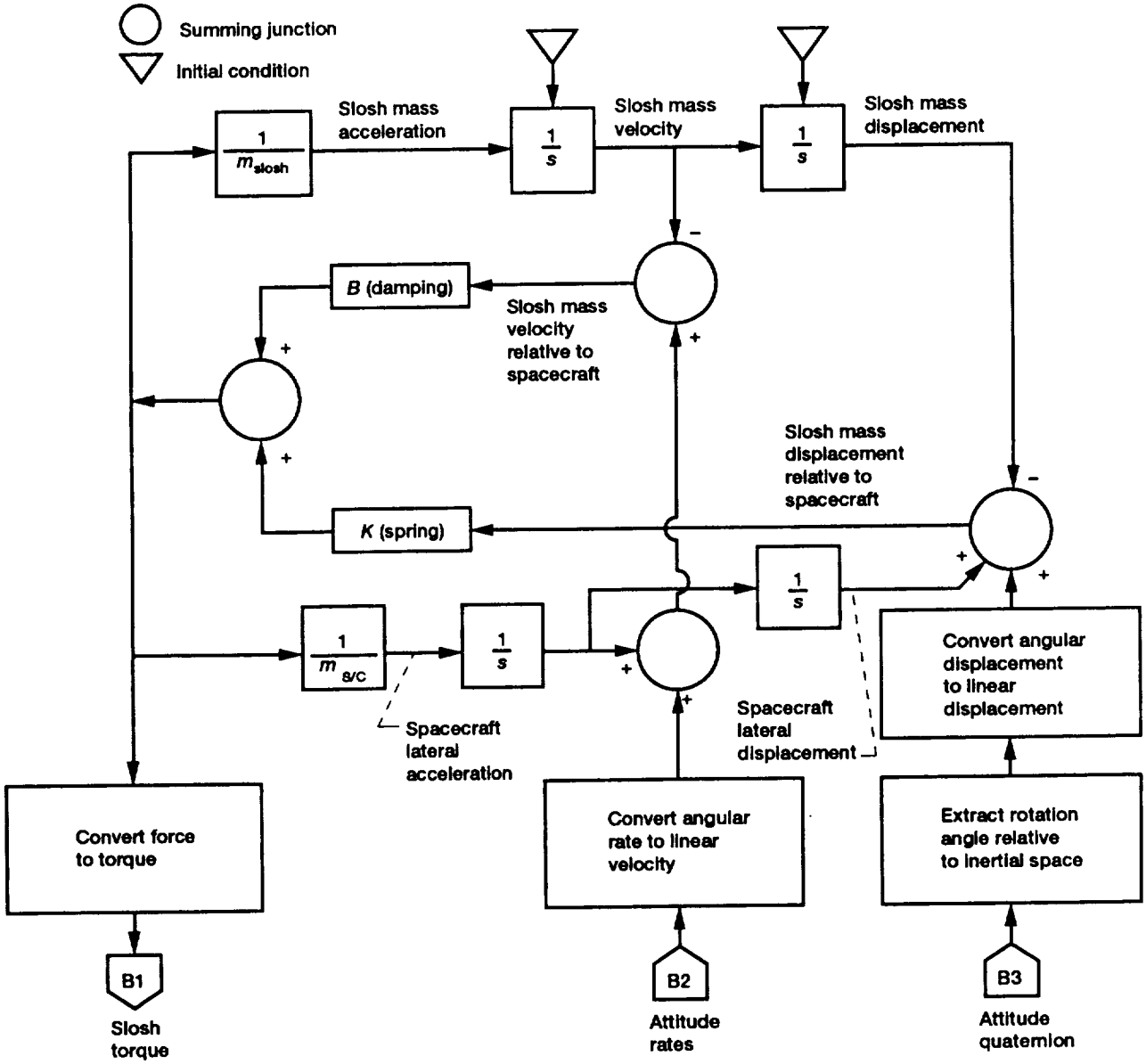

Figure 1.4.—Slosh model.

2.0 Translation Model

The translation model propagates the position and velocity vectors from an assumed initial on-orbit state for a spacecraft under the influence of various forces. The initial state is computed in the model as a function of the following user-specified orbital elements:

(1) Perigee altitude

(2) Eccentricity

(3) Inclination

(4) Argument of perigee

(5) Right ascension of the ascending node

(6) Time since perigee passage

Other inputs to the translation model are the initial date and time (in GMT) used to compute the position of the Sun and the desired attitude option and orientation. A block diagram of the translation model is shown in figure 1.2.

Three rectangular, right-handed coordinate systems are used for the translation model. They are discussed briefly here and in more detail in appendix C:

(1) True-of-date (TOD) coordinate system (fig. 2.1): A pseudo-inertial, equatorial, Earth-centered system whose X axis points in the direction of the first point of Aries (the vernal equinox) and whose Z axis points in the direction of the North Pole. The axes of this system are designated X, Y, and Z. See figure C.1.

(2) Spacecraft-body system: A coordinate system fixed with the center-of-gravity point (CG) of the spacecraft, where the origin is the actual CG location of the spacecraft. The x axis is defined as parallel to the long axis of the spacecraft, pointing toward the fore end, the y axis is parallel to the solar panel connecting struts, and the z axis points in the direction opposite the spacecraft high-gain antenna. The axes of this system are designated x, y, and z. See figure C.2.

(3) Alternative spacecraft-body system: A coordinate system similar to (2) with the origin located where the plane containing the rear thrusters intersects the line that is parallel to the long axis of the spacecraft and passes through the nominal CG point (thus, if the y and z CG offsets from the nominal are zero, then $y = y'$ and $z = z'$). The axes of this system are specified as x', y', and z'. See figure C.2.

All forces acting on the spacecraft, excluding gravity, are computed in spacecraft-body coordinates and then transformed into TOD coordinates. The gravitational force is computed directly in TOD coordinates, and the integration of the resulting accelerations from all applied forces is carried out in the TOD coordinate system.

Because the model was required to accurately simulate the spacecraft orbit for periods of time extending up to 60 days, changes in the spacecraft mass were also modeled. The mass changes of the COLD–SAT spacecraft are significantly larger than those associated with a typical spacecraft because a

high percentage of the spacecraft mass is composed of expendable fluids, which include liquid hydrogen in addition to hydrazine (N_2H_4).

The translation model includes a number of other auxiliary functions that are not directly associated with the computation of the spacecraft position and the velocity vectors. These include the computation of the desired attitude matrix and subsequent extraction of an equivalent quaternion and the computation of the Sun vector and a vector normal to the ecliptic plane. These two vectors are required for the computation of a desired attitude quaternion for certain attitude options. Also included in the translation model are computations of the Greenwich hour angle (GHA) and the conversion of the calendar date and the Greenwich mean time (GMT) to the Julian date.

The remainder of this section provides detailed descriptions of the various elements of the translation model as follows:

(1) Conversion of initial orbital elements into an initial state vector in TOD coordinates

(2) Computation of the Julian date, the Sun vector, the ecliptic-normal vector, and the GHA

(3) Computation of all simulated forces acting on the spacecraft and transformation of these forces to TOD coordinates by using the attitude quaternion

(4) Approximation of the spacecraft mass

(5) Integration of the resulting accelerations to obtain velocity and position vectors

(6) Computation of the desired spacecraft attitude quaternion

(7) Computation of torque due to axial thruster misalignment

(8) Computation of classical or osculating orbital elements from the state vector for printing and plotting

2.1 Interfaces of Translation Model

Interfaces between the translation model and other parts of the overall COLD–SAT dynamic model, as well as input and output quantities, are as follows:

(1) The following quantities are computed by the translation model and passed to the rotation model:

(a) The position vector is used for disturbance-torque computations.

(b) The atmospheric drag forces are used for (aerodynamic drag) disturbance-torque computations.

(c) The Sun position is used for (solar pressure) disturbance-torque computations.

(d) The desired attitude quaternion is used to compute attitude error.

(e) The GHA is used for (magnetic) disturbance-torque computations.

(f) The desired attitude quaternion at the beginning of the simulation is used to initialize the actual spacecraft attitude quaternion.

(2) The desired attitude quaternion at the beginning of the simulation is passed to the slosh model to provide a rotation reference. There are no other interfaces between the translation model and the slosh model.

(3) The following quantities are computed by the rotation model and passed to the translation model:

(a) The actual spacecraft attitude quaternion, which is used to transform forces acting on the spacecraft from body coordinates to TOD coordinates. (If the translation model is used alone, the desired attitude quaternion is used in place of the actual attitude quaternion).

(b) The translational RCS accelerations resulting from unpaired thrusters. (A constant, average value is used to represent the translational RCS force resulting from uncoupled thrusters if the translation model is used alone.)

(4) The following quantities, which are specified by the user at the start of simulation, are input to the translation model:

(a) Initial orbital elements (see beginning of section 2.0)

(b) Initial calendar date and GMT

(c) Spacecraft attitude option and axis alignment (see section 2.6)

(5) The primary outputs of the translation model are numerous classical or osculating orbital elements, which can be plotted or presented in tabular form as a function of time.

2.2 Computation of Initial Position and Velocity Vectors From Given Orbital Elements

An initial state vector, which consists of the initial position vector $\vec{R}_0$ and the initial velocity vector $\vec{v}_0$, must be specified at the beginning of the simulation. It is computed from the specified orbital elements. This section is concerned with this computation. The following standard orbital elements are used as initial conditions. From these values the initial position and velocity vectors can be computed. Some of these orbital elements are illustrated in figure 2.2.

a semimajor axis, ft

e eccentricity

i orbit inclination from equatorial plane, deg

Ω right ascension of ascending node, deg

ω argument of perigee, deg

T_P time since perigee passage, sec

From these given elements, additional orbital elements are computed as follows: The mean anomaly (in radians) is given by

$$M = T_P \sqrt{\frac{\mu}{a^3}}$$

where μ is the Earth gravitational constant (see appendix A). The eccentric anomaly E may be computed by the following iterative pseudocode:

$E = M + e \sin M$
Loop: $M_e = E - e \sin E$
If (abs($M - M_e$) < TOL) STOP, answer is E.
$E = E + (M - M_e)/(1 - e \cos E)$
Go to loop

where TOL is a small number (TOL << 1) that indicates the accuracy of the result.

An Earth-centered, right-handed coordinate system is defined with x and y axes lying in the spacecraft orbit plane. The x axis is in the direction of orbit perigee, and the z axis is in the direction of the spacecraft angular momentum vector. This coordinate system is called the spacecraft orbit (SCO) system. Refer to appendix C for a detailed description of all coordinate systems used in the model. The position and velocity vectors in spacecraft orbital coordinates, $\vec{R}_{SCO}$ and $\vec{v}_{SCO}$, respectively, are computed as follows:

$$\vec{R}_{SCO} = \begin{bmatrix} a(\cos E - e) \\ a \sin E\sqrt{1 - e^2} \\ 0 \end{bmatrix}$$

$$\vec{v}_{SCO} = \begin{bmatrix} -\dfrac{\sqrt{\mu a}\ \sin E}{R} \\ \dfrac{\sqrt{\mu a(1 - e^2)}\cos E}{R} \\ 0 \end{bmatrix}$$

Position and velocity vectors are then transformed to TOD coordinates as follows:

$$\vec{R}_0 = [\text{SCO} \rightarrow \text{TOD}]\vec{R}_{SCO}$$

$$\vec{v}_0 = [\text{SCO} \rightarrow \text{TOD}]\vec{v}_{SCO}$$

where

$$[\text{SCO} \rightarrow \text{TOD}] = \begin{bmatrix} \cos\Omega & \sin\Omega & 0 \\ -\sin\Omega & \cos\Omega & 0 \\ 0 & 0 & 1 \end{bmatrix} \begin{bmatrix} 1 & 0 & 0 \\ 0 & \cos i & \sin i \\ 0 & -\sin i & \cos i \end{bmatrix} \begin{bmatrix} \cos\omega & \sin\omega & 0 \\ -\sin\omega & \cos\omega & 0 \\ 0 & 0 & 1 \end{bmatrix}$$

and

Ω right ascension of ascending node, deg

i inclination, deg

ω argument of perigee, deg

There are two special cases of spacecraft orbit where one or more of the input orbital elements are not defined:

Case 1; $e = 0$, $i \neq 0$: If the spacecraft orbit is circular, orbit perigee is undefined, and the orientation of the SCO x axis is arbitrary. For a circular orbit the argument of perigee input ω should be set to zero, so that the SCO x axis is coincident with the ascending node. Thus, the T_P input is interpreted, in this case, as the time since the spacecraft passed the ascending node.

Case 2; $e = 0$, $i = 0$: If the orbit is circular and lies in the equatorial plane, both the argument of perigee and the right ascension of the ascending node are undefined. In this case, both of the input quantities (ω,Ω) should be set to zero, so that the SCO coordinate system becomes identical to the TOD system and the T_P input is interpreted, in this case, as the time since the spacecraft passed the TOD X axis.

2.3 Computation of Forces Acting on Spacecraft

2.3.1 Gravity

The Earth gravity model computes the linear acceleration of the spacecraft due to the gravitational field of the Earth. The fundamental component (spherical-Earth component) and as many as three additional terms resulting from the oblateness of the Earth (zonal harmonics) can be computed, so that nodal regression and apsidal progression can be accurately simulated.

The gravitational potential function of the Earth (from ref. 1) is as follows:

$$\Phi(R,\theta) = \frac{\mu_{\text{Earth}}}{R}\left[1 + \frac{J_2 R_{\text{Earth}}^2}{2R^2}(1 - 3\sin^2\theta) + \frac{J_3 R_{\text{Earth}}^3}{2R^3}(3 - 5\sin^2\theta)\sin\theta - \frac{J_4 R_{\text{Earth}}^4}{8R^4}(3 - 30\sin^2\theta + 35\sin^4\theta)\right]$$

where

R magnitude of spacecraft position vector, ft

θ geocentric latitude of spacecraft

μ_{Earth} Earth gravitational constant, 1.4076469×10^{16} ft^3/sec^2

R_{Earth} Earth equatorial radius, 20 925 656 ft

J_2 second zonal-harmonic coefficient, 1.0827×10^{-3}

J_3 third zonal-harmonic coefficient, -2.56×10^{-6}

J_4 fourth zonal-harmonic coefficient, -1.58×10^{-6}

The terms J_2, J_3, and J_4 in the preceding equation are called zonal harmonics and result from the oblateness (flattening of the poles) of the Earth, which is the cause of the nodal regression of the orbit plane and the apsidal progression of the argument of perigee. Tesseral harmonics (resulting from longitudinal variations in the density of the Earth), zonal harmonics beyond the fourth, and solar and lunar gravitational effects were considered negligible for these purposes and are not modeled.

The gravitational acceleration can be found by taking the gradient of the potential function as follows:

$$\nabla\Phi(R,\theta) = \vec{\upsilon}_R g_R + \vec{\upsilon}_\theta g_\theta = \vec{\upsilon}_R \frac{\partial\Phi(R,\theta)}{\partial R} + \vec{\upsilon}_\theta \frac{1}{R} \frac{\partial\Phi(R,\theta)}{\partial\theta}$$

where $\vec{\upsilon}_R$ and $\vec{\upsilon}_\theta$ are unit vectors in the R and θ directions in spherical coordinates, respectively. Refer to figure 2.1 for an illustration of this coordinate system.

By evaluating the appropriate partial derivatives, the radial and latitudinal components of the gravitational acceleration (in spherical coordinates) can be determined as follows:

$$g_R = -\frac{\mu_{Earth}}{R^2} - \frac{3}{2}\mu_{Earth}J_2R_{Earth}^2R^{-4}(1 - 3\sin^2\theta) - 2\mu_{Earth}J_3R_{Earth}^3R^{-5}(3 - 5\sin^2\theta)\sin\theta + \frac{5}{8}\mu_{Earth}J_4R_{Earth}^4R^{-6}(3 - 30\sin^2\theta + 35\sin^4\theta)$$

$$g_\theta = -3\mu_{Earth}J_2R_{Earth}^2R^{-4}\sin\theta\cos\theta + \frac{1}{2}\mu_{Earth}J_3R_{Earth}^3R^{-5}(3\cos\theta - 15\sin^2\theta\cos\theta) - \frac{1}{8}\mu_{Earth}J_4R_{Earth}^4R^{-6}(-60\sin\theta\cos\theta + 140\sin^3\theta\cos\theta)$$

As there is no longitudinal variation in the potential function, the longitudinal component of gravitational acceleration is zero.

$$g_\phi = 0$$

The gravitational acceleration of the spacecraft in spherical coordinates is then converted to Cartesian TOD coordinates as follows:

$$\vec{g} = \begin{bmatrix} g_x \\ g_y \\ g_z \end{bmatrix} = \begin{bmatrix} \cos\eta\cos\theta & -\cos\eta\sin\theta \\ \sin\eta\cos\theta & -\sin\eta\sin\theta \\ \sin\theta & \cos\theta \end{bmatrix} \begin{bmatrix} g_R \\ g_\theta \end{bmatrix}$$

where η is the right ascension of the spacecraft position vector.

Right ascension and latitude are computed from the spacecraft position vector $\vec{R}$ as follows:

$$\theta = \tan^{-1}\left[\frac{R_z}{\sqrt{R_x^2 + R_y^2}}\right]$$

$$\eta = \tan^{-1}\left(\frac{R_y}{R_x}\right)$$

(Note that all arctangent functions used in this document are of the four-quadrant form, which considers the numerator and denominator of the argument separately so that the range of the function is the interval $[-\pi,+\pi]$ with no singularities.)

2.3.2 Aerodynamic Drag

An aerodynamic drag force results when the moving spacecraft interacts with the rarified atmosphere, producing a force that opposes motion. Because this force is, in general, not symmetrical with respect to the spacecraft CG, a disturbance torque results as well. (This is discussed in section 3.2.1.3.) The general equation for computing aerodynamic drag is

$$F = \frac{1}{2} c_D \rho_A v^2 A$$

where

F aerodynamic drag force

ρ_A atmospheric density

c_D drag coefficient (assumed ≈2.6)

v spacecraft velocity

A projected area of spacecraft normal to spacecraft velocity vector

The atmospheric drag force is computed for each axis by applying the preceding equation while using the velocity (in spacecraft body coordinates) along each axis and by considering the projected area of the spacecraft normal to each spacecraft axis. It should be emphasized that this method is an approximate one but is sufficiently accurate for the purposes of this model. Because the drag torque must also be computed, the centroid of this projected area must be specified as well. Therefore, using vector notation,

$$\vec{F}_{drag} = \begin{bmatrix}(F_{drag})_x \\ (F_{drag})_y \\ (F_{drag})_z\end{bmatrix} = -\frac{1}{2} c_D \rho_A \begin{bmatrix}\mathrm{sgn}(v_{S/C})_x (v_{S/C}^2)_x (A_x) \\ \mathrm{sgn}(v_{S/C})_y (v_{S/C}^2)_y (A_y) \\ \mathrm{sgn}(v_{S/C})_z (v_{S/C}^2)_z (A_z)\end{bmatrix}$$

where

$\vec{F}_{drag}$ drag force vector (in spacecraft coordinates), lbf

c_D drag coefficient (dimensionless, equal to 2.6)

ρ_A atmospheric density in spacecraft vicinity (from Jacchia's 1970 model), slug/ft^3

$\vec{v}_{S/C}$ spacecraft velocity vector, ft/sec, transformed into spacecraft coordinates (using attitude quaternion)

A_x, A_y, A_z projected area of spacecraft normal to spacecraft x, y, and z axes, respectively, ft^2

The atmospheric density ρ_A is computed by means of a subroutine that utilizes Jacchia's 1970 model. A complete description of this atmospheric density model can be found in reference 2.

2.3.3 Axial Thrust

2.3.3.1 Thrust vector.—The linear force acting on spacecraft due to axial thrust is desired to be in the spacecraft positive x direction; however, because of the thruster-gimbal system and unintentional thruster misalignments, there are typically small y and z components of axial thrust as well. The magnitude of the thrust for blowdown systems varies with time and is as given in section 2.3.3.3. The thrust magnitude for regulated systems is assumed to be constant at some specified value. The thrust vector (in spacecraft coordinates) is expressed as

$$\vec{F}_T = \begin{bmatrix} F_{TG} \cos \gamma_y \cos \gamma_z \\ F_{TG} \sin \gamma_z \\ -F_{TG} \sin \gamma_y \cos \gamma_z \end{bmatrix}_{\substack{\text{gimballed} \\ \text{thruster}}} + \begin{bmatrix} T_{TF} \cos \varepsilon_y \cos \varepsilon_z \\ F_{TF} \sin \varepsilon_z \\ -F_{TF} \sin \varepsilon_y \end{bmatrix}_{\substack{\text{fixed} \\ \text{thruster}}}$$

where

$\vec{F}_T$ resultant thrust vector in spacecraft coordinates, lbf

F_{TG} magnitude of thrust produced by gimballed thruster, lbf

F_{TF} total of thrust magnitude produced by fixed thrusters, lbf

γ_y gimbal angle about y axis, rad

γ_z gimbal angle about z axis, rad

ε_y angular misalignment of fixed thrusters about y axis, rad

ε_z angular misalignment of fixed thrusters about z axis, rad

Positive angles are defined as counterclockwise about the positive axis in question. The fixed thruster term uses small angle approximations; the gimballed thruster force is derived in section 2.3.3.2.

For COLD–SAT the thrust level of the gimballed thruster F_{TG} is 0.04 lbf and corresponds to the minimum thrust level required to conduct some of the onboard experiments. When an experiment requires axial thrust levels higher than 0.04 lbf, F_{TF} is commanded to produce a force equal to the required thrust less 0.04 lbf. This arrangement provides the required thrust vector control by gimballing a single, low-thrust thruster.

The gimbal angles γ_y and γ_z are determined by the attitude control system in a manner to reduce attitude error. Refer to section 3.7.2 for a description of this calculation.

2.3.3.2 Gimbal model.—The gimballed thruster system consists of a 0.04-lbf hydrazine thruster mounted on two single-axis antenna gimbal mechanisms. Gimbal #1 is attached to the spacecraft and can rotate as much as ±20° about the spacecraft y axis; gimbal #2 is mounted on gimbal #1 and can rotate as much as ±20° about the z axis. The rotation angle of gimbal #1 is designated as γ_y, and the rotation angle of gimbal #2 as γ_z. Therefore, if by defining a coordinate system fixed in the thruster itself and assuming that the thruster force vector is directed along the $+x$ axis of the thruster coordinate system, the thrust vector produced by the gimballed thruster in spacecraft coordinates can be determined by applying this coordinate transformation:

$$\vec{F}_{TG} = \begin{bmatrix} \cos\gamma_y & 0 & \sin\gamma_y \\ 0 & 1 & 0 \\ -\sin\gamma_y & 0 & \cos\gamma_y \end{bmatrix} \begin{bmatrix} \cos\gamma_z & -\sin\gamma_z & 0 \\ \sin\gamma_z & \cos\gamma_z & 0 \\ 0 & 0 & 1 \end{bmatrix} \begin{bmatrix} 0.04\ (\text{lbf}) \\ 0 \\ 0 \end{bmatrix}$$

Multiplying the matrices in the proper order gives the gimballed-thruster thrust vector in terms of the gimbal angles, which is the first term of the equation given in section 2.3.3.1. The desired gimbal angles are computed by the rotation model as a function of attitude error, integral of attitude error, and attitude rate.

2.3.3.3 Thrust decay (blowdown system).—In order to accurately model the thrust produced by a blowdown system, the thrust magnitude $F_T = F_{TF} + F_{TG}$ is allowed to vary as a function of hydrazine usage in the model by means of a table-lookup algorithm. For a blowdown system F_T is a linear function of pressure, which drops as hydrazine is expended. The tank is repressurized with helium as required during the spacecraft life in order to maintain a workable hydrazine pressure. A typical graph of system pressure P_{sys} as a function of hydrazine expended is shown in figure 2.3. The thrust level is related to the system pressure by

$$F_T = (F_T)_{\text{nom}} \frac{P_{\text{sys}}}{P_{\text{nom}}}$$

where $(F_T)_{\text{nom}}$ is the nominal thrust level, P_{sys} is the system pressure (as given in fig. 2.3), and P_{nom} is the nominal system pressure (assumed to be 150 psia for COLD–SAT). The rate of change of hydrazine mass (denoted $m_{N_2H_4}$) is a function of the actual thrust F_T as follows:

$$\frac{dm_{N_2H_4}}{dt} = -\frac{F_T}{I_{\text{sp}}}$$

where I_{sp} is the specific impulse, a function of the system design. If a pressure-regulated hydrazine supply system is used, then the effect of system pressure can be eliminated by setting the system pressure variable P_{sys} (as a function of hydrazine mass) to a constant value.

2.3.4 Translational Force Resulting From Unpaired RCS Thrusters

The baseline COLD–SAT RCS system is an uncoupled-thruster system with eight thrusters, which produce torque couples only about the x axis (see section 3.2.3.2). When control thrusters are fired to produce torques about the y and z axes with such a system, a linear acceleration will be produced in the $+x$ direction. The COLD–SAT dynamic model accounts for this linear acceleration in the translation model as $\vec{F}_{RCS}$.

2.4 Approximation of Spacecraft Mass

The mass of the COLD–SAT spacecraft varies over the life of the mission because of the various experimental and propulsion system fluids used. For the purposes of the model the total spacecraft mass is considered to be the sum of three components:

$$m_{S/C} = m_{dry} + m_{H_2} + m_{N_2H_4}$$

where m_{dry} is the mass of the spacecraft minus the mass of all expendable fluids, $m_{N_2H_4}$ is the mass of hydrazine used for all axial thrusters, which is computed as indicated in section 2.3.3.3, and m_{H_2} is the mass of all other expendable fluids onboard, primarily liquid H_2, which is entered into the model as a table of mass versus time.

2.5 Computation of Spacecraft Position and Velocity Vectors

The resulting acceleration due to all external forces acting on the spacecraft in body coordinates is given as follows:

$$(\vec{a}_{ext})_{S/C} = \frac{\vec{F}_T + \vec{F}_{RCS} + \vec{F}_{drag}}{m_{S/C}}$$

This acceleration vector is then transformed into TOD coordinates as follows:

$$\begin{bmatrix} 0 \\ \hline (\vec{a}_{ext})_{TOD} \end{bmatrix} = \bar{q} * \begin{bmatrix} 0 \\ \hline (\vec{a}_{ext})_{S/C} \end{bmatrix} * \bar{q}^{\,c}$$

where

$\bar{q}$ actual spacecraft attitude quaternion (When the translation model is used alone, the desired attitude quaternion is used in place of the actual attitude quaternion because the latter must be computed by the rotation model.)

$\bar{q}^c$ conjugate of spacecraft attitude quaternion

$(\vec{a}_{ext})_{TOD}$ spacecraft linear acceleration due external forces in TOD coordinates

$*$ signifies quaternion multiplication

The notation

$$\begin{bmatrix} 0 \\ --- \\ \vec{a} \end{bmatrix}$$

represents a quaternion whose scalar part is zero and whose vector part is equal to the vector $\vec{a}$. Refer to appendix B for a description of quaternion algebra.

Thus, the total linear acceleration acting on the spacecraft due to all modeled forces is expressed as

$$\vec{a} = \vec{g} + (\vec{a}_{ext})_{TOD}$$

where

$\vec{a}$ total spacecraft linear acceleration in TOD coordinates

$\vec{g}$ spacecraft linear acceleration due to Earth gravity in TOD coordinates

The spacecraft velocity and position vectors can now be computed as

$$\vec{v}(t) = \int_{t_0}^{t} \vec{a}(\tau)d\tau + \vec{v}_0$$

$$\vec{R}(t) = \int_{t_0}^{t} \vec{v}(\tau)d\tau + \vec{R}_0$$

where

$\vec{R}$ spacecraft position vector in TOD coordinates

$\vec{v}$ spacecraft velocity vector in TOD coordinates

$\vec{R}_0$ initial position vector (see section 2.2)

$\vec{v}_0$ initial velocity vector (see section 2.2)

2.6 Computation of Desired Attitude Quaternion

2.6.1 Overview

The COLD–SAT attitude model computes a quaternion that represents the desired attitude of the spacecraft. The actual spacecraft attitude quaternion is computed by the rotation model. The purpose of the desired attitude quaternion is to provide a reference attitude so that the attitude error (a measure of the difference between this desired attitude and the actual attitude) can be computed. The attitude control system then uses this information to correct the actual spacecraft attitude so that it is as close to the desired attitude as possible. The desired spacecraft attitude options are defined by the alignment of certain spacecraft axes with certain base unit vectors, which are defined in TOD coordinates.

The COLD–SAT dynamic model allows an attitude to be selected from among nine basic options. Within each option several suboptions are permitted. The attitude may then be further modified by specifying a fixed or time-varying rotation about any one of the spacecraft axes. Figures 2.4 to 2.12 are pictorial representations of each of the attitude options. The computation of the desired spacecraft attitude proceeds as follows depending upon the user-specified attitude option, axis alignment, and optional spacecraft rotation:

(1) Computation of the position of the Sun in TOD coordinates based upon the Julian date at the start of the simulation and the simulation time

(2) Computation of two orthogonal unit vectors, which are called base vectors in the discussion that follows and are expressed in TOD coordinates. Nine combinations of base vectors, called attitude options, are predefined in the model. The desired attitude option is specified by the user at the start of the simulation.

(3) Determination of the spacecraft axes that are to be aligned with each base vector; either positive or negative spacecraft axes may be specified. This results in 12 possible attitude variations for each pair of base vectors selected. The desired spacecraft axis alignment is specified by the user at the start of the simulation.

(4) Computation of the rotation axis and the rotation angle for the optional spacecraft rotation. The rotation axis may be any positive or negative spacecraft axis; the rotation angle is expressed as

$$\varepsilon(t) = \dot{\varepsilon} t + \varepsilon_0$$

The rotation axis, as well as the values of $\dot{\varepsilon}$ and ε_0, is specified by the user at the start of the simulation.

(5) Computation of the desired attitude matrix (direction-cosine matrix) based on steps (1) through (4)

(6) Extraction of the desired attitude quaternion from the desired attitude matrix

Each of these steps is described in detail in sections 2.6.3 to 2.6.8.

2.6.2 Sun Model

The Sun model computes the position of the Sun in TOD coordinates on a given Julian date, as well as a unit vector normal to the plane of the ecliptic, also expressed in TOD coordinates (ref. 3). The mean solar longitude with respect to the TOD vernal equinox ξ_{ms}, in degrees, is computed in Earth-centered ecliptic coordinates (see appendix C for a description of this coordinate system) as follows:

$$\xi_{ms} = 280.46° + 0.9856474°(JD_{2000})$$

where (JD_{2000}) is the Julian date referenced to the year 2000. The Sun's mean anomaly M, in degrees, is now computed as

$$M = 357.528° + 0.9856003°(JD_{2000})$$

The ecliptic longitude of the Sun ξ_{ecl}, in degrees, is computed as

$$\xi_{ecl} = \xi_{ms} + 1.915° \sin(M) + 0.020° \sin(2M)$$

The unit vector in the direction of the Sun $\vec{\upsilon}_{Sun}$ and a vector normal to the plane of the ecliptic $\vec{\upsilon}_{ecl}$ are expressed as follows in ecliptic coordinates:

$$\vec{\upsilon}_{Sun_{(e)}} = \begin{bmatrix} \cos(\xi_{ecl}) \\ \sin(\xi_{ecl}) \\ 0 \end{bmatrix}$$

$$\vec{\upsilon}_{ecl_{(e)}} = \begin{bmatrix} 0 \\ 0 \\ 1 \end{bmatrix}$$

The same vectors are expressed in TOD coordinates as follows:

$$\vec{\upsilon}_{Sun} = \begin{bmatrix} (\upsilon_{Sun})_x \\ (\upsilon_{Sun})_y \\ (\upsilon_{Sun})_z \end{bmatrix} = \begin{bmatrix} (\upsilon_{Sun})_{x(e)} \\ (\upsilon_{Sun})_{y(e)} \cos\left\{23.439° - 4\times10^{-7}(JD_{2000})\right\} \\ (\upsilon_{Sun})_{z(e)} \sin\left\{23.439° - 4\times10^{-7}(JD_{2000})\right\} \end{bmatrix}$$

$$\vec{\upsilon}_{ecl} = \begin{bmatrix} (\upsilon_{ecl})_x \\ (\upsilon_{ecl})_y \\ (\upsilon_{ecl})_z \end{bmatrix} = \begin{bmatrix} 0 \\ -\sin(23.439° - 4\times10^{-7}JD_{2000}) \\ \cos(23.439° - 4\times10^{-7}JD_{2000}) \end{bmatrix}$$

2.6.3 Base Vectors

Two orthonormal base vectors, designated $\vec{v}_1$ and $\vec{v}_2$, are used to define each of the nine options built into the COLD–SAT dynamic model. These base vectors are selected from the normalized position, velocity, Sun, and ecliptic-normal vectors or from some mathematical combination of two or more of these vectors. Each of the nine attitude options is defined in table 2.1 and illustrated in figures 2.4 to 2.12.

The two base vectors are chosen from the following list of unit vectors as defined in table 2.1, depending on which of the nine attitude options is selected:

$\vec{v}_{\text{Sun}}$ unit vector in direction of Sun (This vector is computed by the Sun model.)

$\vec{v}_{\text{ecl}}$ unit vector normal to plane of ecliptic (This vector is also computed by the Sun model.)

$\vec{v}_R$ unit spacecraft geocentric position vector (This vector is the normalized spacecraft position vector $\vec{R}$.)

$\vec{v}_v$ unit spacecraft velocity vector (This vector is the normalized spacecraft velocity vector $\vec{v}$.)

$\vec{v}_N$ unit vector normal to spacecraft orbit plane, $\left[\dfrac{\vec{v}_R \times \vec{v}_v}{|\vec{v}_R \times \vec{v}_v|}\right]$

$\vec{v}_{sx}$ unit vector in direction of projection of Sun vector into spacecraft orbit plane,

$$\left[\frac{\vec{v}_N \times \vec{v}_{\text{Sun}}}{|\vec{v}_N \times \vec{v}_{\text{Sun}}|}\right] \times \vec{v}_N$$

$\vec{v}_{sy}$ unit vector in plane formed by Sun vector and spacecraft velocity vector and normal to spacecraft velocity vector, $\left[\dfrac{\vec{v}_v \times \vec{v}_{\text{Sun}}}{|\vec{v}_v \times \vec{v}_{\text{Sun}}|}\right] \times \vec{v}_v$

$\vec{v}_P$ unit vector in orbit plane and normal to Sun vector, $\left[\dfrac{\vec{v}_N \times \vec{v}_{\text{Sun}}}{|\vec{v}_N \times \vec{v}_{\text{Sun}}|}\right]$

2.6.4 Spacecraft Axis Alignment With Base Vectors

Once the base vectors are defined, two of the spacecraft coordinate axes are aligned with the two base vectors to establish the desired spacecraft attitude. This alignment of spacecraft axes with base vectors is controlled by the manner in which the attitude matrix is constructed, as described next.

2.6.5 Computation of Desired Attitude (Direction-Cosine) Matrix

The attitude matrix (sometimes called a direction-cosine matrix) defines the transformation of a vector from the TOD coordinate system to the spacecraft body coordinate system. The attitude matrix is a 3×3 matrix with the property that each column (and each row as well) is a unit vector. If $\vec{v}_{TOD}$ is a vector defined in TOD coordinates and $\vec{v}_{S/C}$ is the same vector expressed in spacecraft body coordinates, the relationship between the two representations is

$$\vec{v}_{S/C} = [\text{TOD} \rightarrow \text{S/C}]\vec{v}_{TOD}$$

where [TOD → S/C] is defined as the attitude matrix.

The attitude matrix is formed by substituting the two base vectors for the selected attitude option into the two columns of the matrix that correspond to the two spacecraft axes which are to be aligned with these base vectors. The first column of the matrix corresponds to the x axis, the second column to the y axis, and the third column to the z axis. If the negative of a given axis is to be aligned with a base vector, that vector is negated before substitution into the matrix. Because the base vectors are unit vectors by definition, the remaining column of the matrix is found by taking the crossproduct of the two vectors in the proper order to form a right-handed system.

In equation form, in order to align the spacecraft $-x$ axis with the base vector $\vec{v}_2$ and the z axis with the base vector $\vec{v}_1$, the attitude matrix would be as follows:

$$\left[-\vec{v}_2 \mid \vec{v}_1 \times (-\vec{v}_2) \mid \vec{v}_1\right]$$

As an example, for the attitude selected for COLD–SAT (attitude option 4, with the spacecraft $-x$ axis aligned with $\vec{v}_2$ and the spacecraft z axis aligned with $\vec{v}_1$), the attitude matrix would be as follows:

$$\left[-\vec{v}_{sx} \mid \vec{v}_N \times (-\vec{v}_{sx}) \mid \vec{v}_N\right]$$

2.6.6 180° Spacecraft Rotation

For attitude options 4, 7, and 8, the spacecraft is required to execute a 180° rotation about a given axis whenever the Sun crosses the spacecraft orbit plane. This maneuver is necessary to allow the side of the spacecraft along which the cryogenic lines are run to remain shaded at all times and to minimize the angle between the solar panel normal and the Sun vector. This rotation axis, expressed in TOD coordinates, is as shown in table 2.2. The corresponding axis in spacecraft coordinates depends upon which axis is aligned with the TOD vector.

It is undesirable to allow the desired spacecraft attitude to change instantaneously by 180° because this would result in a sudden 180° attitude error. The subsequent response by the attitude control system (ACS) to compensate would result in poor transient behavior, including large attitude rates, with significant overshoot of the desired attitude and subsequent oscillation about the desired attitude with a very long settling time. In order to avoid this problem, the change in desired attitude is executed over a finite time t_f.

The minimum achievable value for t_f is

$$(t_f)_{\min} = 2\sqrt{\pi I/\tau}$$

where

I spacecraft moment of inertia about rotation axis

τ maximum control torque that ACS can produce about rotation axis

This equation assumes that the spacecraft undergoes a constant angular acceleration at the maximum achievable rate during the first half of the 180° rotation maneuver and then decelerates at an equal rate for the remainder of the maneuver.

For any time $t_f \geq (t_f)_{\min}$ the desired attitude matrix is computed as follows:

$$\mathbf{A}(t) = \mathbf{R}_1(\Psi)\mathbf{A}(t_{0f})$$

where

$\mathbf{A}(t)$ desired attitude matrix at time t, where t is with respect to the start of the rotation (t_{0f})

$\mathbf{A}(t_{0f})$ desired attitude matrix at instant before time of desired attitude change

$\mathbf{R}_1(\Psi)$ Euler matrix representing single rotation about appropriate spacecraft axis through angle Ψ

The angle Ψ is expressed in radians as

$$\Psi = \frac{1}{2}at^2 \qquad \text{for} \quad 0 \leq t \leq \frac{1}{2}t_f$$

$$\Psi = \pi - 0.5a(t_f - t)^2 \quad \text{for} \quad \frac{1}{2}t_f < t \leq t_f$$

and

$$a = \frac{\pi}{t_f^2}$$

This formulation for Ψ and a assumes a constant angular acceleration for the first 90° of rotation and a constant deceleration for the remaining 90° of rotation. Other time functions for Ψ could be used but are not included in the current version of the model. The attitude quaternion is then extracted from the desired attitude matrix in the usual manner.

2.6.7 Optional Spacecraft Rotation

For certain attitude options it may be desired to specify a fixed angular offset from the nominal attitude or a constant-rate rotation about a given axis (perhaps to keep solar arrays pointing toward the Sun for continuously rotating attitude options). The rotation angle is specified as

$$\varepsilon(t) = \dot{\varepsilon} t + \varepsilon_0$$

where

$\dot{\varepsilon}$ rate of continuous spacecraft rotation, rad/sec

t simulation time, sec

ε_0 constant spacecraft angular displacement, rad

The desired attitude matrix is formed as follows:

$$\mathbf{A}(t) = \mathbf{R}[\varepsilon(t)]\mathbf{A}_{nom}$$

where

$\mathbf{R}(\varepsilon)$ Euler rotation matrix of angle ε about specified axis

$\mathbf{A}_{nom}$ nominal spacecraft desired attitude matrix (before rotation)

2.6.8 Quaternion Extraction From Desired Attitude Matrix

A vector transformation (and thus the spacecraft attitude) can be equivalently represented by means of a unit quaternion. Because quaternions are used throughout the model, it is required that the attitude matrix representing the desired spacecraft attitude be converted into quaternion form. This is a fairly straightforward procedure and is described here. If $\mathbf{A}$ is the desired attitude matrix and $\bar{p}$ is the equivalent desired attitude unit quaternion, reference 4 gives $\mathbf{A}$ in terms of $\bar{p}$ as

$$\mathbf{A} = \begin{bmatrix} 2(p^{\langle 0 \rangle})^2 + 2(p^{\langle 1 \rangle})^2 - 1 & 2p^{\langle 1 \rangle}p^{\langle 2 \rangle} - 2p^{\langle 0 \rangle}p^{\langle 3 \rangle} & 2p^{\langle 1 \rangle}p^{\langle 3 \rangle} + 2p^{\langle 0 \rangle}p^{\langle 2 \rangle} \\ 2p^{\langle 1 \rangle}p^{\langle 2 \rangle} + 2p^{\langle 0 \rangle}p^{\langle 3 \rangle} & 2(p^{\langle 0 \rangle})^2 + 2(p^{\langle 2 \rangle})^2 - 1 & 2p^{\langle 2 \rangle}p^{\langle 3 \rangle} - 2p^{\langle 0 \rangle}p^{\langle 1 \rangle} \\ 2p^{\langle 1 \rangle}p^{\langle 3 \rangle} - 2p^{\langle 0 \rangle}p^{\langle 2 \rangle} & 2p^{\langle 2 \rangle}p^{\langle 3 \rangle} + 2p^{\langle 0 \rangle}p^{\langle 1 \rangle} & 2(p^{\langle 0 \rangle})^2 + 2(p^{\langle 3 \rangle})^2 - 1 \end{bmatrix}$$

and

$$\bar{p} = \begin{bmatrix} p^{\langle 0 \rangle} \\ p^{\langle 1 \rangle} \\ p^{\langle 2 \rangle} \\ p^{\langle 3 \rangle} \end{bmatrix}$$

where $p^{\langle 0 \rangle}$ is the scalar part of the quaternion.

Thus, by rearranging terms in the **A** matrix, the desired attitude quaternion elements can be solved for in terms of the attitude matrix elements.

$$T = Tr[\mathbf{A}] = A_{11} + A_{22} + A_{33}$$

Because $(p^{\langle 0 \rangle})^2 + (p^{\langle 1 \rangle})^2 + (p^{\langle 2 \rangle})^2 + (p^{\langle 3 \rangle})^2 = 1$ for a unit quaternion,

$$p^{\langle 0 \rangle} = \frac{\sqrt{T + 1}}{2}$$

The magnitudes of the three vector elements of the quaternion can be computed as follows:

$$|p^{\langle i \rangle}| = + \sqrt{\left[\frac{A_{ii}}{2} + \frac{1 - Tr(\mathbf{A})}{4}\right]} \qquad \text{for} \quad i = 1,2,3$$

The signs of the three vector elements of the quaternion can be computed from the off-diagonal elements. The indices i, j, and k are determined in cyclic order so that

$$|p^{\langle i \rangle}| \geq |p^{\langle j \rangle}|, \qquad |p^{\langle i \rangle}| \geq |p^{\langle k \rangle}|$$

Now the vector elements of the quaternion can be determined as

$$p^{\langle i \rangle} = \text{sgn}(A_{kj} - A_{jk})|p^{\langle i \rangle}|$$

$$p^{\langle j \rangle} = \text{sgn}[p^{\langle i \rangle}(A_{ji} + A_{ij})]|p^{\langle j \rangle}|$$

$$p^{\langle k \rangle} = \text{sgn}[p^{\langle i \rangle}(A_{ki} + A_{ik})]|p^{\langle k \rangle}|$$

where $\text{sgn}(x)$ is the sign function (i.e., $\text{sgn}(x)$ returns +1 if the argument x is positive, 0 if the argument is zero, and −1 if the argument is negative).

Thus, by using the preceding equations, the four elements of the quaternion can be computed. The resulting quaternion is then normalized by means of

$$\bar{p} \leftarrow \frac{\bar{p}}{|p|}$$

where

$$|p| = \sqrt{(p^{\langle 0 \rangle})^2 + (p^{\langle 1 \rangle})^2 + (p^{\langle 2 \rangle})^2 + (p^{\langle 3 \rangle})^2}$$

2.7 Miscellaneous Calculations in Translation Model

2.7.1 Greenwich Hour Angle

The Greenwich hour angle is the angle between the Greenwich meridian and the TOD X axis. It is computed by the following:

$$\mathrm{GHA} = \mathrm{GHA}_0 + \Omega_{\mathrm{Earth}} t$$

where

GHA_0 Greenwich hour angle at beginning of simulation, determined by given date and GMT at start of simulation (ref. 3)

Ω_{Earth} Earth rotation rate, $4.178074216 \times 10^{-3}$ deg/sec

The modulo function is applied to the GHA so that it will remain in the interval (0°, 360°).

2.7.2 Axial-Thrust Misalignment Torque

This torque, which results from the thrust-vector offset from the CG, is computed in the translation model. However, because this torque affects the rotational behavior of the spacecraft, it is discussed in section 3.2.3.3.

TABLE 2.1—BASE VECTOR DEFINITIONS FOR PROPOSED COLD-SAT ATTITUDE OPTIONS

Attitude option	Base vector, $\vec{v}_1$	Base vector, $\vec{v}_2$	Description
1	$\vec{v}_{Sun}$	$\vec{v}_{ecl}$	First axis is in direction of Sun, and second is normal to ecliptic; spacecraft rotates once per year.
2	$\vec{v}_R$	$\vec{v}_N$	First axis points away from center of Earth along position vector, and second is normal to orbit plane; spacecraft rotates once per orbit.
3	$\vec{v}_v$	$\vec{v}_N$	Similar to (2), except that first axis points along velocity vector and second is normal to orbit plane; spacecraft rotates once per orbit.
4	$\vec{v}_N$ or $-\vec{v}_N$[a]	$\vec{v}_{sx}$	One axis points toward projection of Sun vector into orbit plane, and other is normal or negative-normal to orbit plane, in direction opposite the Sun, requiring a 180° rotation when Sun crosses orbit plane; spacecraft rotates once per year; and 180° rotation occurs several times per year for low-Earth orbit.
5	$\vec{v}_N$	$\vec{v}_{sx}$	Same as (4), except second axis is always positive-normal to orbit plane (i.e., no 180° rotation occurs); spacecraft rotates once per year.
6	$\vec{v}_v$	$\vec{v}_{sy}$	One spacecraft axis is in plane defined by Sun and velocity vectors; second axis is aligned with velocity vector.
7	$\vec{v}_R$	$\vec{v}_N$ or $-\vec{v}_N$[a]	One spacecraft axis is aligned with position vector; other axis is normal to orbit plane; spacecraft rotates one revolution per orbit. Includes 180° rotation when Sun crosses orbit plane.
8	$\vec{v}_v$	$\vec{v}_N$ or $-\vec{v}_N$[a]	One spacecraft axis is aligned with velocity vector; a second is aligned with orbit normal that is on same side of orbit plane as Sun. Includes 180° rotation when Sun crosses orbit plane.
9	$\vec{v}_{Sun}$	$\vec{v}_P$	One spacecraft axis is in orbit plane; other points directly at Sun.

[a]Transition from $+\vec{v}_N$ to $-\vec{v}_N$ occurs when the Sun crosses the spacecraft orbit plane. This maneuver is a spacecraft rotation about a given axis and is done to minimize solar panel pointing loss.

TABLE 2.2—180° SPACECRAFT ROTATION AXIS

Attitude option	Rotation axis vector (TOD coordinates)
4	$\vec{v}_{sx}$
7	$\vec{v}_R$
8	$\vec{v}_v$

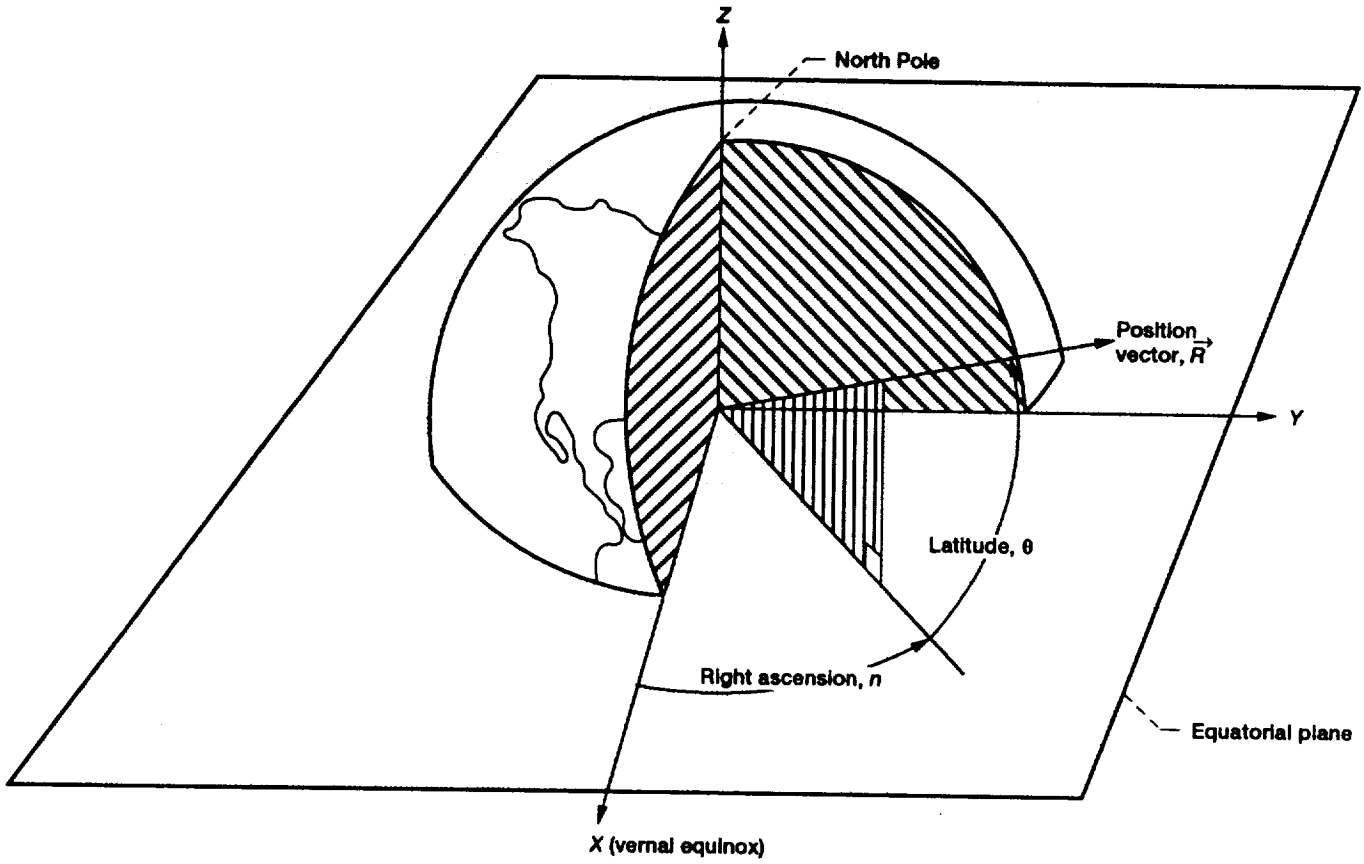

Figure 2.1.—Spherical TOD coordinate system used in gravity model.

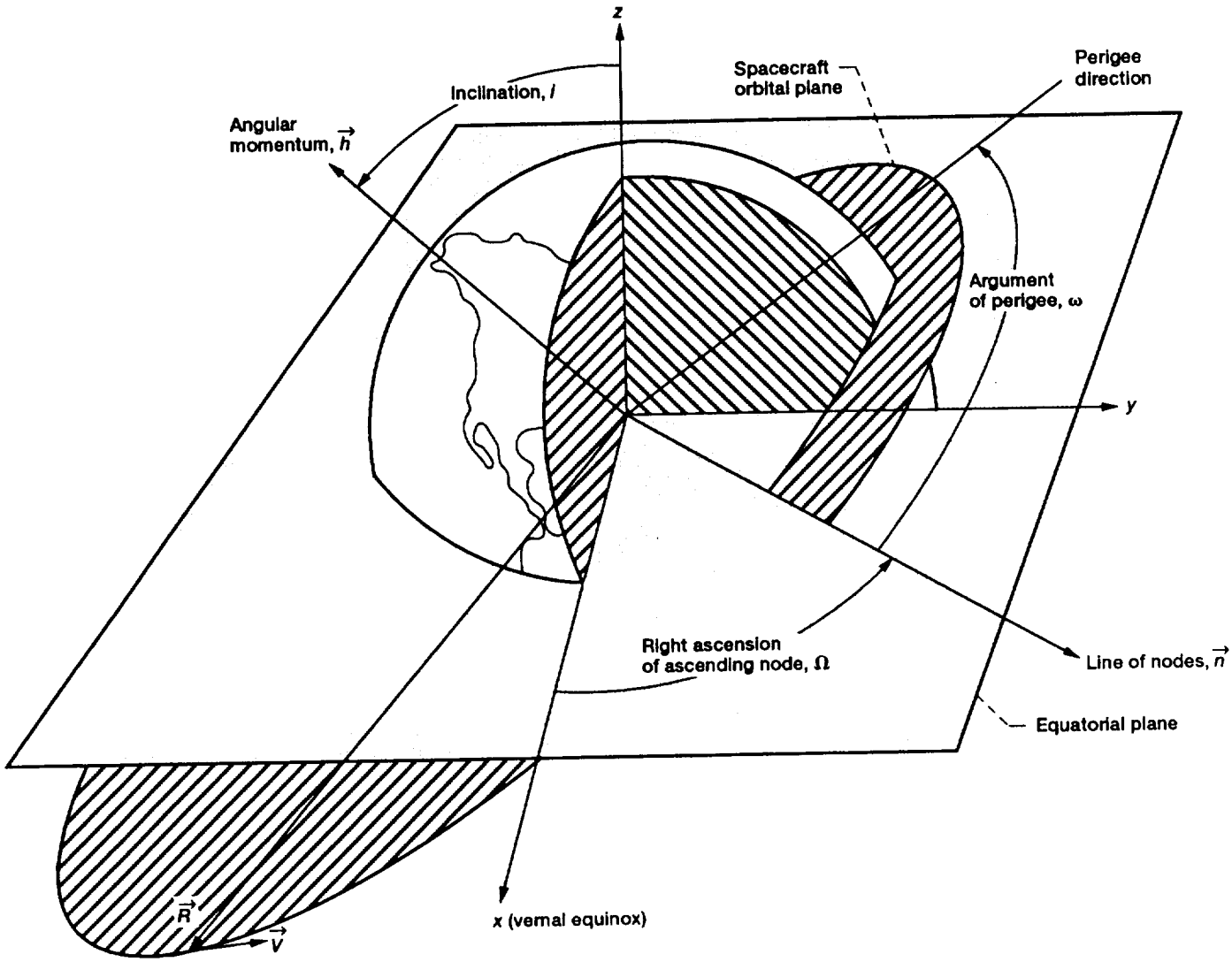

Figure 2.2.—Orbital elements.

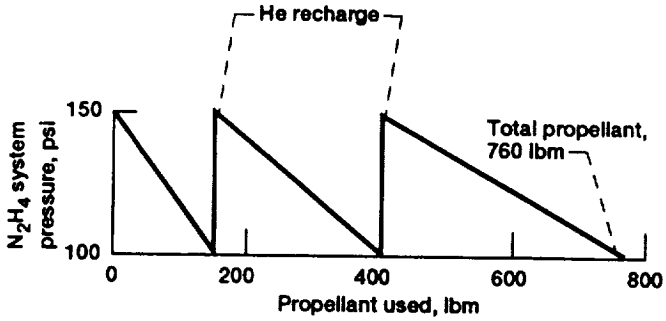

Figure 2.3.—Typical hydrazine pressure profile.

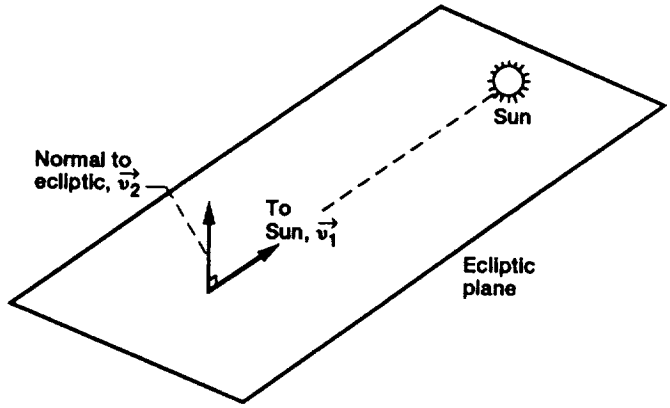

Figure 2.4.–Attitude option 1.

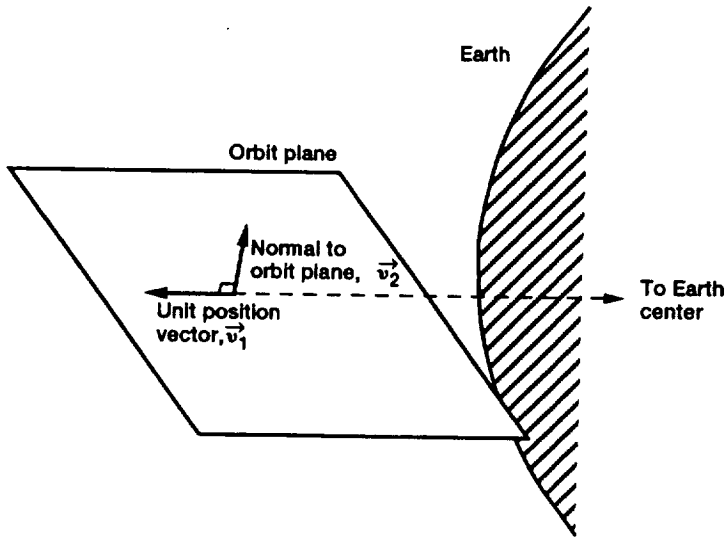

Figure 2.5.—Attitude option 2.

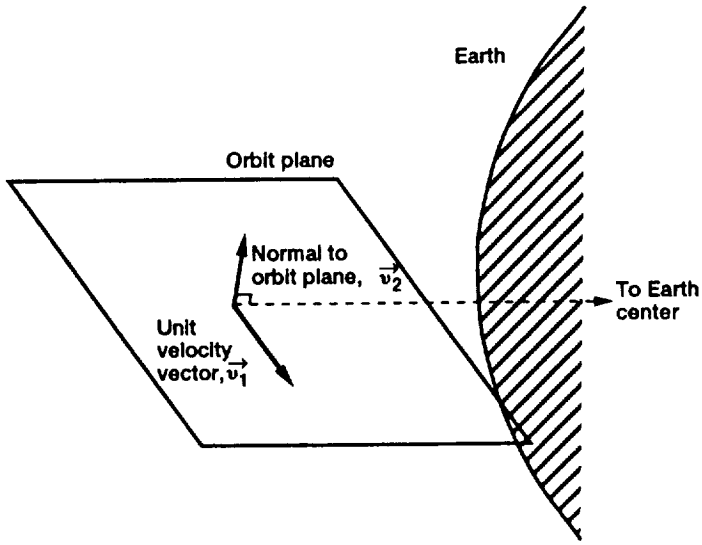

Figure 2.6.—Attitude option 3.

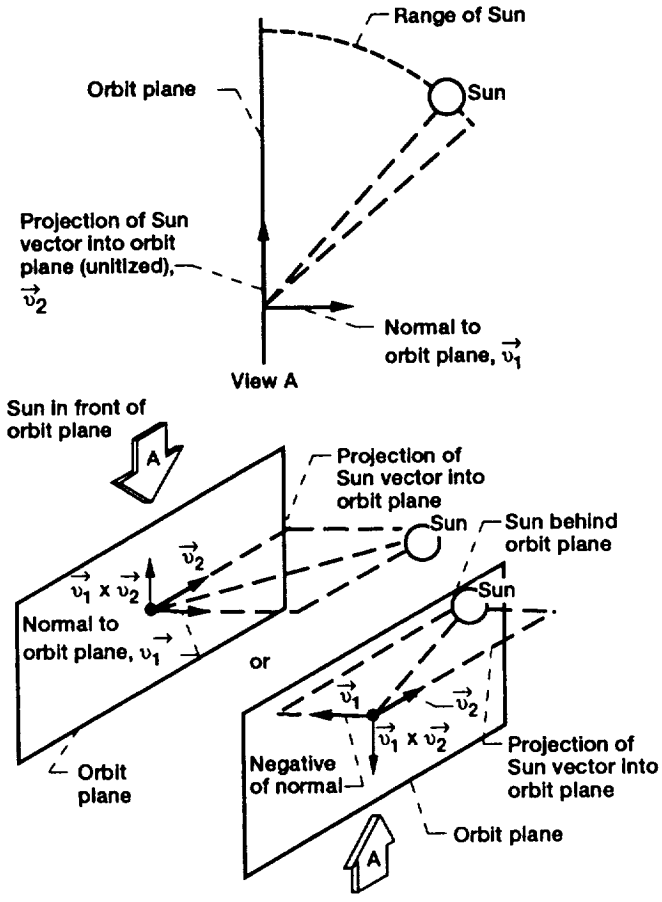

Figure 2.7.—Attitude option 4. (As Sun crosses the orbit plane, the spacecraft is rotated 180° about the spacecraft axis that is in the orbit plane and pointing in the direction of the Sun.)

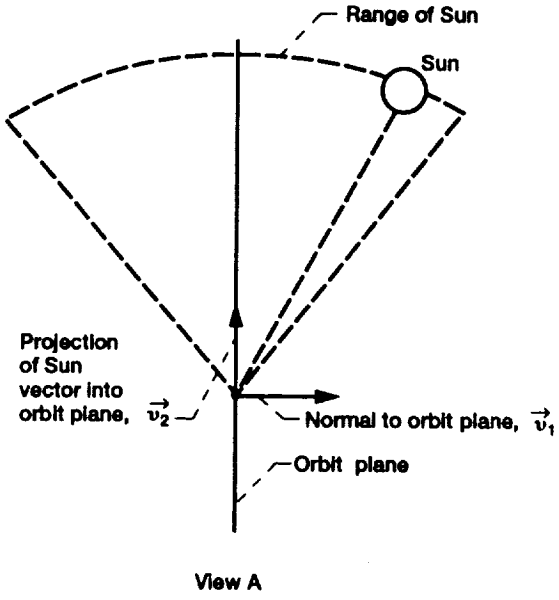

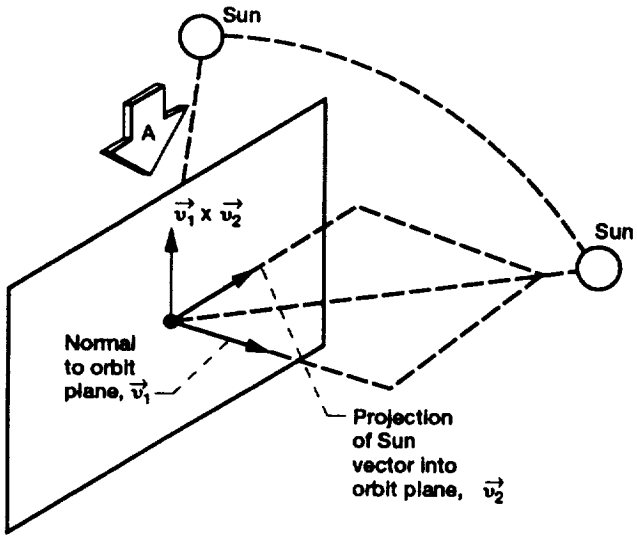

Figure 2.8.—Attitude option 5.

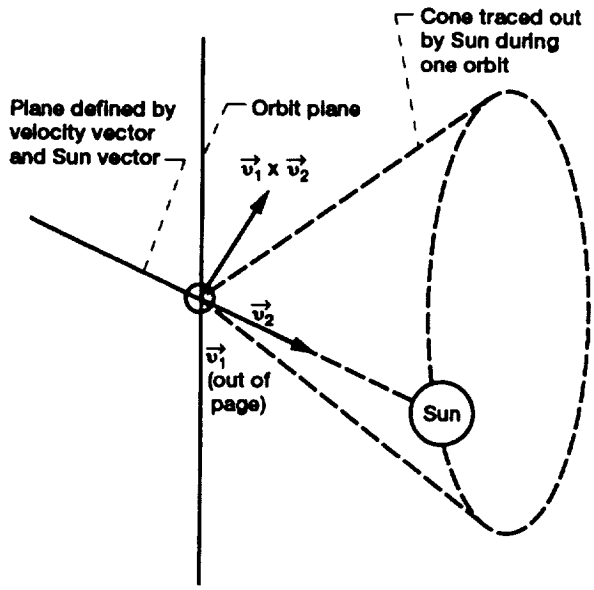

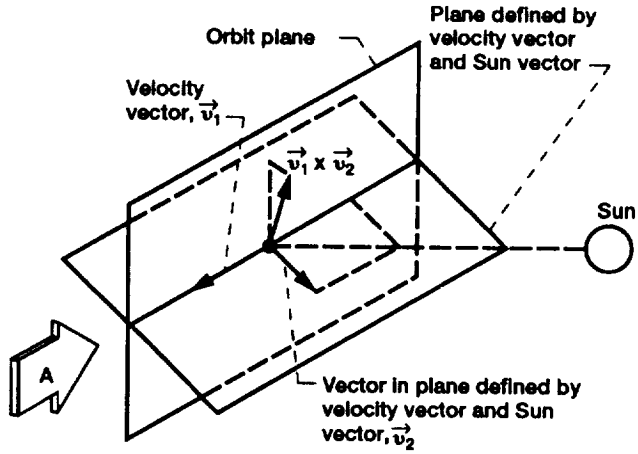

Figure 2.9.—Attitude option 6.

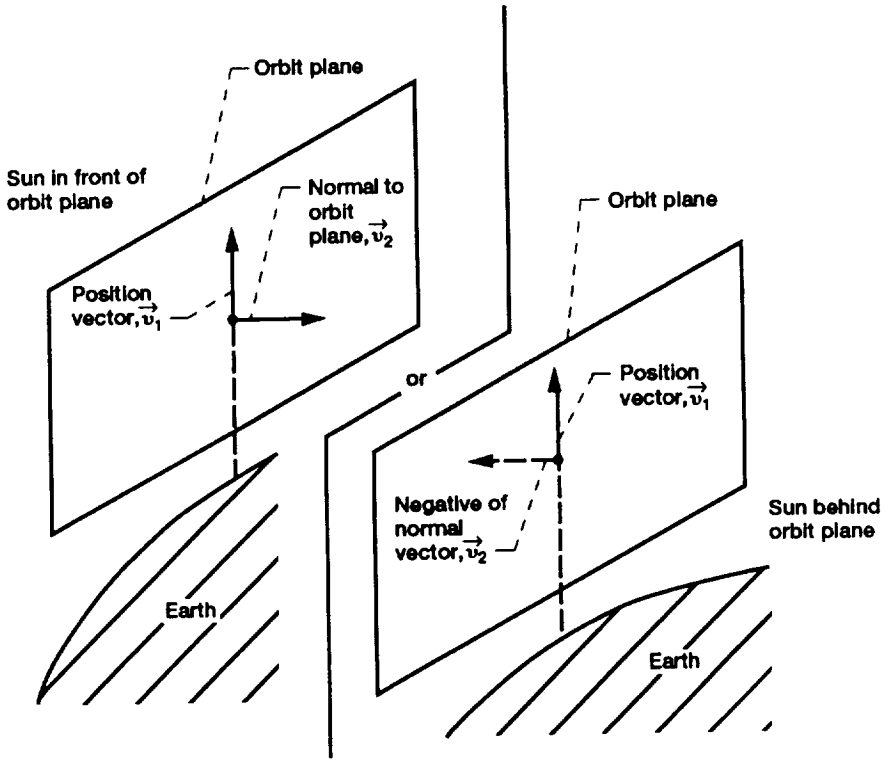

Figure 2.10.—Attitude option 7. (When the Sun crosses the orbit plane, the spacecraft rotates 180° about the velocity vector.)

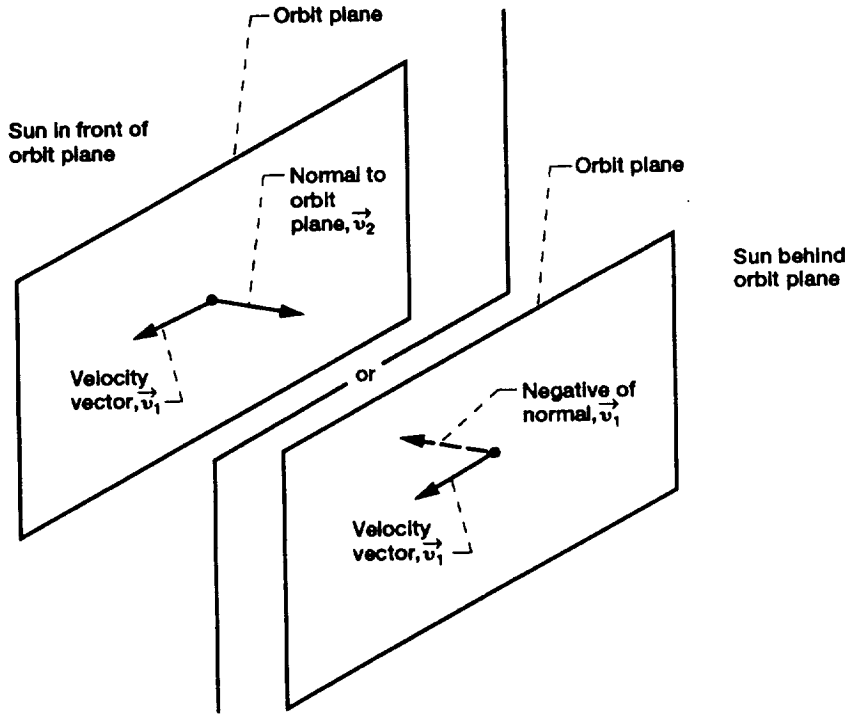

Figure 2.11.—Attitude option 8. (When the Sun crosses the orbit plane, the spacecraft rotates 180° about the velocity vector.)

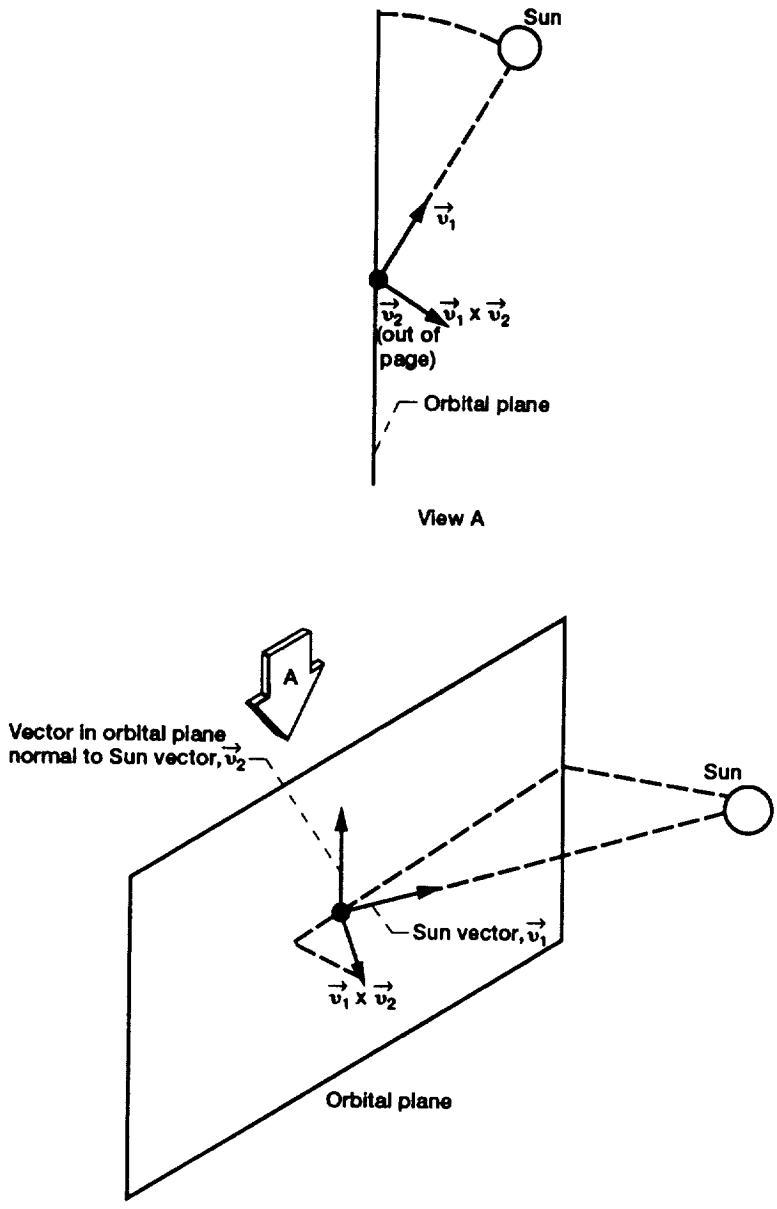

Figure 2.12.—Attitude option 9.

3.0 Rotation Model

The rotation model simulates the attitudinal motion of the spacecraft about its center of gravity. This motion is a consequence of various disturbance torques acting on the spacecraft as well as torques produced by the attitude control system to counteract the undesirable effects of these disturbance torques. The torques that act upon the spacecraft may be categorized into three groups:

(1) External disturbance torques, which include the gravity-gradient, magnetic, solar pressure, and aerodynamic drag torques. These torques are, in general, functions of spacecraft attitude, orbit position, velocity, and spacecraft geometry and mass properties.

(2) Self-induced disturbance torques, which are generated by the spacecraft itself. These torques include those produced by thruster misalignments and slosh. They are not directly functions of attitude, orbit position, or velocity but are related to spacecraft body rates, attitude error, and spacecraft design tolerances.

(3) Control torques, which are intentionally applied to the spacecraft under the command of the attitude control system. These torques are functions of attitude error and attitude rate. In practice many types of systems are used to affect attitude control; the COLD–SAT dynamic model includes

(a) Coupled and uncoupled RCS thrusters

(b) A gimballed thruster, which provides both axial thrust and attitude control about two spacecraft axes

(c) A reaction wheel, which is used to provide control about a single spacecraft axis

The sum of all torques acting on the spacecraft causes the spacecraft to experience angular acceleration, the integral of which is the angular (body) rate. The angular rate in turn produces changes in the spacecraft attitude. In the model the attitude is represented in quaternion form. This attitude quaternion is compared with the desired attitude quaternion computed by the translation model to arrive at the three-axis attitude error. The attitude error, along with the attitude rate, is used by the attitude control system algorithms to produce the appropriate control torques for stabilizing the spacecraft attitude.

This section describes in detail each of the following:

(1) Simulation of all torques included in the model except for the slosh torque. The slosh torque computation, because of its complexity, forms a separate part of the COLD–SAT dynamic model (the slosh model) and is discussed in section 4.0.

(2) Computation of the angular acceleration and the angular rates

(3) Computation of the actual spacecraft attitude quaternion

(4) Computation of the attitude error

(5) Description of the attitude control system algorithms

The rotation model also includes the computation of the microgravity accelerations at arbitrarily selectable points within the spacecraft. A detailed description of these calculations is deferred to section 5.0 of this report. A block diagram of the rotation model is shown in figure 1.3.

3.1 Interfaces of Rotation Model

Interfaces between the rotation model and the translation model were given in section 2.1. The interfaces between the rotation model and the slosh model, as well as input and output quantities of the rotation model, are given here. The following quantities are computed by the rotation model and passed to the slosh model:

(1) The actual spacecraft attitude quaternion

(2) The spacecraft attitude-rate vector

The slosh torque is computed by the slosh model and passed to the rotation model to compute the total disturbance torque.

The following inputs to the rotation model are user specified at the start of the simulation:

(1) Spacecraft rotational mass properties, which include moments and products of inertia

(2) Spacecraft magnetic dipole moment, which is used in computing magnetic torque

(3) Solar and geomagnetic parameters, which are used in computing atmospheric density and hence atmospheric drag torque

(4) Number, location, and thrust of RCS thrusters

(5) Reaction wheel moment of inertia

(6) Initial attitude rates

In addition, numerous program flag variables can be set to disable portions of the model, including attitude control system devices not desired to be simulated. Rotation model outputs typically plotted include, but are by no means limited to, attitude errors and rates, microgravity accelerations, gimbal angles, and total disturbance torques.

3.2 Simulation of Torques Acting on Spacecraft

3.2.1 External Disturbance Torques

3.2.1.1 Gravity-gradient torque model.—Gravitational and centripetal forces, which maintain the spacecraft in its orbit, are equal and opposite only at the spacecraft CG point. At all other points on the spacecraft body there is a slight imbalance between these two forces, which results in a net torque on the spacecraft. This torque is called the gravity-gradient torque and is a function of the orbit altitude as well as the rotational mass properties of the spacecraft.

Gravity-gradient torque in the COLD–SAT dynamic model is computed by using a spherical Earth gravity model as follows:

$$\vec{\tau}_{GG} = \frac{3\mu}{R^5}\left(R_{S/C} \times \mathbf{I}_{MP}\vec{R}_{S/C}\right)$$

where

$\vec{\tau}_{GG}$ gravity-gradient torque acting on spacecraft, ft-lbf

$\mathbf{I}_{MP}$ spacecraft rotational mass-properties matrix (refer to section 3.3.1), ft-lbf-sec^2

μ_{Earth} Earth gravitational constant, 1.4076469×10^{16} ft^3/sec^2

R magnitude of spacecraft position vector, ft

$\vec{R}_{S/C}$ spacecraft position vector transformed into spacecraft body coordinates, ft, which are transformed from TOD coordinates as follows:

$$\begin{bmatrix} 0 \\ \vec{R}_{S/C} \end{bmatrix} = (\bar{q}^{\,c}) * \begin{bmatrix} 0 \\ \vec{R} \end{bmatrix} * \bar{q}$$

A typical plot of gravity gradient torque versus time for the COLD–SAT spacecraft over approximately one orbit, showing x, y, and z components, is given in figure 3.1. The gravity-gradient torque can be seen to exist predominantly about the z axis for this attitude and is of sinusoidal form with a period of one-half the orbit period. This plot, as well as all others to follow, are for zero axial thrust and without the reaction wheel active (because in the final COLD–SAT design the reaction wheel was eliminated). All simulation results in this document are from the same simulation run to allow direct comparison between different plots. The attitude option is that selected for the final design.

3.2.1.2 Magnetic torque.—The spacecraft is assumed to have a net magnetic dipole moment $\vec{M}_{S/C}$ (in ampere-square meters) that is randomly aligned with respect to the spacecraft coordinate axes. The interaction of this magnetic dipole moment with the Earth's magnetic field produces a torque on the spacecraft, which is given as follows:

$$\vec{\tau}_{mag} = (0.73717)\left[\vec{M}_{S/C} \times (\vec{B}_{Earth})_{S/C}\right]$$

where $(\vec{B}_{Earth})_{S/C}$ is the Earth's magnetic flux density vector (in tesla) transformed into spacecraft coordinates. The conversion factor of 0.73717 is required to convert the computed torque (in newton-meters) to English units (foot-pounds-force). COLD–SAT is assumed to be a class 3 spacecraft, with a residual magnetic dipole moment of 30 A-m^2.

In order to compute $\vec{B}_{Earth}$, it is necessary to have a reasonably accurate model of the Earth's magnetic field. In the COLD–SAT dynamic model the Earth's magnetic field is modeled as a tilted dipole with strength $M_{Earth} = 8.1\times10^{22}$ A-m^2. The flux density produced by this dipole $(\vec{B}_{Earth})_M$, in spherical magnetic coordinates, is given by the following expression:

$$(\vec{B}_{\text{Earth}})_M = \begin{bmatrix} B_R \\ B_{\phi_M} \end{bmatrix} = \frac{\mu_0}{4\pi} \frac{M_{\text{Earth}}}{R^3} \begin{bmatrix} 2 \sin \phi_M \\ -\cos \phi_M \end{bmatrix}$$

where

μ_0 permeability constant, $4\pi \times 10^{-7}$ H/m

R magnitude of spacecraft position vector, m

ϕ_M spacecraft magnetic latitude measured from the Earth's magnetic equator, which is computed as

$$\phi_M = \tan^{-1}\left[\frac{R_M}{\sqrt{\left(R_x^2\right)_M + \left(R_y^2\right)_M}}\right]$$

where

$$\vec{R}_M = [\text{TOD} \rightarrow M]\vec{R}$$

and $\vec{R}_M$ is the spacecraft position vector expressed in Earth-centered magnetic coordinates (refer to appendix C). The matrix [TOD → M] is the transformation from TOD to magnetic coordinates and is derived in appendix C.

The vector $(\vec{B}_{\text{Earth}})_M$, as computed previously, is in spherical magnetic coordinates with the R component directed away from the center of the Earth and the positive ϕ_M component directed perpendicular to $\vec{R}$ and toward magnetic north. This vector is converted into the rectangular magnetic coordinates as follows:

$$(\vec{B}_{\text{Earth}})_M = \begin{bmatrix} B_x \\ B_y \\ B_z \end{bmatrix}_{(\text{Earth})_M} = \begin{bmatrix} \cos \theta_M \cos \phi_M & -\cos \theta_M \sin \phi_M \\ \sin \theta_M \cos \phi_M & -\sin \theta_M \sin \phi_M \\ \sin \phi_M & \cos \phi_M \end{bmatrix} \begin{bmatrix} B_R \\ B_{\phi_M} \end{bmatrix}$$

where θ_M is the spacecraft magnetic longitude, which is computed as

$$\theta_M = \tan^{-1}\left[\frac{(R_y)_M}{(R_x)_M}\right]$$

The vector $\vec{B}_{\text{Earth}}$ is now transformed to TOD coordinates:

$$(\vec{B}_{\text{Earth}})_{\text{TOD}} = [TOD \rightarrow M]^T(\vec{B}_{\text{Earth}})_M$$

Finally, the flux density is transformed into spacecraft coordinates by using the usual quaternion transformation as follows:

$$\begin{bmatrix} 0 \\ \hline (\vec{B}_{\text{Earth}})_{\text{S/C}} \end{bmatrix} = (\bar{q}^{\,c})^* \begin{bmatrix} 0 \\ \hline (\vec{B}_{\text{Earth}})_{\text{TOD}} \end{bmatrix} * \bar{q}$$

where $\bar{q}$ is the spacecraft attitude quaternion.

A typical plot of magnetic torque versus time for the COLD–SAT spacecraft over approximately one orbit, showing x, y, and z components, is given in figure 3.2. There is no magnetic torque about the x axis because the spacecraft magnetic dipole moment chosen was aligned with the spacecraft x axis.

3.2.1.3 Aerodynamic drag torque.—Aerodynamic drag torque is produced by the effect of unbalanced (with respect to the CG) drag forces acting on the spacecraft (refer to section 2.3.2 for computation of the aerodynamic drag force). The following quantities are the coordinates of the centroid of the projected spacecraft area along each principal coordinate axis:

x_z, y_z x and y coordinates, respectively, of centroid of projected area normal to spacecraft z axis

y_x, z_x y and z coordinates, respectively, of centroid of projected area normal to spacecraft x axis

x_y, z_y x and z coordinates, respectively, of centroid of projected area normal to spacecraft y axis

The aerodynamic torque can then be computed as follows:

$$\vec{\tau}_{\text{drag}} = \begin{bmatrix} \tau_x \\ \tau_y \\ \tau_z \end{bmatrix}_{\text{drag}} = \begin{bmatrix} z_y(F_{\text{drag}})_y - y_z(F_{\text{drag}})_z \\ x_z(F_{\text{drag}})_z - z_x(F_{\text{drag}})_x \\ y_x(F_{\text{drag}})_x - x_y(F_{\text{drag}})_y \end{bmatrix}$$

where $\vec{F}_{\text{drag}}$, the aerodynamic drag force, was computed in section 2.3.2.

A typical plot of aerodynamic drag versus time for the COLD–SAT spacecraft over approximately one orbit, showing x, y, and z components, is given in figure 3.3. The apparent ripple in the curves results from the fact that the atmospheric density is computed at approximately 1-min intervals to reduce execution time. This computation involves iterative routines, and if computed continuously, would consume excessive central processing unit (CPU) time. Furthermore, this torque is very small

relative to the dominant gravity-gradient torque so that highly accurate computation is not required. There is no drag torque about the x axis because the spacecraft as modeled is completely symmetrical with respect to the x axis. (CG shift from the nominal CG location is neglected for this computation.)

3.2.1.4 Solar pressure torque model.—The Sun shining on a surface is equivalent to the surface being bombarded by photons; it produces a pressure on the surface. Because, in general, the surface area of the COLD–SAT spacecraft upon which the Sun is shining is not symmetrical with respect to the CG, this solar radiation pressure will produce a disturbance torque on the spacecraft.

Highly accurate modeling of the solar pressure torque produced on a spacecraft requires a finite-element approach, which is very costly in terms of CPU time. For the purposes of the COLD–SAT spacecraft, a much simpler, less accurate approach will suffice, because the solar pressure torque is very small relative to the dominant gravity-gradient torque.

The solar pressure torque modeling approach chosen for the COLD–SAT dynamic model will produce correct results only for the attitude option and axis alignment chosen for the COLD–SAT design, which is attitude option 4 with the spacecraft z axis aligned with $\vec{v}_1$, the orbit plane normal, and the $-x$ axis aligned with $\vec{v}_2$, in the orbit plane pointed toward the Sun (refer to section 2.6).

If the COLD–SAT spacecraft is considered to consist of a cylinder and a truncated cone, as shown in figure 3.4, with the CG located at the center of the cylinder, it is apparent that the net torque produced by sunlight striking the cylinder and the solar panels (which are perpendicular to the page in figure 3.4) will be zero, because both are completely symmetrical with respect to the CG. Solar pressure torque will be produced only when sunlight strikes the conical portion of the spacecraft. Since the Sun always lies in the x–z plane and the angle β varies between 0° and 41°, the solar pressure torque will be zero when the angle β is less than 15° because the conical portion of the spacecraft will be in shadow. If β is greater than 15°, sunlight will strike the conical portion of the spacecraft and a negative solar pressure torque will be produced about the spacecraft y axis.

The value of this torque is computed as follows: As given in reference 5 the solar pressure force produced by sunlight striking an object of small surface area dA is given by

$$dF_{solar} = -P_{solar}(1 + \rho)(\vec{v}_{Sun} \cdot \vec{v}_n)^2 \vec{v}_n \, dA$$

where

P_{solar} solar constant, 9.4×10^{-8} lbf/ft^2 at 1 AU

ρ surface reflectivity ($\rho = 1$ for highly reflective surface, $\rho = 0$ for black surface)

$\vec{v}_{Sun}$ unit Sun vector

$\vec{v}_n$ unit vector normal to area dA

The planar projection of the conical area of the spacecraft in any direction normal to the surface is 75.44 ft^2 as shown in figure 3.4. The torque moment arm (the distance between the centroid of the projected conical area and the spacecraft CG) ℓ is 11.3 ft as determined from figure 3.4. Assuming a worst-case reflectivity of 1 and realizing that $\vec{v}_{Sun} \cdot \vec{v}_n = \cos\theta = \sin(\beta - 15°)$, the solar pressure torque can be computed by the following equation:

$$\vec{\tau}_{solar} = -\vec{v}_y K_{solar} S_v \sin^2(\beta - 15°) \qquad \text{for } \beta \geq 15°$$

$$\vec{\tau}_{solar} = \vec{0} \qquad \text{for } \beta < 15°$$

where

K_{solar} solar torque constant, $P_{solar}(1 + \rho)A\ell$, 1.6×10^{-4} ft-lbf for COLD–SAT spacecraft

S_v solar visibility flag, 1 for visible Sun and 0 for eclipse

β solar beta angle, $\cos^{-1}\left[(-\vec{v}_{Sun})_{S/C} \cdot \vec{v}_x\right]$, deg or rad

$\vec{v}_x$ unit vector in direction of spacecraft x axis

$\vec{v}_y$ unit vector in direction of spacecraft y axis

$(\vec{v}_{Sun})_{S/C}$ unit Sun vector, transformed into spacecraft coordinates

It should be emphasized that this solar pressure model is highly specific to COLD–SAT and is generally not applicable to other spacecraft. Furthermore, it is only valid for small attitude errors.

Figure 3.5 is a typical plot of solar pressure torque versus time for the COLD–SAT spacecraft over approximately one orbit, showing x, y, and z components. As previously discussed, this torque is modeled about the y axis only. In the regions designated A on the plot, the Sun is visible and thus the solar pressure torque is nonzero; in region B the Sun is blocked by the Earth and the solar pressure torque is zero.

In order to accurately compute solar pressure torque, it is necessary to determine when the Sun is blocked by the Earth. The solar blockage routine in the COLD–SAT dynamic model determines whether the spacecraft is in sunlight, penumbra, or umbra and sets the value of the solar visibility flag S_v to 1, 1/2, or 0, respectively. Figure 3.6 represents the plane that contains the Sun, the Earth, and the spacecraft, showing the umbra and the penumbra. If an angle θ_{range} is defined as the angle measured from the subsolar point (i.e., the point of intersection between the Earth-center-to-Sun-center line and the spacecraft orbit) to the spacecraft position vector, whether the spacecraft is in umbra, penumbra, or sunlight can be determined by the following:

$$S_v = 1 \qquad \text{for } \theta_{range} < \theta_P \qquad \text{(sunlight)}$$

$$S_v = \frac{1}{2} \qquad \text{for } \theta_P \leq \theta_{range} < \theta_U \qquad \text{(penumbra)}$$

$$S_v = 0 \qquad \text{for } \theta_{range} > \theta_U \qquad \text{(umbra)}$$

Because the umbra and the penumbra are symmetrical with respect to the Earth-center-to-Sun-center line, all angles measured from the subsolar point can be considered to be in the first or second quadrant only (i.e., $0° \leq \theta \leq 180°$). Thus, angles measured from either side of the subsolar point are considered to be positive. The angle θ_{range} is computed by

$$\theta_{range} = \cos^{-1}\left(\vec{\upsilon}_R \cdot \vec{\upsilon}_{Sun}\right)$$

where $\vec{\upsilon}_R$ and $\vec{\upsilon}_{Sun}$ are unit vectors as defined in section 2.6.3. The angles θ_P and θ_U are measured from the subsolar point to the points where the penumbra and umbra each intersect the spacecraft orbit, respectively. They are computed as follows:

$$\theta_U = 90° + \theta_{esdu} + \theta_{ar} + \theta_{alt}$$

where θ_{esdu} is the correction for the difference between the Earth's radius and the Sun's radius for the umbra and is computed as follows:

$$\theta_{esdu} = \tan^{-1}\left(\frac{R_{Sun} - R_{Earth}}{D_{Earth\text{-}Sun}}\right) = 0.26412°$$

and

R_{Sun} solar radius, 2.28346×10^9 ft

R_{Earth} Earth equatorial radius, 20 925 656 ft

$D_{Earth\text{-}Sun}$ Earth-Sun distance, 1 AU or 4.908066×10^{11} ft

The correction for atmospheric refraction, θ_{ar} (in degrees), is given as follows:

$$\theta_{ar} = 1.133 - 0.566e^{-0.17x_{alt}}$$

where x_{alt} is the spacecraft altitude in nautical miles. This term is essentially constant at 1.133 for altitudes above 100 nautical miles. The altitude correction θ_{alt} is computed as follows:

$$\theta_{alt} = \cos^{-1}\left(\frac{R_{Earth}}{|\vec{R}|}\right)$$

For the penumbra,

$$\theta_P = 90° - \theta_{esdp} + \theta_{ar} + \theta_{alt}$$

where θ_{esdp} is the Earth and Sun radii correction term for the penumbra, given as

$$\theta_{esdp} = \tan^{-1}\left(\frac{R_{Sun} + R_{Earth}}{D_{Earth\text{-}Sun}}\right) = 0.26901°$$

and θ_{ar} and θ_{alt} are the same as for the umbra.

3.2.2 Slosh Torque

The torque acting on the spacecraft is computed by the slosh model, which is discussed in detail in section 4.0.

3.2.3 Thruster-Generated Torques

3.2.3.1 General.—Any thruster produces a translational force on the spacecraft in the direction of the thrust vector. If the thrust vector does not pass through the spacecraft CG, it will also produce a torque. A spacecraft thruster is classified as an RCS thruster if its purpose is to produce a control torque on the spacecraft; as a fixed axial thruster if its purpose is to produce a translational force on the spacecraft; or as a gimballed axial thruster if its purpose is to produce both a translational force and a control torque. However, because of thruster misalignments and spacecraft CG shifts, in general all of these classes of thrusters will produce both rotational torques and translational forces, and the undesired force or torque will constitute an additional disturbance on the spacecraft translational or rotational dynamics. All three of these thruster classes are present on the COLD–SAT spacecraft and are discussed in detail in subsequent sections.

The purpose of the RCS is to provide control torques on the spacecraft in order to maintain the desired spacecraft attitude. The primary advantages of an RCS over other attitude control schemes are relatively low cost, less complexity, high reliability, and ability to control both cyclical and secular disturbances for axial-thrust and no-axial-thrust conditions. The principal disadvantage of such a system is that the discontinuous nature of this type of control degrades the experimental microgravity environment (see section 5.0). An RCS can be classified as a coupled or uncoupled scheme, depending on whether or not the torques produced are pure couples. An uncoupled RCS scheme, which is discussed in detail in section 3.2.3.2, will always produce a translational force on the spacecraft regardless of whether thruster misalignments are present. This translational force will result in additional microgravity disturbances and will, over time, affect the spacecraft orbit. However, this uncoupled RCS scheme is advantageous from a cost or complexity point of view, and despite its disadvantages, was chosen as the baseline RCS for COLD–SAT. From a simulation point of view, however, the two types of systems are the same, except that the thrust produced by certain thrusters is set to zero when simulating the uncoupled system.

A fixed axial thruster is designed to produce a translational force on the spacecraft for the purpose of inducing a controlled microgravity acceleration inside the experiment tanks. However, because of CG shift and thruster misalignments, a torque will also be produced as previously discussed. This torque constitutes a disturbance that must be counteracted by the attitude control system.

A gimballed axial thruster is a single low-thrust device attached to a bi-axial gimbal mechanism. This device serves two purposes: First, it augments the thrust produced by the fixed thrusters in order to maintain the desired acceleration of the spacecraft; and second, it constitutes part of the attitude control system because the orientation of the thrust vector produced by this thruster with respect to the CG can be controlled, thus providing a control torque on the spacecraft.

The torque produced by any thruster $\vec{\tau}$ can be computed by the simple crossproduct rule:

$$\vec{\tau} = \vec{r} \times \vec{F}$$

where

$\vec{F}$ thrust vector produced by thruster

$\vec{r}$ vector from location of thruster (i.e., point of application of thrust vector to spacecraft rigid body) to spacecraft CG

For each thruster the values of $\vec{r}$ and $\vec{F}$ are given in tabular form as part of the user-supplied model input data. The preceding equation is used to compute the torque for each thruster that is turned on. The torques from each individual thruster are added to obtain the total thruster-produced torque acting on the spacecraft.

3.2.3.2 RCS thruster torques.—The COLD–SAT dynamic model can model any desired number of RCS thrusters, whose steady-state thrust level, orientation, and location with respect to the CG can be specified by the user. For COLD–SAT two different RCS schemes were considered:

(1) A coupled RCS system, which utilizes twelve 0.06-lbf thrusters located as shown in figure 3.7. The thrusters are always fired in pairs so that the resulting torques are always pure couples (i.e., there is no translational force acting on the spacecraft when a thruster is fired).

(2) An uncoupled RCS system, which utilizes the same eight rear thrusters; however, the four front thrusters (2, 4, 6, and 8) are eliminated. This scheme results in considerable cost savings, because the four front thrusters and the associated hydrazine lines and line heaters running from the tanks in the rear of the spacecraft are eliminated. However, the torques produced about the y and z spacecraft axes are no longer couples (i.e., there is a translational force produced in the $+x$ direction whenever a y axis or z axis RCS thruster is fired). Also less control torque is available about the y and z axes because only a single thruster is fired instead of the two thrusters fired with the coupled scheme. Note that the torques produced about the x axis are still pure couples.

In addition, it was assumed that all RCS thrusters are misaligned with respect to the spacecraft coordinate axes by 1°, so that when a control torque is required about a given axis and the appropriate thruster (or thrusters) is fired, disturbance torques will be produced about the other two spacecraft axes as well. These misalignments are included in the COLD–SAT dynamic model and are chosen such that the resulting disturbance torques are maximized. The following data are entered to simulate any RCS system in the COLD–SAT dynamic model:

(1) The number of RCS thrusters

(2) A table of the steady-state thrust vector produced by each thruster, including any misalignments

(3) A table of the coordinates of each thruster in the x',y',z' system (see section 2.0). The distance of the CG from the plane containing the back thrusters is entered into the axial thrust model. CG shift from nominal along the y and z axes is neglected in RCS torque calculations.

For COLD–SAT the number of thrusters is set to 12 for either the coupled or uncoupled scheme. The thrust vectors produced by each thruster are as given in table 3.1. In order to simulate the uncoupled scheme, the thrust vectors produced by thrusters 2, 4, 6, and 8 are set to zero.

The coordinates of each thruster in the x',y',z' system are specified by the user. The coordinates of the thrusters relative to the spacecraft CG can then be readily computed by specifying the spacecraft

CG location relative to the origin of the x',y',z' system. These torques are computed only once at the beginning of the simulation, in order to reduce CPU time; therefore, subsequent movement of the CG will not be accounted for in the RCS simulation. However, this is not a serious model limitation because simulation of the full-up model rarely, if ever, is run for more than a few hours, over which time the CG can be expected to move very little. Because the y and z CG offsets, $(y - y')$ and $(z - z')$, are very small, these offsets are ignored in computing RCS torques. These thruster locations (table 3.2) assume that the front thruster ring is 286.91 inches from the back ring and that the thruster ring radii are 48 inches for the back thruster ring and 20 inches for the front thruster ring.

From these coordinates a vector $(\vec{r}_{RCS})_i$ is formed from the thruster to the CG for each thruster as follows:

$$(\vec{r}_{RCS})_i = \begin{bmatrix} -(x'_{RCS})_i - (x'_{CG})_i \\ -(y'_{RCS})_i \\ -(z'_{RCS})_i \end{bmatrix}$$

where

$(x'_{RCS})_i$, $(y'_{RCS})_i$, $(z'_{RCS})_i$ — coordinates of ith RCS thruster in spacecraft x', y', z' system as given in table 3.2

x'_{CG} — spacecraft CG x coordinate in x', y', z' spacecraft coordinate system (i.e., distance of CG from rear thruster ring)

Recall that y'_{CG} and z'_{CG} are assumed to be zero and thus are not included in the computation of $(\vec{R}_{RCS})_i$.

Next, the torque produced by each thruster is found by

$$(\vec{\tau}_{RCS})_i = (S_{trans})_i\left[(\vec{r}_{RCS})_i \times (\vec{F}_{RCS})_i\right] \qquad \text{for } i = 1,12$$

where

$(S_{trans})_i$ — factor between 0 and 1 representing startup and shutdown transient of thruster i as discussed in section 3.2.3.2

$(\vec{F}_{RCS})_i$ — thrust vector produced by ith RCS thruster, as given in table 3.1

On the basis of the thruster locations and thrust vectors given for COLD–SAT, the resulting torque and translational force produced by each thruster are computed in the model. The information given in tables 3.3 and 3.4 is presented for informational purposes and illustrates the torques and translational forces for a typical simulation run, for thrusters that are perfectly aligned with the spacecraft primary axes (table 3.3) and for thrusters with selected 1° misalignments (table 3.4). The direction of each thruster misalignment is chosen so that the resulting disturbance torques are

maximized. For both tables x'_{CG} is assumed to be 85.5 inches. Thrusters are always fired in pairs (1&2, 3&4, 5&6, 7&8, 9&10, 11&12) as discussed in later sections.

The design of RCS thrusters is such that when a thruster is fired, it will remain "on" for a predetermined minimum amount of time, designated $t_{\min\ on}$. This is done in order to increase the efficiency of the RCS. Furthermore, each thruster exhibits startup and shutdown transients, denoted t_{su} and t_{sd}, respectively. In reality, the startup transient is a second-order underdamped step response and the shutdown transient is a decaying exponential, but in order to reduce unnecessary overhead, it is reasonable to model these transients linearly as shown in figure 3.8. These transients are modeled by multiplying the steady-state RCS torque for thruster i, as computed previously in this section by a factor $(S_{trans})_i$ of 0 to 1. If thruster i is in a full-on or full-off state, then $S_{(trans)_i} = 1$ or $S_{(trans)_i} = 0$, respectively; if thruster i is in a startup or shutdown transient, then $0 < S_{(trans)_i} < 1$.

3.2.3.3 Axial-thruster-induced torque.—The axial thrust vector $\vec{F}_T$ discussed in section 2.3.3 is the vector sum of the thrust vectors that are produced by the fixed and gimballed thrusters, $\vec{F}_{TF}$ and $\vec{F}_{TG}$, respectively. If this thrust vector does not pass directly through the CG, a torque on the spacecraft will be produced. This torque comprises both a disturbance torque and a control torque. If the gimballed thruster were not present, or if the gimbal mechanism were to fail, the resultant thrust vector would not, in general, pass through the CG, and thus a disturbance torque would result whenever the axial thrusters were fired. With the gimballed thruster in operation, however, the direction of the gimballed-thruster thrust vector can be used to provide an attitude control torque of sufficient magnitude to counteract all expected disturbance torques, including that produced by the thrust-vector–CG offset of the fixed thrusters. This attitude control scheme will eliminate virtually all RCS thruster firings during periods of axial thrust and result in an excellent experimental microgravity environment.

The torque produced by the axial thrusters (fixed and gimballed) is given as

$$\vec{\tau}_T = \vec{r} \times \vec{F}_T$$

where

$\vec{F}_T$ thrust vector computed in section 2.3.3

$\vec{r}$ vector from origin of x'_{SC}, y'_{SC}, z'_{SC} coordinate system to CG

The total thrust vector resulting from fixed and gimballed thrusters is assumed to pass through the origin of the $x'_{S/C}$, $y'_{S/C}$, $z'_{S/C}$ coordinate system. It is defined as follows:

$$\vec{r} = \begin{bmatrix} x'_{CG} \\ y'_{CG} \\ z'_{CG} \end{bmatrix}$$

where x'_{CG}, y'_{CG}, and z'_{CG} are the coordinates of the spacecraft CG.

The gimballed thruster is assumed to be driven by a stepper motor, which is modeled as a second-order system (with quantized input) as follows:

$$M(s) = \frac{\omega_n^2}{S^2 + 2\zeta\omega_n s + \omega_n^2}$$

It is assumed that $\zeta = 0.7071$ and $\omega_n = 0.00584$, which results in 5-percent overshoot and a time to first peak (for a step command) of about 12.6 min. The input of $M(s)$ is quantized with a step size of 0.07815 deg/step.

3.2.4 Reaction Wheel Torque

A single-axis reaction wheel has been considered for COLD–SAT in order to improve the microgravity environment during periods of zero axial thrust. The dominant disturbance torque encountered under these conditions is the gravity-gradient torque. This torque appears predominantly about the spacecraft z axis and is cyclical. Thus, a single, modestly sized reaction wheel would be able to remove this disturbance torque over long periods of time without saturating and would eliminate the need for nearly all RCS firings during periods of zero axial thrust. A block diagram of the reaction wheel model in rotational dynamics is shown as part of figure 1.3.

The single-axis reaction wheel in the model includes static and viscous friction. Viscous friction is computed as follows:

$$\tau_{fv} = F_v \omega_{rw}$$

where

F_v viscous friction coefficient

ω_{rw} reaction wheel angular speed, rad/sec

The torque developed by the motor is given as

$$\tau_{dev} = K_m V_A$$

where

K_m DC motor torque constant, ft-lbf/V

V_A DC voltage applied to motor, V

Thus, the total torque is

$$\tau_{total} = \tau_{dev} - \tau_{fv}$$

A switch state S_{cf} is used to indicate if the wheel is stuck because of static friction. If S_{cf} is positive, the wheel is spinning in a positive direction; if S_{cf} is zero, the wheel is not moving; and if S_{cf} is negative, the wheel is spinning in a negative direction. The value of S_{cf} is determined as follows:

$$S_{cf}(t^+) = +1 \quad \text{for } (S_{cf} = 0) \text{ and } (\tau_{dev} > \tau_c) \text{ or } (S_{cf} = +1) \text{ and } (\omega_{rw} > \text{TOL})$$

$$S_{cf}(t^+) = 0 \quad \text{for } (S_{cf} = 0) \text{ and } (|\tau_{dev}| < \tau_c) \text{ or } (S_{cf} \neq 0) \text{ and } (|\omega_{rw}| < \text{TOL})$$

$$S_{cf}(t^+) = -1 \quad \text{for } (S_{cf} = 0) \text{ and } (\tau_{dev} < -\tau_c) \text{ or } (S_{cf} = -1) \text{ and } (\omega_{rw} < -\text{TOL})$$

where

τ_c static friction torque that is constant based on physical characteristics of reaction wheel, ft-lbf

TOL very small positive number (TOL << 1), typically on order of 10^{-7}

The rate of change of wheel angular speed is given by

$$\dot{\omega}_{rw} = \frac{\tau_{total}}{I_w} \qquad \text{for } S_{cf} \neq 0$$

$$\dot{\omega}_{rw} = 0 \qquad \text{for } S_{cf} = 0$$

where I_w is the wheel moment of inertia; thus,

$$\omega_{rw} = \int_0^t \dot{\omega}_{rw}(\tau) d(\tau)$$

The resulting control torque on the spacecraft when the wheel is spinning is

$$\vec{\tau}_{rw} = \begin{bmatrix} 0 \\ 0 \\ -\tau_{total} \end{bmatrix}$$

If the wheel is stuck because of static friction, the control torque on the spacecraft is zero, even though τ_{total} may be nonzero.

The reaction wheel angular momentum (in inertial coordinates) must be accounted for in the spacecraft equations of motion as follows:

$$\vec{L}_{rw} = \begin{bmatrix} 0 \\ 0 \\ I_w(\omega_{rw} + \omega_z) \end{bmatrix}$$

where ω_z is the z component of the spacecraft angular body rate vector.

3.3 Spacecraft Rotational Dynamics

3.3.1 Rotational Mass Properties

Spacecraft rotational mass properties are in the form of a moment-of-inertia matrix, defined as

$$\mathbf{I}_{MP} = \begin{bmatrix} I_x & I_{xy} & I_{xz} \\ I_{xy} & I_y & I_{yz} \\ I_{xz} & I_{yz} & I_z \end{bmatrix}$$

where I_x, I_y, and I_z are the moments of inertia, defined as

$$I_x = \int_{S/C}(y^2 + z^2)dm, \qquad I_y = \int_{S/C}(x^2 + z^2)dm, \qquad I_z = \int_{S/C}(x^2 + y^2)dm$$

and I_{xy}, I_{xz}, and I_{yz} are the products of inertia, defined as

$$I_{xy} = -\int_{S/C} xy\ dm, \qquad I_{xz} = -\int_{S/C} xz\ dm, \qquad I_{yz} = -\int_{S/C} yz\ dm$$

The matrix $\mathbf{I}_{MP}$ is a user-specified input to the model.

3.3.2 Computation of Angular Body Rates

The rotational dynamic equation of motion is a first-order vector differential equation that allows one to compute the angular rates as a function of the spacecraft mass properties and applied torques. Euler's equation for general rigid-body dynamic motion is as follows:

$$\dot{\vec{h}} = \vec{\tau} - \vec{\omega} \times \vec{h}$$

where

$\vec{h}$ angular momentum, ft-lbf-sec

$\vec{\tau}$ applied torque, ft-lbf

$\vec{\omega}$ spacecraft angular rate vector, rad/sec

Because $\vec{h} = \mathbf{I}_{MP}\vec{\omega}$, where $\mathbf{I}_{MP}$ is a constant matrix, Euler's equation can be expressed as

$$\mathbf{I}_{MP}\dot{\vec{\omega}} = \vec{\tau} - \vec{\omega} \times (\mathbf{I}_{MP}\vec{\omega})$$

Both sides of the equation can then be premultiplied by $(\mathbf{I}_{MP})^{-1}$ to obtain the rate equation

$$\dot{\vec{\omega}} = \mathbf{I}_{MP}^{-1}\{\vec{\tau} - \vec{\omega} \times (\mathbf{I}_{MP}\vec{\omega})\}$$

Expanding gives

$$\dot{\vec{\omega}} = \begin{bmatrix} \dot{\omega}_x \\ \dot{\omega}_y \\ \dot{\omega}_z \end{bmatrix} = \begin{bmatrix} I_x & I_{xy} & I_{xz} \\ I_{xy} & I_y & I_{yz} \\ I_{xz} & I_{yz} & I_z \end{bmatrix}^{-1} \left\{ \begin{bmatrix} \tau_x \\ \tau_y \\ \tau_z \end{bmatrix} - \begin{bmatrix} \omega_x \\ \omega_y \\ \omega_z \end{bmatrix} \times \left(\begin{bmatrix} I_x & I_{xy} & I_{xz} \\ I_{xy} & I_y & I_{yz} \\ I_{xz} & I_{yz} & I_z \end{bmatrix} \begin{bmatrix} \omega_x \\ \omega_y \\ \omega_z \end{bmatrix} \right) \right\}$$

The sum of all torques, both disturbance and control, acting on the spacecraft $\vec{\tau}$ is defined as

$$\begin{bmatrix} \tau_x \\ \tau_y \\ \tau_z \end{bmatrix} = \vec{\tau} = \vec{\tau}_{disturb} + \vec{\tau}_{control}$$

where $\vec{\tau}_{disturb}$ are disturbance torques acting on the spacecraft:

$$\vec{\tau}_{disturb} = \vec{\tau}_{GG} + \vec{\tau}_{drag} + \vec{\tau}_{solar} + \vec{\tau}_{mag} + \vec{\tau}_{slosh}$$

and $\vec{\tau}_{control}$ are torques produced by the attitude control system and the axial thrusters:

$$\vec{\tau}_{control} = \vec{\tau}_{RCS} + \vec{\tau}_{RW} + \vec{\tau}_{T}$$

The angular rates are then found by integrating the dynamic equation of motion as follows:

$$\vec{\omega}(t) = \int_0^t \dot{\vec{\omega}}(\tau)d\tau + \vec{\omega}_0$$

where $\vec{\omega}_0$ is the initial angular rate vector.

A typical plot of attitude rate versus time for the COLD–SAT spacecraft over approximately one orbit, showing x, y, and z components, is given in figure 3.9. This figure is discussed in more detail in section 3.7.1.1.

3.4 Spacecraft Attitude Computation

The spacecraft attitude represents the orientation of the spacecraft axes (x, y, and z) with respect to the inertial (TOD) frame (X, Y, and Z). This orientation can be conveniently specified in terms of a quaternion, which represents the rotation required to transform the TOD axes to be coincident with the spacecraft axes. The equation describing the time evolution of the quaternion is a first-order vector differential equation that specifies the rate of change of the attitude quaternion in terms of the spacecraft angular rates and the instantaneous spacecraft attitude as follows:

$$\dot{\bar{q}} = \frac{1}{2}\mathbf{M}_{ss}\bar{q}$$

where $\mathbf{M}_{ss}$ is a time-varying, skew-symmetric matrix formed from the spacecraft angular rates as follows:

$$\mathbf{M}_{ss} = \begin{bmatrix} 0 & -\omega_x & -\omega_y & -\omega_z \\ \omega_x & 0 & \omega_z & -\omega_y \\ \omega_y & -\omega_z & 0 & \omega_x \\ \omega_z & \omega_y & -\omega_x & 0 \end{bmatrix}$$

and

$$\vec{\omega} = \begin{bmatrix} \omega_x \\ \omega_y \\ \omega_z \end{bmatrix}$$

are the angular body rates about the spacecraft x, y, and z axes, respectively, and

$$\bar{q} = \begin{bmatrix} q^{\langle 0 \rangle} \\ q^{\langle 1 \rangle} \\ q^{\langle 2 \rangle} \\ q^{\langle 3 \rangle} \end{bmatrix}$$

is the attitude quaternion. The quantity $\dot{\bar{q}}$ is the attitude quaternion rate, which is integrated to obtain the attitude quaternion at any time t.

$$\bar{q}(t) = \int_0^t \dot{\bar{q}}(\tau)d\tau + \bar{q}_0$$

where $\bar{q}_0$ is the initial attitude.

3.5 Attitude Error Computation

The attitude error is a measure of the difference between the spacecraft's actual attitude $\bar{q}$ and the desired attitude computed by the attitude model $\bar{p}$ (see section 2.6). It is expressed in terms of angles about the spacecraft x, y, and z axes, which are denoted θ_x, θ_y, and θ_z, respectively. The error quaternion (which represents the transformation between the desired spacecraft axes and the actual spacecraft axes) is the product of the conjugate of the actual spacecraft attitude quaternion and the desired attitude quaternion.

$$\bar{q}_{err} = (\bar{q}^{\,c})^* \bar{p}$$

The three-axis attitude error is defined as

$$\hat{\theta} = \begin{bmatrix} \theta_x \\ \theta_y \\ \theta_z \end{bmatrix} = \begin{bmatrix} \varepsilon q_{err}^{\langle 1 \rangle} \\ \varepsilon q_{err}^{\langle 2 \rangle} \\ \varepsilon q_{err}^{\langle 3 \rangle} \end{bmatrix}$$

where

$$\varepsilon = \frac{-2\phi}{\sin \phi} \qquad \text{for } \phi \neq 0$$

$$\varepsilon = -2 \qquad \text{for } \phi = 0$$

and

$$\phi = \cos^{-1} q_{err}^{\langle 0 \rangle}$$

Angle ϕ must be in the first or fourth quadrant, so that if $(\phi > \pi/2)$ then let $\phi = \phi - \pi$.

A typical plot of attitude error versus time for the COLD–SAT spacecraft over approximately one orbit, showing x, y, and z components, is given in figure 3.10. This figure is discussed in more detail in section 3.7.1.1.

3.6 Attitude Determination System and Error and Rate Quantization

For the purposes of this model the attitude determination system is assumed to provide perfect knowledge of the actual spacecraft attitude errors and attitude rates. For COLD–SAT the actual attitude determination system consists of rate-integrating gyros, which are updated by information from redundant Sun sensors and horizon sensors. These systems, and any errors that they may introduce into knowledge of the attitude errors and rates, are not included in the COLD–SAT dynamic model. However, the effect of digital quantization of both the attitude errors and rates is included in the simulation (although all floating-point numbers stored in a digital computer are quantized, the quantization discussed in this section is many orders of magnitude "coarser" than that encountered with a 64-bit word length and is meant to represent that found on a spacecraft computer). For COLD–SAT the following values are used:

(1) Attitude-error quantization, 1.43×10^{-4} deg/step

(2) Attitude-rate quantization, 1.43×10^{-4} deg/sec-step

These values were chosen to be consistent with the numerical accuracy of the spacecraft computer selected for COLD–SAT.

3.7 Attitude Control System Algorithms

3.7.1 RCS Thruster Control Algorithm

RCS thrusters can have one of two possible command states: full on or full off. The decision to fire a given thruster is determined by comparing, for each of the three axes, the spacecraft attitude errors and angular rates against a set of switchlines on the phase plane $(\theta, \dot{\theta})$. Depending on the results of these comparisons, a table lookup is implemented to determine which thrusters, if any, need to be commanded "on" in order to produce the required corrective torques.

3.7.1.1 Switchline control.—Reaction control systems are commonly controlled by means of switchlines. For COLD–SAT the switchline configuration used consists of a pair of parallel straight-line segments plotted on the state plane of attitude rate versus attitude error that divide the plane into three control regions. One of the switchlines intercepts the ordinate (attitude-rate axis) at a positive attitude rate; the other intercepts it at a negative attitude rate. Both have a negative slope and corresponding segments have equal slopes. One switchline crosses the abscissa (attitude-error axis) at the maximum allowable positive attitude error; the other crosses the abscissa at the maximum allowable negative attitude error. The slopes and intercepts of the switchlines for a given axis are computed from the RCS-produced maximum acceleration and spacecraft moment of inertia about that axis.

A typical set of switchlines, such as those used for COLD–SAT, is shown in figure 3.11. The switchlines divide the $(\theta, \dot{\theta})$ plane into three control regions: a zero-torque region in the vicinity of the origin, a negative-torque region above and to the right of the right switchline, and a positive-torque region below and to the left of the left switchline. This scheme is implemented for each of the three spacecraft axes.

A typical phase-plane plot of the z-component of attitude rate versus attitude error is given in figure 3.12 for approximately one cycle (~65 min). The presence of the switchlines is clearly evident

on the right and left sides of this figure. The regions A, B, and C are marked as in figures 3.9 and 3.10. As shown in figures 3.9 and 3.10 the primary attitudinal activity occurs about the z axis because the dominant disturbance torque (in the absence of axial thrust) is the gravity-gradient torque, which exists predominantly about the z axis. Recall that this torque is sinusoidal with a period of one-half the orbit period. Thus, when the gravity-gradient torque is positive, it produces a positive angular acceleration about the z axis, which causes both the attitude error and the attitude rate to increase (region A in figs. 3.9, 3.10, and 3.12). This continues until an RCS switchline is reached. When the switchline is crossed, the appropriate RCS thrusters are fired, quickly reducing the attitude rate to a very small value. The thrusters are fired about five times per minute, with thrust duration of 0.2 sec ($t_{\text{min on}}$) per firing, to oppose the gravity-gradient torque (region B in figs. 3.9, 3.10, and 3.12). The phase trajectory hovers around the 1° (0 rev/day) point until the gravity-gradient torque becomes negative. The spacecraft then experiences an angular acceleration in the opposite direction toward the opposite switchline (region C) until that switchline is crossed and the appropriate RCS thrusters are fired. This limit-cycle behavior continues indefinitely as long as there is no axial thrust.

3.7.1.2 Computing switchlines.—A switchline is specified by means of a slope and an intercept with the attitude-rate axis. The slope and the intercept are chosen so that a positive or negative attitude rate outside the "zero torque" region will result in a continuous RCS thruster firing that will reduce this attitude rate to zero along a parabolic trajectory in the state plane. Consequently, the slope and intercept for a given switchline are functions of the moment of inertia and the steady-state RCS torque about that axis.

For a given maximum-attitude-error specification, steady-state RCS torque, and moment of inertia for each axis, the switchlines for each control axis are computed as follows:

$$\alpha_i = \frac{\tau_i}{I_i}$$

$$(L_{\text{slope}})_i = -\sqrt{\frac{\alpha_i}{(\theta_i)_{\max}}}$$

$$(L_{\text{intcpt}})i = \pm\sqrt{\alpha_i(\theta_i)_{\max}}$$

where $i = x, y, z$, and

τ_i magnitude of steady-state, RCS-produced torque about *i*th axis

I_i moment of inertia about *i*th axis from mass properties matrix

α_i resulting steady-state angular acceleration about *i*th axis

$(\theta_i)_{\max}$ magnitude of maximum allowable attitude error about *i*th axis

3.7.1.3 Thruster commanding.—In the COLD–SAT model the decision of which thrusters to fire proceeds in two steps. First, the attitude error and the attitude rate are compared against the switchlines to determine the "required torque region" (i.e., either positive, negative, or zero, as

discussed in section 3.7.1.1). This is done for each spacecraft axis. Next, the model searches through a thruster control table to determine which thrusters are to be turned on. The thruster control table is created by the user and reflects the physical arrangement of control thrusters. Table 3.6 is the thruster control table used for the COLD–SAT spacecraft. For example, if the attitude error and attitude rate about the x axis indicate a point on the x switchline plot in the positive-torque region while the attitude error and attitude rate about the y axis give rise to a point on the y switchline plot in the zero-torque region and the attitude error and attitude rate about the z axis indicate a point on the z switchline plot in the positive-torque region, this combination corresponds to the eleventh line in table 3.6. Therefore, for this case thrusters 7, 8, 11, and 12 are fired until there is a change of torque region on one or more of the three axes.

3.7.2 Gimballed Thruster Control Algorithm

A linearized, small-angle, block diagram representation of the gimballed thruster and the spacecraft rotational dynamics is shown in figure 3.13. This representation is reasonably accurate for gimbal angles as large as about 20° and thus can be utilized for the purposes of designing the control law. It should be emphasized, however, that the actual model simulates the complete nonlinear dynamics of the gimbal mechanism, including the fact that the two gimbal angles are not completely independent (because one gimbal mechanism is mounted on the other).

A control law was designed to command the gimballed thruster based upon the spacecraft attitude-error and attitude-rate vectors. The control law should meet the following goals:

(1) The control law must result in a stable closed-loop system for all expected spacecraft perturbations.

(2) The control law must result in a reasonably fast transient response, with a time to first peak of approximately 10 to 15 min.

(3) The control law should not result in excessive overshoot or oscillation.

(4) The control law must result in acceptable operation for all expected thrust levels.

The following should be noted concerning the system to be controlled:

(1) The open-loop system has two poles at the origin (two integrations) as a result of the spacecraft dynamics. Any proportional control scheme acting upon the attitude error will result in closed-loop poles in the right-half s plane, and thus an unstable system will result.

(2) An integration in the forward loop is required to have zero steady-state error between the attitude error and the gimbal angle. The system as it is, with no integration in the forward path, will require a nonzero steady-state attitude error in order to drive the gimbal angle to a nonzero value. Because a zero steady-state attitude error is desired, the controller must have one integration (i.e., a pole at the origin of the s plane).

(3) This additional integration in the forward path results in three poles at the origin and thus in an even more unstable system.

The following approach is used in order to solve this problem.

(1) If an additional attitude-rate feedback loop is added, one of the poles at the origin is moved into the left-half s plane.

(2) An additional controller zero at some point in the left-half plane near the origin will cause the closed-loop root locus to circle about this zero, so that the remaining two closed-loop poles will move into the left-half s plane for increasing controller gain. A finite zero and integration can be provided by a proportional-integral (P–I) control law.

(3) Thus, the control law should be a P–I scheme acting on the attitude error, along with a constant attitude-rate feedback. Root locus analysis of the system indicates that the following is a suitable control law:

$$C(s) = \frac{2.5(s + 0.0037)}{s} = 2.5 + \frac{0.00925}{s}$$

$$K_{\text{rate}} = -400$$

Note that this control law is not necessarily optimal but will result in acceptable response for all expected conditions.

3.7.3 Reaction Wheel Control Algorithm

The control law used for the reaction wheel is a proportional law that acts on the attitude error about the z axis and gives the voltage applied to the reaction wheel drive motor:

$$V_A = K_p \theta_{e_z}$$

where

K_p proportional control constant, 300 V/rad

θ_{e_z} z component of spacecraft attitude error (see section 3.5), rad

TABLE 3.1—STEADY-STATE THRUST VECTORS FOR COLD-SAT RCS THRUSTERS

Thruster	Thrust vector, including 1° misalignments, lbf		
	x component	*y* component	*z* component
1	+0.06 cos 1°	+0.06 sin 1°	0
2[a]	−0.06 cos 1°	↓	↓
3	+0.06 cos 1°	↓	↓
4[a]	−0.06 cos 1°	↓	↓
5	+0.06 cos 1°	0	+0.06 sin 1°
6[a]	−0.06 cos 1°	↓	↓
7	+0.06 cos 1°	↓	↓
8[a]	−0.06 cos 1°	↓	↓
9	+0.06 sin 1°	−0.06 cos 1°	0
10	↓	+0.06 cos 1°	↓
11	↓	−0.06 cos 1°	↓
12	↓	+0.06 cos 1°	↓

[a]For an uncoupled RCS system, thrusters 2, 4, 6, and 8 are deleted.

TABLE 3.2.—COLD-SAT RCS THRUSTER COORDINATES

Thruster	Thruster coordinates in spacecraft system, in.		
	x′	y′	z′
1	0	0	−48
2	+286.91	↓	+20
3	0	↓	+48
4	+286.91	↓	−20
5	0	+48	0
6	+286.91	−20	↓
7	0	−48	↓
8	+286.91	+20	↓
9	0	0	−48
10	↓	↓	+48
11	↓	↓	+48
12	↓	↓	−48

TABLE 3.3.—RCS TORQUES AND FORCES FOR STEADY-STATE COUPLED SYSTEM WITH MISALIGNMENT

Pair	RCS thruster	Steady-state torque, in.-lbf			Translational force, lbf		
		About x axis	About y axis	About z axis	Along x axis	Along y axis	Along z axis
1	1	-----	−2.88	-----	+0.06	-----	-----
	2[a]	-----	−1.20	-----	−.06	-----	-----
2	3	-----	+2.88	-----	+.06	-----	-----
	4[a]	-----	+1.20	-----	−.06	-----	-----
3	5	-----	-----	−2.88	+.06	-----	-----
	6[a]	-----	-----	−1.20	−.06	-----	-----
4	7	-----	-----	+2.88	+.06	-----	-----
	8[a]	-----	-----	+1.20	−.06	-----	-----
5	9	−2.88	-----	+5.13	-----	−0.06	-----
	10	−2.88	-----	−5.13	-----	+.06	-----
6	11	+2.88	-----	+5.13	-----	−.06	-----
	12	+2.88	-----	−5.13	-----	+.06	-----

[a]For uncoupled RCS system, thrusters 2, 4, 6, and 8 are deleted.

TABLE 3.4.—STEADY-STATE RCS TORQUES WITH 1° ANGULAR MISALIGNMENTS

[Boldface type indicates desired torque produced; normal type indicates misalignment torque.]

Pair	RCS thruster	Steady-state torque, in.-lbf			Translational force, lbf		
		About x axis	About y axis	About z axis	Along x axis	Along y axis	Along z axis
1	1	+0.0502629	**−2.87956**	−0.0895309	+0.0599991	+0.0010471	0
	2[a]	−.0209429	**−1.19982**	+.210895	−.0599991	↓	↓
2	3	−.0502629	**+2.87956**	−.0895309	+.0599991		
	4[a]	+.0209429	**+1.19982**	+.210895	−.0599991		
3	5	+.0502629	+.0895309	**−2.87956**	+.0599991	0	+0.0010471
	6[a]	−.0209429	−.210895	**−1.19982**	−.0599991	↓	↓
4	7	−.0502629	+.0895309	**+2.87956**	+.0599991		
	8[a]	+.0209429	−.210895	**+1.19982**	−.0599991		
5	9	**−2.87956**	−.0502629	**+5.12922**	+.0010471	−.0599991	0
	10	**−2.87956**	+.0502629	**−5.12922**	↓	+.0599991	↓
6	11	**+2.87956**	+.0502629	**+5.12922**		−.0599991	
	12	**+2.87956**	−.0502629	**−5.12922**		+.0599991	

[a]For uncoupled RCS system thrusters 2, 4, 6, and 8 are deleted.

TABLE 3.5.—RCS THRUSTER STATES

Thruster state	Description	Value of S_{trans}
0	Thruster off	$S_{trans} = 0$
1	Thruster in startup transient	$0 < S_{trans} < 1$, S_{trans} increasing linearly
2	Thruster full on	$S_{trans} = 1$
−1	Thruster in shutdown transient	$0 < S_{trans} < 1$, S_{trans} decreasing linearly

TABLE 3.6.—RCS THRUSTER CONTROL TABLE

Torque region (from switchline plots)			Thruster											
x axis	*y* axis	*z* axis	1	2	3	4	5	6	7	8	9	10	11	12
0	0	0												
0	0	+							On	On				
0	0	−					On	On						
0	+	0			On	On								
0	+	+			On	On			On	On				
0	+	−			On	On	On	On						
0	−	0	On	On										
0	−	+	On	On					On	On				
0	−	−	On	On			On	On						
+	0	0											On	On
+	0	+							On	On			On	On
+	0	−					On	On					On	On
+	+	0			On	On							On	On
+	+	+			On	On			On	On			On	On
+	+	−			On	On	On	On					On	On
+	−	0	On	On									On	On
+	−	+	On	On					On	On			On	On
+	−	−	On	On			On	On					On	On
−	0	0									On	On		
−	0	+							On	On	On	On		
−	0	−					On	On			On	On		
−	+	0			On	On					On	On		
−	+	+			On	On			On	On	On	On		
−	+	−			On	On	On	On			On	On		
−	−	0	On	On							On	On		
−	−	+	On	On					On	On	On	On		
−	−	−	On	On			On	On			On	On		

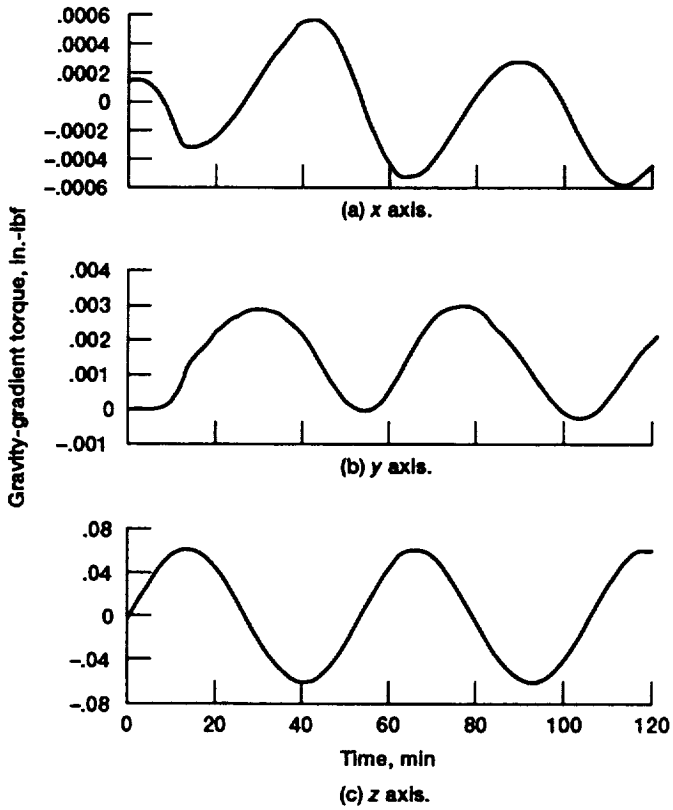

Figure 3.1.—Typical plot of gravity-gradient torque versus time for COLD–SAT spacecraft. (Orbit period, 105 min.)

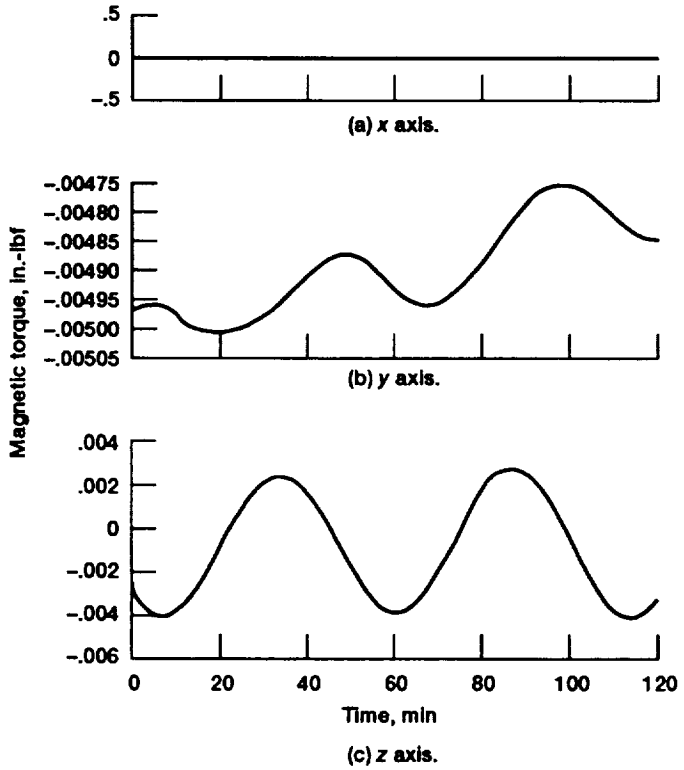

Figure 3.2.—Typical magnetic torque plot. (Spacecraft dipole moment aligned with x axis.)

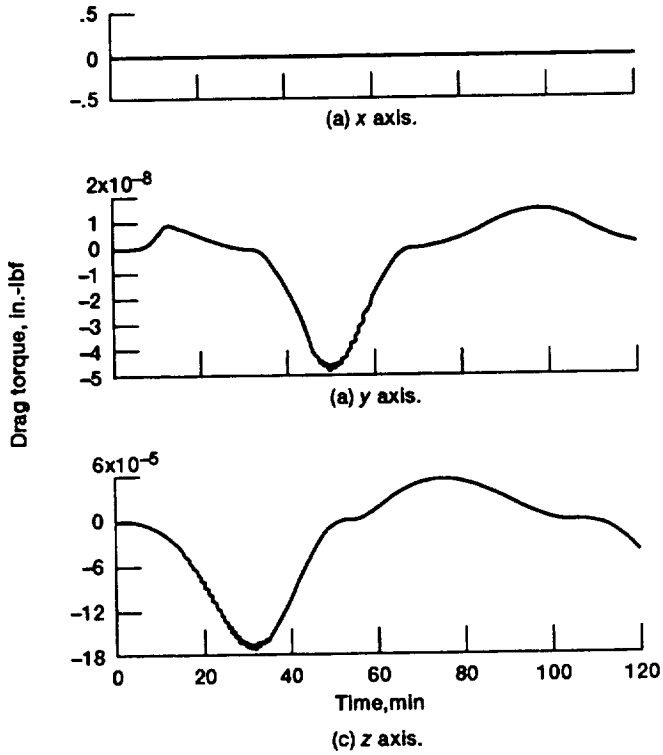

Figure 3.3.—Typical aerodynamic drag torque. (Apparent ripple is due to the fact that atmospheric density is computed at intervals of 1 minute to reduce CPU time.)

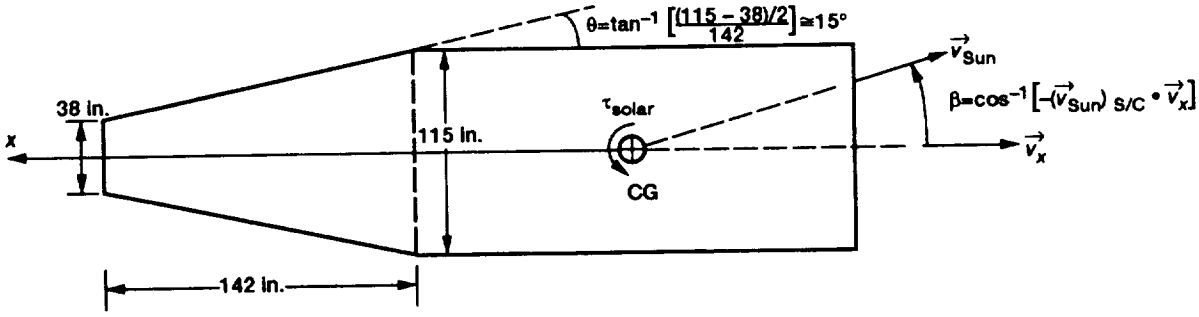

Figure 3.4.—Solar pressure torque computation. (The y axis is perpendicular to and into the page.)

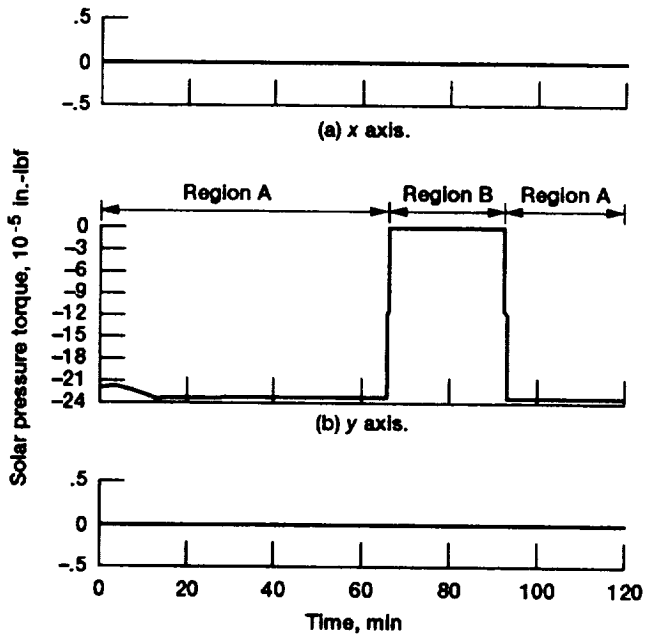

Figure 3.5.—Typical solar pressure torque plot.

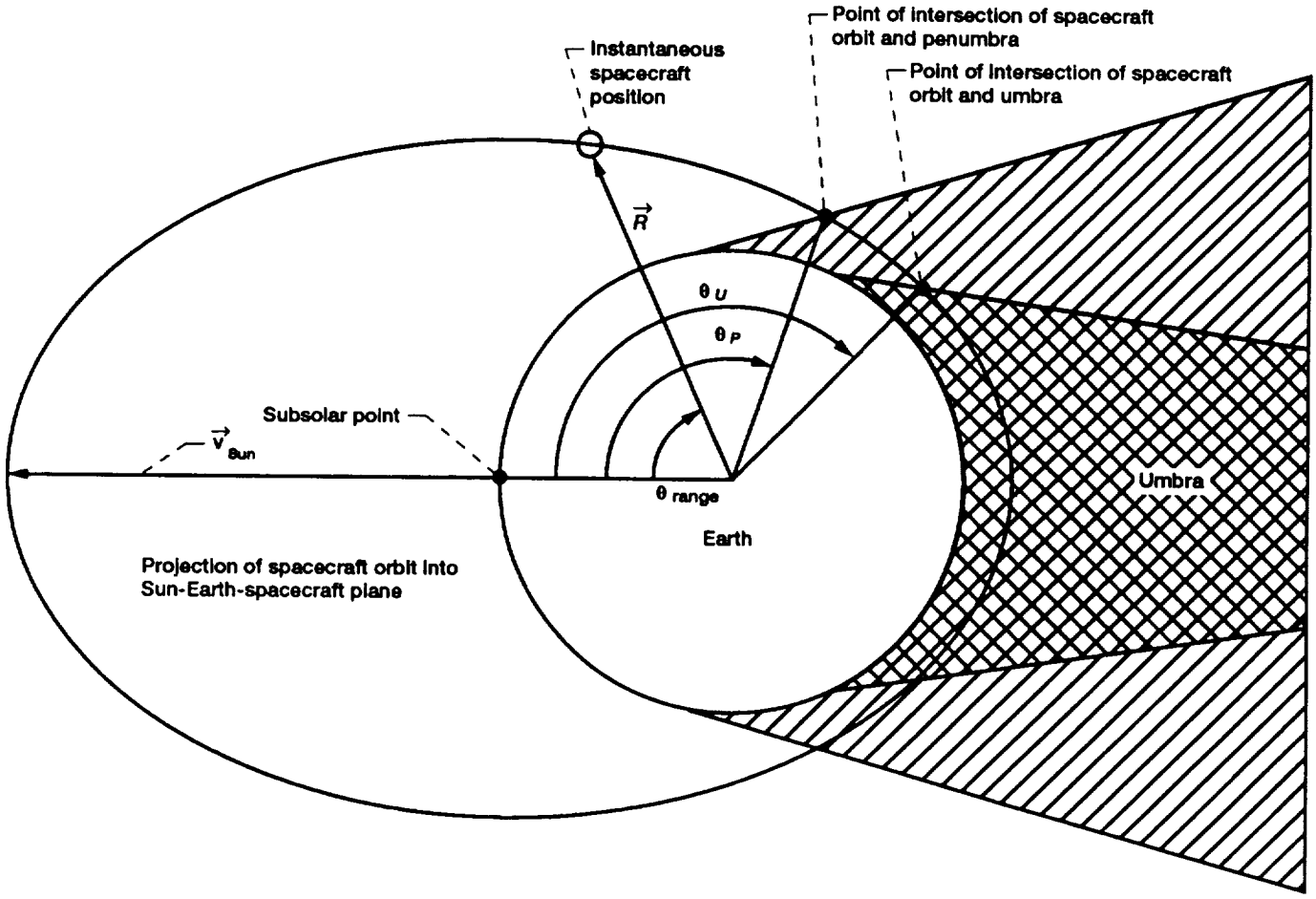

Figure 3.6.—Sun blockage.

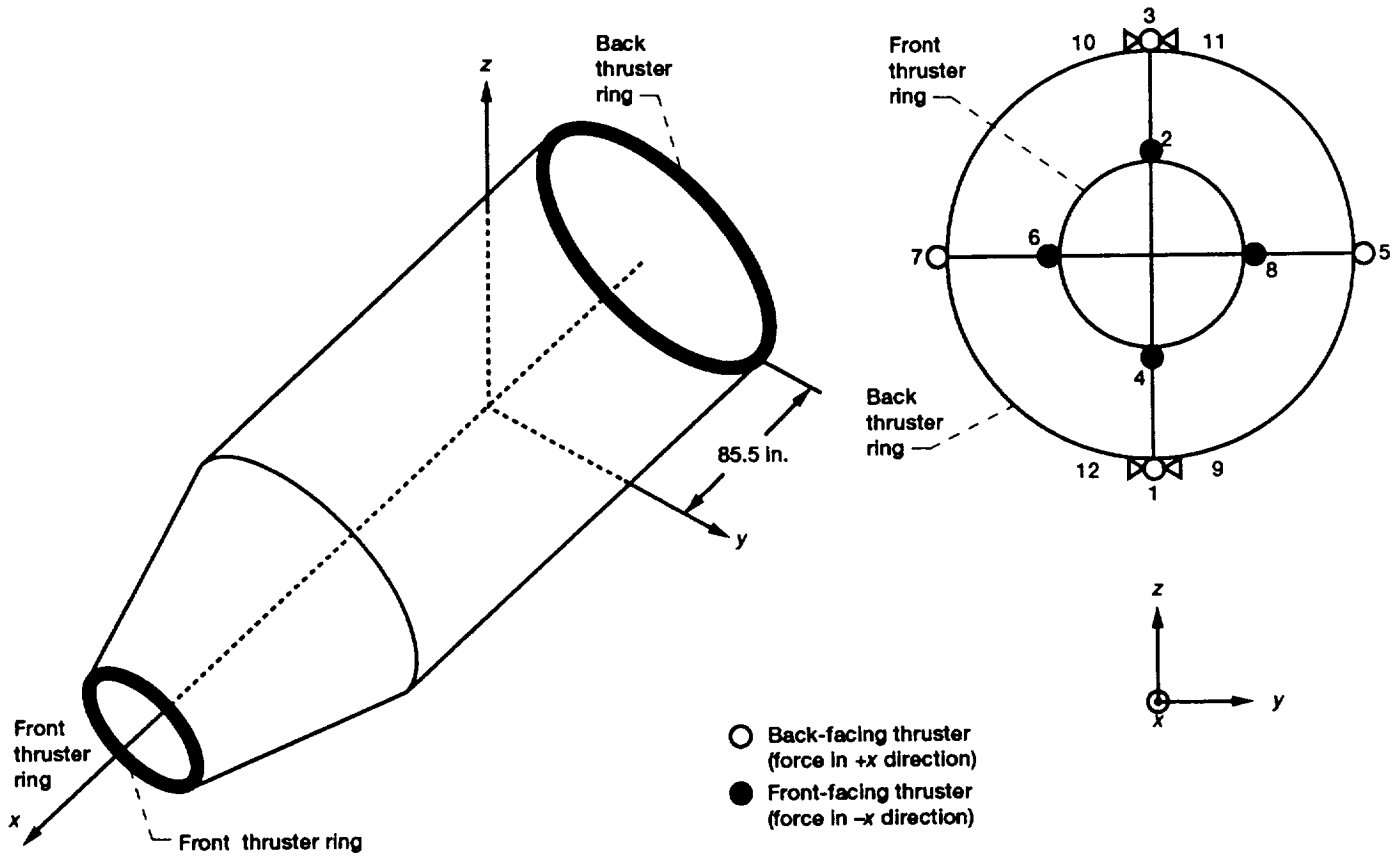

Figure 3.7.—RCS thruster location for COLD–SAT spacecraft. (For an uncoupled system the front thruster ring is deleted.)

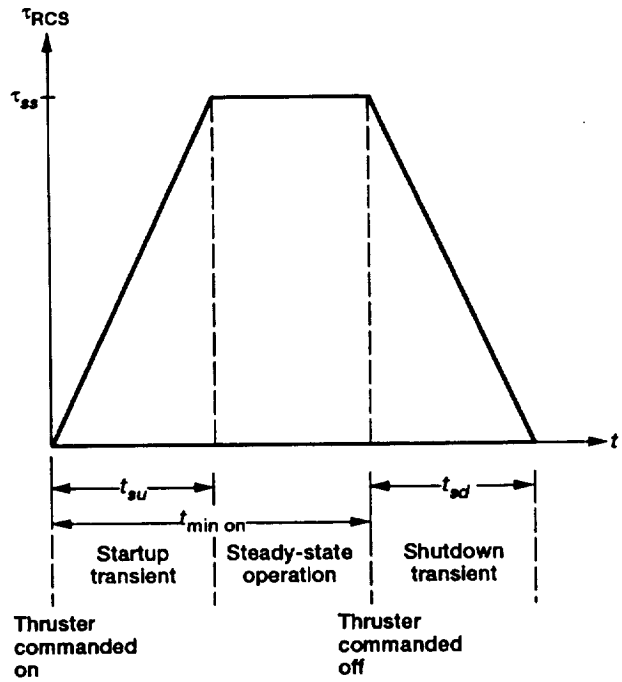

Figure 3.8.—Typical RCS thruster pulse, including transients.

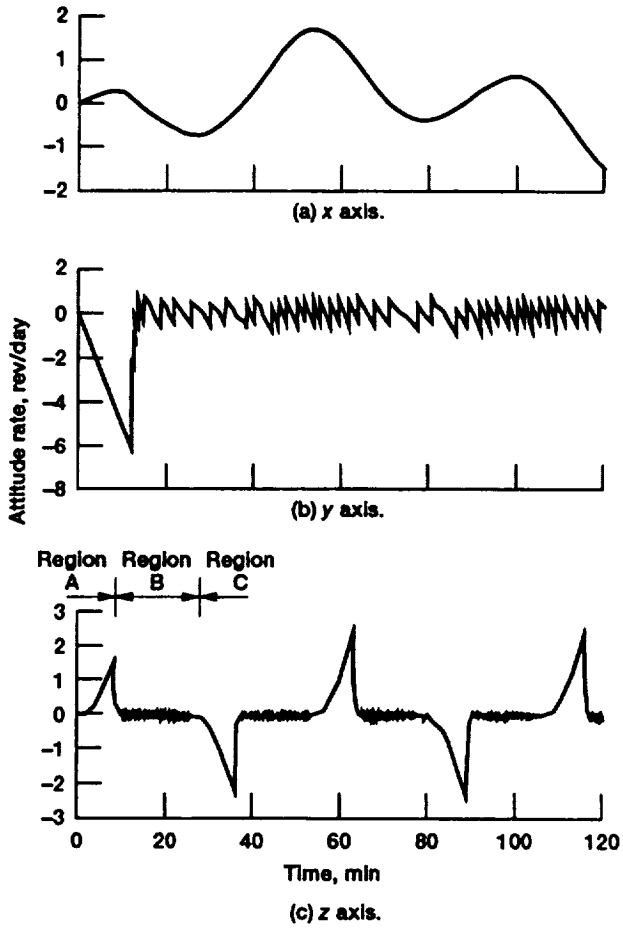

Figure 3.9.—Typical attitude-rate plot.

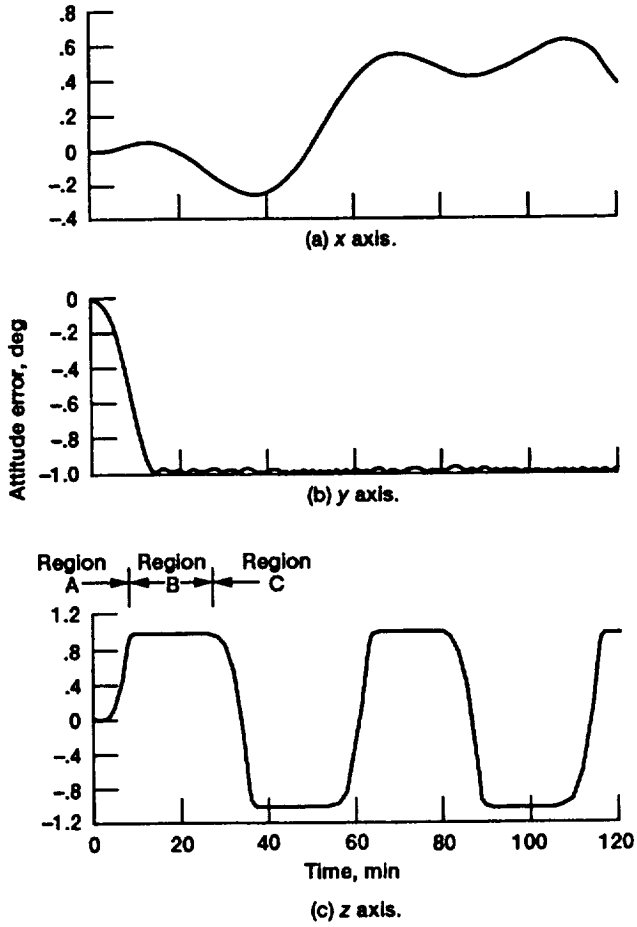

Figure 3.10.—Typical attitude-error plot.

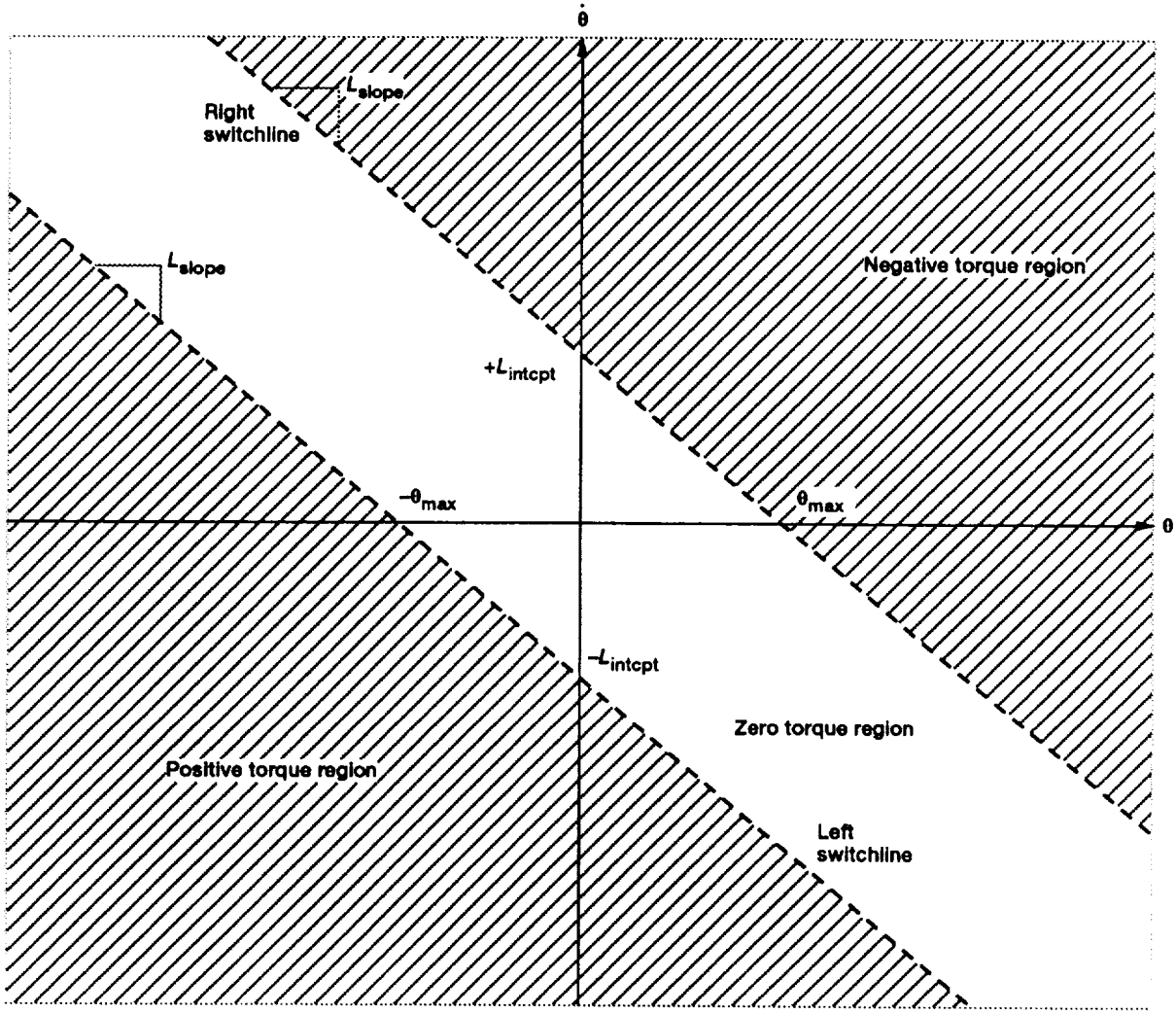

Figure 3.11.—Typical RCS switchline.

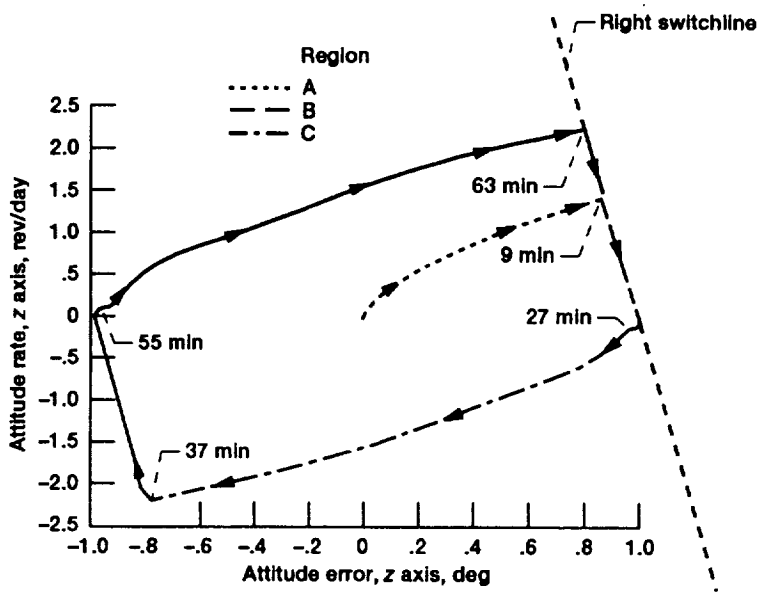

Figure 3.12.—Attitude-error and attitude-rate phase-plane trajectory.

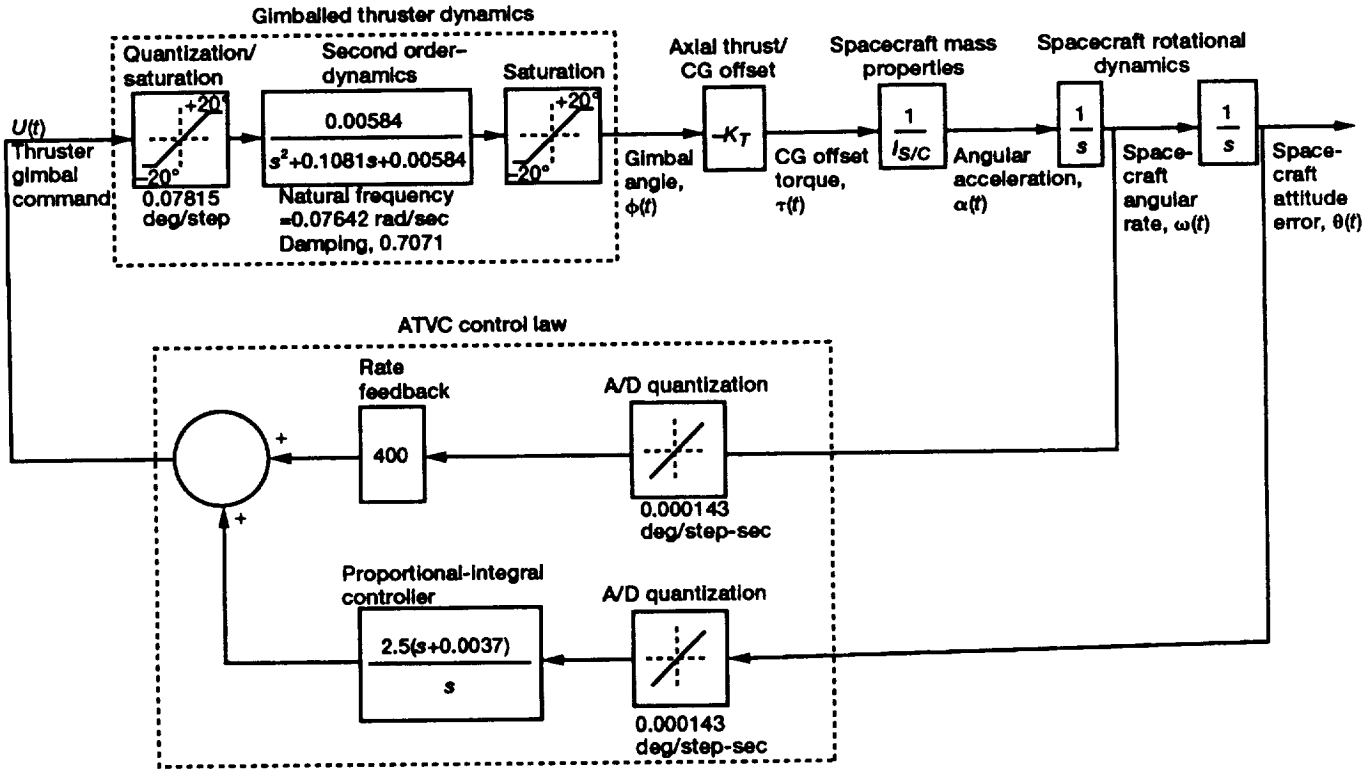

Figure 3.13.—Gimballed thruster control loop (linearized, one axis).

4.0 Slosh Model

One of the major design issues of the COLD–SAT spacecraft was the effect of fluid slosh on spacecraft dynamic stability and attitude control system performance because of the large mass of liquid hydrogen onboard. Therefore, one of the goals of the COLD–SAT dynamic model was to develop a slosh model that would approximate slosh with sufficient accuracy to permit the torques produced on the spacecraft by slosh to be evaluated for the conditions that the COLD–SAT spacecraft was expected to encounter.

An equivalent mechanical model is used to represent the fluid in the experiment tanks. This model consists of two independent linear spring-mass-dashpot (SMD) systems per tank: one coupled to the spacecraft y axis rotational dynamics and the other to the z axis rotational dynamics. The equivalent mechanical model used for slosh is shown in figure 4.1.

4.1 Computation of Equivalent Mechanical Model Parameters From Physical Parameters

Two orthogonal mechanical SMD systems are used to represent fluid slosh; each is attached to the tank wall so that the equilibrium, or null, position of the sloshing mass is on the tank centerline. If the proper values of spring constant, mass, damping, and distance below the free surface are selected, the mechanical model's dynamic behavior will under most conditions approximate that of the actual sloshing fluid in terms of such externally observable characteristics as reaction force produced on the tank wall, slosh frequency, and amplitude. This section is concerned with determining these mechanical model quantities in terms of actual physical properties, such as tank dimensions, fluid properties, fill level, and local acceleration, so that the dynamic behavior of the mechanical model will best approximate the actual sloshing fluid (ref. 6).

Cylindrical geometry is assumed for all tanks. Other assumptions are simplifying assumptions for the slosh model:

(1) Only the fundamental slosh frequency is considered.

(2) Sloshes in pitch and yaw are assumed independent.

(3) Bare, smooth tanks are used.

(4) Slosh can be modeled in any of the three tanks or any combination thereof.

All parameters are computed at the start of the simulation only and thus are assumed not to change significantly during the course of the simulation.

The equivalent spring constant, K_{sl} (in pounds force per foot), for each tank is computed as follows:

$$K_{sl} = m_T\left(\frac{a_x}{1.19h}\right)\left(\tanh\ 3.68\frac{h}{d}\right)^2 + \Delta K_{sl}(a_x,h,d)$$

where

m_T total mass of liquid hydrogen in tank, $(1/4)\pi\rho_{H_2}d^2h$, lbm

ρ_{H_2} density of liquid hydrogen, lbm/ft^3

a_x	x component of spacecraft linear acceleration produced by axial thrust $(F_T)_x/m_{S/C}$, ft/sec^2 (For the purposes of the slosh model only, other accelerations in the x direction, as well as y-directed and z-directed accelerations, are neglected.)
h	nonsloshing height of fluid in tank, $x_{tank}f$, ft
f	fill level of tank, percent
d	diameter of tank, ft
$\Delta K_{sl}(a_x,h,d)$	correction factor for low acceleration levels, slug/sec^2 or lbf/ft (For COLD–SAT, this term is essentially zero for the three axial-thrust-induced, nonzero acceleration levels and is only significant for simulation of slosh under zero-acceleration conditions. This term cannot be computed analytically and is computed in the model by interpolating actual experimental data given in reference 7.)
x_{tank}	height (i.e., x-axis dimension) of tank, ft

The mass of the equivalent SMD system, m_{sl} (in pounds mass), is computed as follows:

$$m_{sl} = (m_T)\left(\frac{d}{4.4h}\right)\tanh\ 3.68\frac{h}{d}$$

The distance of the equivalent SMD system below the free surface, ℓ_{sl} (in feet), which causes the SMD system dynamic behavior to best approximate that of the fluid, is given by

$$\ell_{sl} = \frac{d}{3.68}\tanh\ 3.68\frac{h}{d}$$

The actual distance of the sloshing mass from the spacecraft CG, D_{CG} (in feet), is given by

$$D_{CG} = x_{\text{tank base}} + h - \ell_{sl}$$

where $x_{\text{tank base}}$ is the x coordinate of the tank bottom (in feet).

For local acceleration levels above zero gravity, the damping ratio of the SMD system, ζ_{sl} (dimensionless), is estimated as follows:

$$\zeta_{sl} \cong \frac{4.98}{2\pi}\nu^{0.5}\left(\frac{d}{2}\right)^{-0.75}a_x^{-0.25} \qquad \text{for bare tank, } a_x > 0$$

where

ν kinematic viscosity of liquid hydrogen, 0.00197 cm^2/sec

a_x linear acceleration in x direction, cm/sec^2

d diameter of tank, cm

Note that the value of damping given by this expression becomes infinite as local acceleration approaches zero. For values of a_x less than 1 μg, it is assumed that $\zeta = 10^{-6}$.

The damping coefficient, B_{sl} (in pounds force-seconds per foot) for the tank, is used to express damping in the slosh dynamical equations given in section 4.3. It is related to the damping ratio as follows:

$$B_{sl} = 2\zeta_{sl}\,\omega_{n,sl}\,m_{sl} = 2\zeta_{sl}\sqrt{k_{sl}m_{sl}}$$

where $\omega_{n,sl}$ is the slosh natural frequency (in radians per second), $\sqrt{k_{sl}/m_{sl}}$.

4.2 Effect of Spacecraft Rotational Motion and Slosh-Model Tank Motion

The slosh model consists of two independent SMD systems; each system is separately coupled to the spacecraft *y*-axis and *z*-axis rotational dynamics. Each SMD system is forced by the inertial angular displacement (with respect to some arbitrary reference) and the angular rotation about the corresponding spacecraft body axis. In turn, the reaction force produced by each SMD system produces a torque about the corresponding spacecraft axis. Because the slosh model is a translational mechanical system and not a torsional one, it is necessary to develop the relationships between the rotational motion of the spacecraft and the corresponding motion of the tank walls, which forces the slosh model, as well as the relationship between the reaction forces produced on the tank walls and the resulting torque produced on the spacecraft about its CG. The coupling between the spacecraft angular motion and the slosh model is given in this section. The coupling between the slosh model and the resultant torque produced on the spacecraft is given in section 4.4.

4.2.1 Displacement of Tank Wall Due to Spacecraft Rotation

As the spacecraft rotates about the *y* or *z* axis, the null point of the sloshing mass moves along an arc of radius D_{CG}. If the angular displacement of the spacecraft is small, this arc can be approximated by a straight line tangent to this arc at the null point. Thus, the tank wall is considered to move in a straight line as the spacecraft rotates, as given by the following relations:

y-Axis slosh	z-Axis slosh
$y_{tw} = D_{CG}\theta_y$	$z_{tw} = D_{CG}\theta_z$

where

D_{CG} distance of slosh-mass null point from spacecraft CG, ft

y_{tw}, z_{tw} *y* and *z* components, respectively, of linear displacement of null point (and tank walls) with respect to inertial space due to spacecraft rotation, ft

θ_y, θ_z *y* and *z* components, respectively, of spacecraft rotation about its CG with respect to some arbitrary reference, rad

The angles θ_y and θ_z are extracted from the spacecraft attitude quaternion in a manner similar to the extraction of attitude error discussed in section 3.5. The attitude quaternion at the beginning of the simulation is used as the attitude reference. The Euler rotation angle extracted from the quaternion will always be in the range 0° to 180°, which leads to the restriction that slosh cannot be simulated for non-inertially-fixed attitudes: A spacecraft rotation of more than 180°, in any direction, from the initial attitude would cause a discontinuity in the computed values of y_{tw}, z_{tw}, or both, which would cause the slosh model to produce incorrect results. The relationship between the Euler rotation axis, the Euler rotation angle, and the quaternions is given in appendix B.

The computation of the angles θ_y and θ_z from the spacecraft attitude quaternion is given in equation form as follows: The slosh rotation quaternion is computed as

$$\bar{q}_{\text{slosh}} = \bar{q}^{\,c} * \bar{q}_0$$

where

$\bar{q}$ actual spacecraft attitude quaternion

$\bar{q}_0$ spacecraft attitude quaternion at start of simulation (reference attitude)

The slosh rotation angles are given by

y-Axis slosh	z-Axis slosh
$\theta_y = \varepsilon q_{\text{slosh}}^{\langle 2 \rangle}$	$\theta_z = \varepsilon q_{\text{slosh}}^{\langle 3 \rangle}$

where

$$\varepsilon = -2\frac{\phi}{\sin\phi}, \qquad \phi = \cos^{-1} q_{\text{slosh}}^{\langle 0 \rangle}$$

4.2.2 Velocity of Tank Wall Due to Spacecraft Angular Rates

The slosh SMD system is also forced by the inertial velocity of the tank wall, which is related to the spacecraft angular rates about the y and z axes. As was the case for the displacement computation, this velocity is actually the tangential velocity at the null point of the sloshing mass. It can be computed as follows:

y-Axis slosh	z-Axis slosh
$\dot{y}_{tw} = D_{CG}\omega_y$	$\dot{z}_{tw} = D_{CG}\omega_z$

where

$\dot{y}_{tw}, \dot{z}_{tw}$ y and z components, respectively, of tangential velocity of tank wall, ft/sec

ω_y, ω_z attitude rates about spacecraft y and z axes, respectively, rad/sec

4.3 Slosh-Model Implementation

An SMD slosh representation was chosen because of its simplicity and because, unlike a pendulum analogy, it is valid at all acceleration levels down to zero. Because of the COLD–SAT spacecraft geometry and the orientation of the axial thrust vector, it can validly be assumed that slosh about the spacecraft x axis is negligible; thus, the fundamental slosh frequency can be modeled by two independent SMD systems that are coupled to the spacecraft rotational dynamics about the y and z axes, as was previously discussed. It is assumed that the slosh harmonics beyond the fundamental are insignificant and that there is no coupling between the two SMD systems themselves (although coupling exists through the rotation model). Both are valid assumptions if the system is not near resonance.

The mechanical equivalent system, shown inside one tank relative to the fluid free surface, is illustrated in figure 4.1. All tanks are assumed to be cylindrical. The parameters m_{sl}, K_{sl}, B_{sl}, and ℓ_{sl} are computed from the fluid density, fill level, tank diameter, and linear acceleration (produced by the axial thrusters), as was discussed in section 4.1. Slosh is assumed to significantly affect the spacecraft rotational dynamics only; the effect on the spacecraft trajectory is assumed to be negligible and is not fed back to the translation model although lateral motion of the spacecraft is accounted for in the slosh model itself. Refer to figure 1.4 for a block diagram representation of the slosh model.

The relative displacement of the sloshing mass for tank i with respect to its null point is computed as follows:

y-Axis slosh	z-Axis slosh
$y_{rel} = y_{tw} - y_{si} + y_{S/C}$	$z_{rel} = z_{tw} - z_{si} + z_{S/C}$

where

y_{si}, z_{si} y and z components, respectively, of displacement of sloshing mass with respect to inertial space for tank, ft (This is computed by integrating the accelerations resulting from forces applied to the sloshing masses.)

$y_{S/C}, z_{S/C}$ y and z components, respectively, of translational displacement of spacecraft due to the effects of slosh, ft (This displacement is *not* fed back to the translation model.)

The relative velocity of the slosh mass with respect to the tank wall is computed as follows:

y-Axis slosh	z-Axis slosh
$\dot{y}_{rel} = \dot{y}_{tw} - \dot{y}_{si} + \dot{y}_{S/C}$	$\dot{z}_{rel} = \dot{z}_{tw} - \dot{z}_{si} + \dot{z}_{S/C}$

where

$\dot{y}_{si}, \dot{z}_{si}$ y and z components, respectively, of velocity of sloshing mass with respect to inertial space, ft/sec

$\dot{y}_{S/C}, \dot{z}_{S/C}$ y and z components, respectively, of translational velocity of spacecraft due to effects of slosh, ft/sec (This velocity is *not* fed back to the translation model.)

The force vector acting on the slosh mass, $\vec{F}_{sl}$ (in pounds force), is computed as follows. The negative of this force vector produces a disturbance torque on the spacecraft, as discussed in section 4.4, and a translational motion of the spacecraft, which is discussed here.

$$\vec{F}_{sl} = \begin{bmatrix} 0 \\ K_{sl} y_{rel} + B_{sl} \dot{y}_{rel} \\ K_{sl} z_{rel} + B_{sl} \dot{z}_{rel} \end{bmatrix}$$

Integrating the acceleration produced by this force yields the velocity and position of this mass with respect to inertial space:

y-Axis slosh	z-Axis slosh
$\dot{y}_{sl} = \frac{1}{m_{sl}} \int_0^t \left[F_{sl}(\tau)\right]_y \, d\tau$	$\dot{z}_{sl} = \frac{1}{m_{sl}} \int_0^t \left[F_{sl}(\tau)\right]_z \, d\tau$
$y_{sl} = \int_0^t \dot{y}_{sl}(\tau) d\tau + y_{sl}(0)$	$z_{sl} = \int_0^t \dot{z}_{sl}(\tau) d\tau + z_{sl}(0)$

The translational acceleration acting on the spacecraft due to slosh in tank i is computed as follows:

y-Axis slosh	z-Axis slosh
$(\ddot{y}_{S/C})_i = -\frac{\left[(F_{sl})_i\right]_y}{m_{S/C} - \sum_j (m_{sl})_j}$	$(\ddot{z}_{S/C})_i = -\frac{\left[(F_{sl})_i\right]_z}{m_{S/C} - \sum_j (m_{sl})_j}$

The translational velocities and displacements of the spacecraft due to slosh are computed by integrating these accelerations as shown here:

y-Axis slosh	z-Axis slosh
$\dot{y}_{S/C} = \int_0^t \left[\sum_i (\ddot{y}_{S/C})_i(\tau)\right] d\tau$	$\dot{z}_{S/C} = \int_0^t \left[\sum_i (\ddot{z}_{S/C})_i(\tau)\right] d\tau$

and

$$y_{S/C} = \int_0^t \dot{y}_{S/C}(\tau) d\tau \qquad z_{S/C} = \int_0^t \dot{z}_{S/C}(\tau) d\tau$$

4.4 Disturbance Torque Produced on Spacecraft by Slosh

The reaction force on the tank wall $\vec{F}_{sl}$ was computed in section 4.3. This is the sum of the forces produced by the spring and the dashpot; it translates into a torque on the spacecraft. This is the slosh torque, which was discussed in section 3.2.2.

$$\vec{\tau}_{\text{slosh}} = - \sum_i (D_{CG})_i \, (\vec{F}_{sl})_i$$

A typical plot of slosh torque (resulting from slosh in all three tanks) for the COLD–SAT spacecraft for approximately one orbit, showing x, y, and z components, is given in figure 4.2.

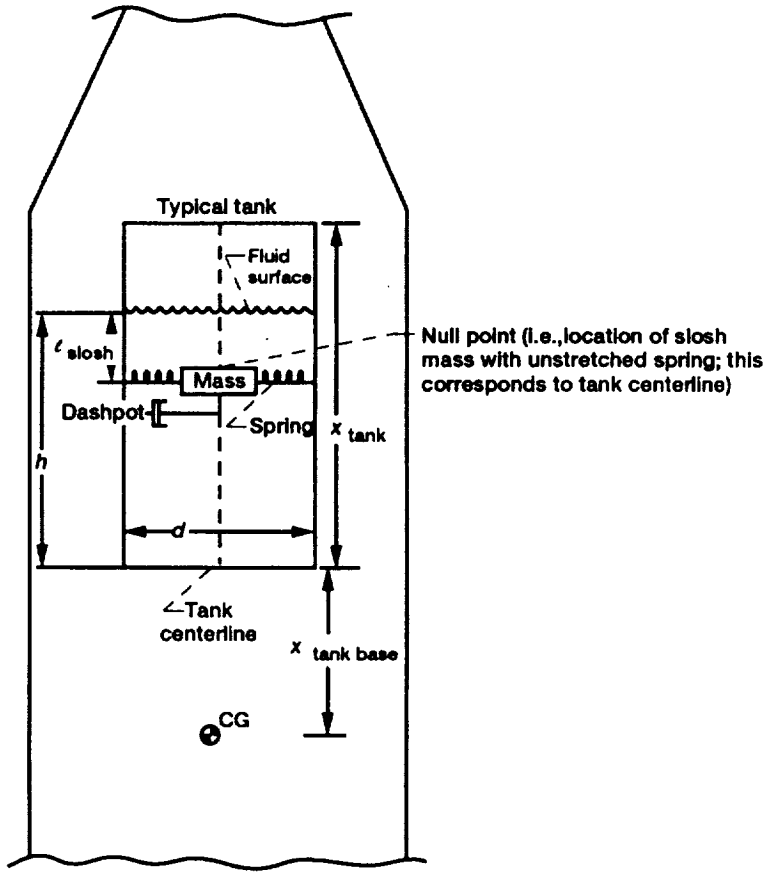

Figure 4.1.—Mechanical equivalent of slosh model.

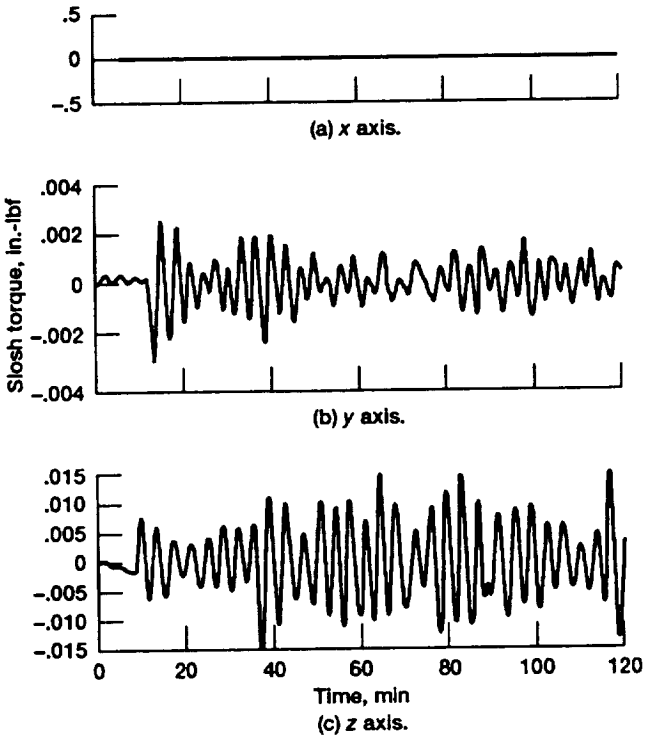

Figure 4.2.—Typical slosh torque (slosh in all three tanks).

5.0 Microgravity Accelerations in Experiment Environment

While on orbit the COLD–SAT spacecraft was to perform a series of experiments to investigate the behavior of cryogenic fluids in a near-zero-gravity environment. For some of these experiments it was desired to control both the magnitude and direction of the accelerations acting on the spacecraft, particularly at the fluid surface, as precisely as possible. In addition, it was desired that the acceleration level remain constant throughout the course of the experiment. Three levels of acceleration were desired. The acceleration was to be directed along the positive spacecraft x axis, with zero acceleration along the y and z axes. Axial thrusters were provided on the aft end of the spacecraft for this purpose. The thrusters were sized to provide the following levels of thrust: 0.04, 0.16, and 0.52 lbf. The acceleration levels generated by these thrust levels will depend upon the spacecraft mass at the time that the thrusters are operating. With a spacecraft nominal mass of 6000 lbm, the three resulting acceleration levels are 6.7, 26.7, and 86.7 μg directed along the $+x$ axis.

These desired acceleration conditions are not obtainable in practice because a number of factors act to alter the desired acceleration. These undesired accelerations are termed parasitic accelerations and are caused by the following conditions:

(1) Axial thruster misalignment: If the thrust vector generated by the fixed axial thrusters is not parallel with the spacecraft x axis, undesired components of acceleration in the y and z directions will be produced.

(2) Gimballed thruster: The gimballing action of the gimballed thruster causes the thrust vector to change in direction, thereby creating components of thrust in the spacecraft y and z directions and causing the x component of thrust to vary in magnitude.

(3) Spacecraft mass changes: During the course of the mission the spacecraft mass decreases owing to consumption of hydrazine and overboard loss of experiment fluids. Thus, for axial thrusters with constant thrust level the acceleration level gradually increases throughout the mission.

(4) Aerodynamic drag: Aerodynamic drag modifies the spacecraft acceleration. The direction of this disturbance acceleration, in body coordinates, depends upon the spacecraft attitude selected and the spacecraft orbit.

(5) Spacecraft angular accelerations: Angular accelerations acting on the spacecraft are produced by disturbance torques (including slosh) and the action of the attitude control system. Linear accelerations result that are tangentially directed with respect to the CG.

(6) Spacecraft angular rotation: The body rates of the spacecraft produce linear accelerations that are radially directed with respect to the CG.

(7) Gravity gradient: A gravity-gradient acceleration field is produced by the nonuniformity of the gravitational field throughout the spacecraft body.

(8) Uncoupled RCS thrusters: The firing of an uncoupled control thruster, whose function is to produce a control torque, will cause linear accelerations of the spacecraft body. For COLD–SAT these accelerations are always directed in the $+x$ direction.

(9) Angular misalignment of RCS thrusters: If the thrust vectors produced by the RCS are not parallel to the principal spacecraft axes because of thruster misalignment, a parasitic linear acceleration will be produced in the direction of misalignment when an RCS thruster is fired.

To gain an understanding of these microgravity disturbances and to evaluate the effect of various attitude control systems on the microgravity environment, the rotation model was expanded to include the computation of these accelerations at various user-selectable points throughout the spacecraft. A qualitative assessment of these accelerations was obtained by plotting the computed acceleration levels, typically for one complete orbit. A typical plot of the microgravity environment for a point at the front of the supply tank, showing x, y, and z components, is given in figure 5.1 for approximately one orbit. The RCS thruster firings are clearly evident, superimposed on the background gravity-gradient acceleration. Comparison with figures 3.9, 3.10, and 3.12 reflects a correlation between the microgravity environment and the location in the attitude-error/attitude-rate phase plane.

To obtain a quantitative measure of the degree to which the total accelerations at the selected points deviate from the desired acceleration levels, two parameters were defined as follows:

(1) The maximum instantaneous deviation (MID)

(2) The root-mean-square deviation (RMSD)

Precise definitions of these parameters are provided in section 5.5. It was found that these measures of microgravity deviation from the ideal acceleration requirements correlated well with the visual impressions created by the graphical representation. For the plot shown in figure 5.1 the maximum instantaneous deviation is 19.35 μg along the x axis, 6.916 μg along the y axis, and 8.151 μg along the z axis. The RMSD is 1.181 μg along the x axis, 0.7282 μg along the y axis, and 0.2647 μg along the z axis.

In the model the linear accelerations (conditions (1) to (4)) are computed in the translation model, and the remaining effects are computed in the rotation model. The acceleration level may be computed at as many as 10 points. At each of the 10 points the components of the total acceleration along the three body axes is computed.

The following subsections describe in detail the computation of the various components of the microgravity disturbances. Also described are the computation of the MID and RMSD parameters.

5.1 Microgravity Acceleration Resulting From Spacecraft Linear Acceleration

This component of microgravity acceleration results from translational spacecraft acceleration, which is produced by the fixed and gimballed axial thrusters, from aerodynamic drag, and from linear forces produced by uncoupled and/or misaligned RCS thrusters: Of these, only the x component of axial thrust produces a desired acceleration; the y and z components of axial thrust, as well as all of the other causes indicated, produce parasitic accelerations. Computing this acceleration is simply a

matter of converting the total external[1] accelerations acting on the spacecraft, which were computed by the translation model, into microgravity units. This computation, in equation form, is as follows:

$$\vec{s}_{tr} = \left\{ \frac{10^6}{32.175} \right\} (\vec{a}_{ext})_{S/C}, \ \mu g$$

where $(\vec{a}_{ext})_{S/C}$ was given (in feet per second squared) in section 2.5. This acceleration is independent of location within the spacecraft.

5.2 Microgravity Acceleration Resulting From Spacecraft Rotational Dynamics and Gravity-Gradient Effects

The remaining three components of microgravity acceleration are unique in the sense that the magnitudes and directions of these accelerations at a given point in the spacecraft are a function of the coordinates of that point with respect to the CG. Therefore, it is necessary to define the location at which the microgravity accelerations are to be computed. This is done by means of a vector from the CG to the point of microgravity computation, denoted $\vec{r}_p$, which is used in all of the acceleration computations that follow. The microgravity accelerations discussed in this section are entirely parasitic.

5.2.1 Angular-Rate-Induced Centrifugal Acceleration

Owing to centrifugal effects, spacecraft rotation about the CG produces a radially directed acceleration that is a function of angular rates and relative distance from the CG. Because COLD–SAT's attitude control scheme results in extremely low angular rates, this acceleration is typically insignificant. However, it is included in the model for generality.

The centrifugal microgravity acceleration is computed as follows:

$$\vec{s}_{cen} = \left\{ \frac{10^6}{32.175} \right\} \vec{\omega} \times (\vec{\omega} \times \vec{r}_p), \ \mu g$$

where

$\vec{\omega}$ spacecraft angular rate vector, rad/sec

$\vec{r}_p$ vector from CG to point of computation, ft

[1]Because the spacecraft is in free fall, the gravitational acceleration does not affect the microgravity environment and thus is not included in the computation.

5.2.2 Angular-Acceleration-Induced Tangential Acceleration

Spacecraft angular acceleration about its CG produces a tangentially directed linear acceleration that is a function of the distance from the CG and the spacecraft angular acceleration vector. This acceleration is produced by all torques that act on the spacecraft, including both disturbance and control torques. For COLD–SAT, because of the large magnitude of the RCS control torques with respect to other torques acting on the spacecraft, this component of microgravity acceleration is dominant when RCS thrusters are firing. This acceleration is predominantly in the form of large-magnitude, short-duration pulses that correspond to RCS activity. This effect can be clearly seen in figure 5.1.

The tangential microgravity acceleration is computed as follows:

$$\vec{s}_{\tan} = \left\{ \frac{10^6}{32.175} \right\} \dot{\vec{\omega}} \times \vec{r}_p, \ \mu g$$

where $\dot{\vec{\omega}}$ the spacecraft angular acceleration vector (in radians per second squared).

5.2.3 Microgravity Acceleration Resulting From Gravity-Gradient Effects

Gravity-gradient microgravity acceleration results from the fact that (like the gravity-gradient disturbance torque acting on the spacecraft rigid body) only the CG of the spacecraft is truly in free fall and nowhere else inside the spacecraft does the orbital centrifugal acceleration (away from the Earth) exactly balance the gravitational acceleration (toward the Earth). This results in a "gravity-gradient field" that is zero at the CG and increases as one moves away from the CG.[2] The variation of the field is different along the direction of the spacecraft position vector $\vec{R}$ than it is in the remaining two orthogonal coordinate directions.

Computation of the gravity-gradient acceleration requires that the vector $\vec{r}_p$ be transformed into the local-horizon (LH) coordinate system. This system has its origin located at the spacecraft CG, with the z axis in the direction of the zenith and the y axis perpendicular to the spacecraft orbit plane. The x axis is chosen to form a right-handed system and will coincide with the velocity vector for a circular orbit only.

The vector $\vec{r}_p$ in spacecraft body coordinates is transformed into TOD coordinates $(\vec{r}_p)_{\text{TOD}}$ by means of vector transformation and by using the spacecraft actual attitude quaternion as follows:

$$\begin{bmatrix} 0 \\ \hline (\vec{r}_p)_{\text{TOD}} \end{bmatrix} = \bar{q} * \begin{bmatrix} 0 \\ \hline \vec{r}_p \end{bmatrix} * (\bar{q}^{\,c})$$

where $\bar{q}$ is the attitude quaternion.

---

[2] Note that the microgravity acceleration that is produced by the gravity-gradient field is in addition to the microgravity acceleration that is caused by gravity-gradient-disturbance-torque-induced angular acceleration on the spacecraft, as previously discussed.

The transformation between TOD coordinates and LH coordinates is now derived. The LH system can easily be defined in terms of previously defined base vectors (see section 2.6.3) as follows: The LH z axis is the unit position vector $\vec{v}_R$. The LH y axis is a unit vector normal to the orbit plane, $\vec{v}_N = \vec{v}_R \times \vec{v}_v$, where $\vec{v}_v$ is the unit velocity vector. The LH x axis is the crossproduct $\vec{v}_N \times \vec{v}_R$. Thus, the transformation matrix from TOD to LH coordinates is

$$[\text{TOD} \rightarrow \text{LH}] = [\vec{v}_N \times \vec{v}_R \mid \vec{v}_N \mid \vec{v}_R]$$

The vector $\vec{r}_p$ can now be expressed in LH coordinates $(\vec{r}_p)_{\text{LH}}$ as

$$(\vec{r}_p)_{\text{LH}} = [\text{TOD} \rightarrow \text{LH}](\vec{r}_p)_{\text{TOD}}$$

The microgravity acceleration vector due to gravity-gradient effects, denoted $\vec{s}_{GG}$, is computed in LH coordinates as follows:

$$(\vec{s}_{GG})_{\text{LH}} = \left\{\frac{10^6}{32.175}\right\}\left\{\frac{\mu_{\text{Earth}}}{R^3}\right\}\begin{bmatrix} r_{px} \\ r_{py} \\ -2r_{pz} \end{bmatrix}_{\text{LH}}, \mu g$$

where

R magnitude of spacecraft position vector, ft

μ_{Earth} Earth gravitational constant, 1.4076469×10^{16} ft^3/sec^2

The acceleration vector is now transformed to TOD coordinates $(\vec{s}_{GG})_{\text{TOD}}$ and finally to spacecraft body coordinates $(\vec{s}_{GG})$ as follows:

$$(\vec{s}_{GG})_{\text{TOD}} = [\text{TOD} \rightarrow \text{LH}]^T(\vec{s}_{GG})_{\text{LH}}$$

$$\begin{bmatrix} 0 \\ \hline \vec{s}_{GG} \end{bmatrix} = (\bar{q}^{\,c}) * \begin{bmatrix} 0 \\ \hline (\vec{s}_{GG})_{\text{TOD}} \end{bmatrix} * \bar{q}$$

5.3 Total Microgravity Acceleration

The total microgravity acceleration is the vector sum of the four components:

$$\vec{s} = \vec{s}_{tr} + \vec{s}_{GG} + \vec{s}_{cen} + \vec{s}_{tan}$$

5.4 Plotting Total Acceleration

It is required to graphically plot the total microgravity acceleration, which is the sum of the translational, gravity-gradient, centrifugal, and tangential accelerations as previously discussed. When there is no RCS activity, the dominant torque acting on the spacecraft is the gravity-gradient torque, and perhaps the reaction-wheel- and gimballed-thruster-produced torques if these systems are included in the simulation. In any event the torques produced by these three entities are smooth curves that can easily be plotted. However, if one or more RCS thrusters are fired, the torques produced by these thrusters are by far the largest torques acting on the spacecraft for the duration of the thruster on-time. But because this on-time is very short, typically with a value of $t_{\text{min on}}$ (see section 3.2.3.2) or slightly greater, the resulting tangential acceleration profile consists of very narrow pulses of large magnitude whose width matches the thruster on-time. These pulses are too short in duration to plot in most cases (typical spacing between plot points is on the order of 5 to 10 sec, whereas $t_{\text{min on}}$ for COLD–SAT is 200 msec). In theory, the number of data points plotted could be increased so that the spacing between points is on the order of 200 msec, but this would result in excessively large data files. A better solution to this problem is to exaggerate the width of the RCS pulses (for plotting purposes only) from their actual width of about 200 msec to several seconds so that the resulting plots will faithfully illustrate the microgravity environment.

Because these short pulses occur only when an RCS thruster is fired, the algorithm implemented simply checks the states of all RCS thrusters; when one or more RCS thruster is in a full-on state (i.e., it has passed the startup transient), the algorithm holds the value of microgravity acceleration computed at this point (which is the maximum value) for time t_{hold}, which may be several seconds, and allows the plotting program to catch at least one point at this maximum value. After t_{hold} seconds have passed, the value of the stretched acceleration variable is again set to that computed by the simulation. This results in pulses that are clearly visible on the plotted output. The value of t_{hold} is selected so that $t_{\text{hold}} > t_{\text{inc}}$, where t_{inc} is the time between plotted points.

5.5 Computation of Microgravity Deviation Parameters

It is desirable to develop a numerical measure of how much the actual microgravity environment deviates from the ideal microgravity acceleration for each point. Two vectors are defined for each point where the microgravity environment is to be computed:

(1) Maximum instantaneous deviation (MID): This parameter represents the largest magnitude of deviation of the actual acceleration from the desired acceleration for one orbit.

(2) Root-mean-square deviation (RMSD): This parameter represents an average deviation of the actual acceleration from the desired value over one orbit.

The MID and RMS deviations are expressed as follows:

$$\overrightarrow{\text{MID}} = \begin{bmatrix} \max\left[s_x(t) - s_{\text{nom}}\right] \\ \max\left[s_y(t)\right] \\ \max\left[s_z(t)\right] \end{bmatrix}, \ \mu\text{g, over one orbit}$$

$$\overrightarrow{\text{RMSD}} = \left(\frac{1}{t} \int_0^t \left\{ \begin{matrix} [s_x(\tau) - s_{\text{nom}}]^2 \\ s_y^2(\tau) \\ s_z^2(\tau) \end{matrix} \right\} d\tau \right)^{1/2}, \ \mu g, \text{ over one orbit}$$

where

s_{nom} nominal acceleration in $+x$ direction (computed at beginning of simulation only), $(F_{T,x})_{\text{nom}}/(m_{\text{S/C}})_{\text{nom}}$

$(F_{T,x})_{\text{nom}}$ nominal thrust level (0.04, 0.16, or 0.52 lbf) in $+x$ direction

$(m_{\text{S/C}})_{\text{nom}}$ nominal spacecraft mass, slug

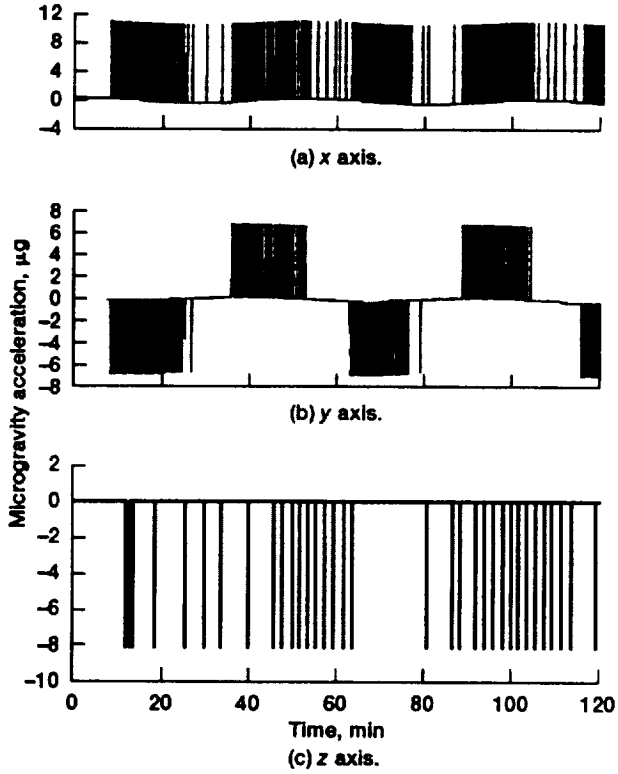

Figure 5.1.—Typical microgravity plot. (Point of computation is located on x axis at front of supply tank.)

Appendix A
Notation and Constants

TABLE A.1.—NOTATION CONVENTIONS

Symbol	Typical usage
$\vec{v}_v$, $\vec{v}_R$	unit vector; subscript indicates which one (in this case, v subscript indicates unit velocity vector, R subscript indicates unit position vector, etc.
$\vec{v}_x$, $\vec{v}_y$ $\vec{v}_\chi$, $\vec{v}_R$, $\vec{v}_\phi$, etc.	unit vectors along coordinate axis as indicated by subscript
$\vec{v}$, $\vec{R}$, $\vec{a}$, etc.	vector (in general, not unit vector)
v_x, v_y, v_z	x, y, and z components of vector $\vec{v}$
$\vec{v}_R$, $\vec{v}_\phi$, $\vec{v}_\theta$	R, ϕ, and θ components of vector $\vec{v}$ (spherical coordinates)
$\vec{v}_{S/C}$	vector referenced to coordinate system other than one in which vector was originally defined (e.g., $\vec{v}_{S/C}$ is spacecraft velocity vector expressed in spacecraft coordinates; original definition of this vector was in TOD coordinates)
$\bar{q}$	quaternion
$q^{\langle 0 \rangle}$	scalar part of quaternion $\bar{q}$
$q^{\langle 1 \rangle}$, $q^{\langle 2 \rangle}$, $q^{\langle 3 \rangle}$	vector part (x, y, and z components, respectively) of quaternion $\bar{q}$
$\hat{\theta}$	three-axis attitude error (in strict mathematical sense, not a vector)
$\mathbf{I}$	rectangular matrix
I_{ij}	single element of matrix $\mathbf{I}$ (ith row, jth column)
$\mathbf{I}^T$	transpose of matrix $\mathbf{I}$
$\mathbf{I}^{-1}$	inverse of square matrix $\mathbf{I}$
$\dot{x}$, $\dot{\vec{v}}$, $\dot{\bar{q}}$	time derivative (rate of change) of scalar, vector, and quaternion, respectively
$[A \rightarrow B]$	transformation matrix from coordinate system A to coordinate system B

TABLE A.2.—FUNDAMENTAL PHYSICAL CONSTANTS

Symbol	Name	Value
μ_{Earth}	Earth gravitational constant (product of universal gravitational constant and Earth mass)	1.4076469×10^{16} ft^3/sec^2 3.986005×10^{14} m^3/sec^2
J_2	Earth gravitational second zonal harmonic coefficient	1.0827×10^{-3}
J_3	Earth gravitational third zonal harmonic coefficient	-2.56×10^{-6}
J_4	Earth gravitational fourth zonal harmonic coefficient	-1.58×10^{-6}
R_{Earth}	Earth equatorial radius	20 925 656 ft 3443.920 n mi 6378.15 km
S_{Sun}	Solar radius (visible surface)	2.283436×10^{9} ft
$D_{Earth\text{-}Sun}$	Earth-Sun distance (semimajor axis), AU	4.908066×10^{11} ft
M_{Earth}	Earth magnetic dipole strength	8.1×10^{22} A-m^2
μ_0	Magnetic permeability	$4\pi\times10^{-7}$ H/m

Appendix B
Quaternion Algebra

Because quaternions are used throughout this model to represent spacecraft attitude, it is essential to provide some background information on the mathematics of quaternions.

B.1 Introduction

A quaternion is an ordered quadruple that appears to be a complex number with an imaginary part consisting of a three-element vector. Quaternions can be expressed in many different forms, but two forms are of concern here. The unit-vector form is expressed as follows:

$$\bar{q} = q^{\langle 0 \rangle} + q^{\langle 1 \rangle}\vec{i} + q^{\langle 2 \rangle}\vec{j} + q^{\langle 3 \rangle}\vec{k}$$

where $\vec{i}, \vec{j}$, and $\vec{k}$ are unit vectors similar to those encountered in vector analysis. Alternatively, a quaternion can be expressed in column-vector form as

$$\bar{q} = \begin{bmatrix} q^{\langle 0 \rangle} \\ q^{\langle 1 \rangle} \\ q^{\langle 2 \rangle} \\ q^{\langle 3 \rangle} \end{bmatrix}$$

where q_0 is called the scalar part and q_1, q_2, and q_3 make up the vector part. The column-vector form is used throughout this document when referring to quaternions in general. However, the unit-vector form is convenient when dealing with quaternion multiplication, as will be shown shortly.

A special type of quaternion is the unit quaternion. The unit quaternion simply satisfies the property that

$$\sqrt{\left(q^{\langle 0 \rangle}\right)^2 + \left(q^{\langle 1 \rangle}\right)^2 + \left(q^{\langle 2 \rangle}\right)^2 + \left(q^{\langle 3 \rangle}\right)^2} = 1$$

Because many of the properties defined herein are only valid for unit quaternions, all quaternions used in this model, unless otherwise indicated, are assumed to be unit quaternions.

B.2 Advantages of Quaternion Attitude Representation

A unit quaternion actually represents a single three-dimensional rotation of a given angle about a given vector. Thus, a unit quaternion can be used to express a transformation between two different coordinate systems and is used to represent the attitude of the spacecraft in the COLD–SAT dynamic model.

Alternative representations of spacecraft attitude are the use of Euler angles and the attitude matrix (sometimes called a direction-cosine matrix). Euler angles represent three sequential two-dimensional rotations to describe a rotation in three dimensions. The equations of motion for the Euler angle representation contain nonlinear functions. Singularities occur for certain rotation angles, making the Euler angle approach valid only for small-angle rotations. The attitude matrix, on the other hand, has linear equations of motion but requires integration of nine values per time step, as opposed to three for the Euler angle representation. Another problem with the attitude matrix representation is the tendency of the matrix to drift away from orthonormality because of numerical inaccuracies in the integration. Restoration of orthonormality is a nontrivial procedure that requires many operations. The quaternion representation suffers from none of the aforementioned problems. It requires only four integrations per time step, is valid for any rotation, and has no singularities anywhere in the equations of motion. The only condition that must be maintained is normality of the quaternion, which is easily checked and corrected.

B.3 Quaternion Mathematics

B.3.1 Addition

Quaternions are added together just like vectors or column matrices. If $\bar{p}$ and $\bar{q}$ are quaternions, the quaternion sum is found as follows:

$$\begin{bmatrix} p^{\langle 0 \rangle} \\ p^{\langle 1 \rangle} \\ p^{\langle 2 \rangle} \\ p^{\langle 3 \rangle} \end{bmatrix} + \begin{bmatrix} q^{\langle 0 \rangle} \\ q^{\langle 1 \rangle} \\ q^{\langle 2 \rangle} \\ q^{\langle 3 \rangle} \end{bmatrix} = \begin{bmatrix} p^{\langle 0 \rangle} + q^{\langle 0 \rangle} \\ p^{\langle 1 \rangle} + q^{\langle 1 \rangle} \\ p^{\langle 2 \rangle} + q^{\langle 2 \rangle} \\ p^{\langle 3 \rangle} + q^{\langle 3 \rangle} \end{bmatrix}$$

B.3.2 Multiplication by Scalar

Quaternions can be multiplied by a scalar like vectors and matrices. If $\bar{q}$ is a quaternion and a is a scalar, then

$$a \begin{bmatrix} q^{\langle 0 \rangle} \\ q^{\langle 1 \rangle} \\ q^{\langle 2 \rangle} \\ q^{\langle 3 \rangle} \end{bmatrix} = \begin{bmatrix} aq^{\langle 0 \rangle} \\ aq^{\langle 1 \rangle} \\ aq^{\langle 2 \rangle} \\ aq^{\langle 3 \rangle} \end{bmatrix}$$

B.3.3 Quaternion Multiplication

If $\bar{p}$ and $\bar{q}$ are quaternions defined as

$$\bar{p} = \begin{bmatrix} p^{\langle 0 \rangle} \\ p^{\langle 1 \rangle} \\ p^{\langle 2 \rangle} \\ p^{\langle 3 \rangle} \end{bmatrix} = p^{\langle 0 \rangle} + p^{\langle 1 \rangle}\vec{i} + p^{\langle 2 \rangle}\vec{j} + p^{\langle 3 \rangle}\vec{k}$$

and

$$\bar{q} = \begin{bmatrix} q^{\langle 0 \rangle} \\ q^{\langle 1 \rangle} \\ q^{\langle 2 \rangle} \\ q^{\langle 3 \rangle} \end{bmatrix} = q^{\langle 0 \rangle} + q^{\langle 1 \rangle}\vec{i} + q^{\langle 2 \rangle}\vec{j} + q^{\langle 3 \rangle}\vec{k}$$

where $\vec{i}, \vec{j}$, and $\vec{k}$ are unit vectors, multiplication of the quaternions $\bar{p}$ and $\bar{q}$, denoted $\bar{p} * \bar{q}$, is defined as follows by using the unit-vector representation.

(1) Multiply each element of $\bar{p}$ by each element of $\bar{q}$, preserving the order of multiplication (16 multiplications).

(2) Simplify the resulting terms by using the following rules. Note that this operation is not commutative:

$$\begin{array}{lll} \vec{i}*\vec{i} = -1 & \vec{j}*\vec{j} = -1 & \vec{k}*\vec{k} = -1 \\ \vec{i}*\vec{j} = \vec{k} & \vec{j}*\vec{k} = \vec{i} & \vec{k}*\vec{i} = \vec{j} \\ \vec{k}*\vec{j} = -\vec{i} & \vec{j}*\vec{i} = -\vec{k} & \vec{i}*\vec{k} = -\vec{j} \end{array}$$

Note the similarity to complex number multiplication and vector crossproduct.

B.3.4 Conjugation

If $\bar{q}$ is a quaternion, the conjugate of $\bar{q}$, denoted by $\bar{q}^{\,c}$, is found by negating the vector part of the quaternion $\bar{q}$:

$$\bar{q}^{\,c} = \begin{bmatrix} q^{\langle 0 \rangle} \\ -q^{\langle 1 \rangle} \\ -q^{\langle 2 \rangle} \\ -q^{\langle 3 \rangle} \end{bmatrix}$$

Note the similarity to the conjugation of a complex number.

B.3.5 Inverse

The inverse of a quaternion $\bar{q}$, another quaternion denoted by $\bar{q}^{-1}$, satisfies the following property:

$$\bar{q} * (\bar{q}^{-1}) = \begin{bmatrix} 1 \\ 0 \\ 0 \\ 0 \end{bmatrix} = 1$$

If $\bar{q}$ is a unit quaternion, then $\bar{q}^{-1} = \bar{q}^{\,c}$ (i.e., the inverse and conjugate of any unit quaternion are equal.

B.3.6 Extraction of Rotation Angle and Rotation Vector

Because a quaternion represents a rotation of a given angle about a given vector, the rotation angle θ and rotation vector $\vec{v} = [v_x \quad v_y \quad v_z]^T$ that a given unit quaternion $\bar{q}$ represents can be depicted as follows:

$$\bar{q} = \begin{bmatrix} q^{\langle 0 \rangle} \\ q^{\langle 1 \rangle} \\ q^{\langle 2 \rangle} \\ q^{\langle 3 \rangle} \end{bmatrix} = \begin{bmatrix} \cos\frac{\theta}{2} \\ v_x \sin\frac{\theta}{2} \\ v_y \sin\frac{\theta}{2} \\ v_z \sin\frac{\theta}{2} \end{bmatrix}$$

The rotation angle θ is found from the scalar part of the quaternion. If θ is restricted to two quadrants, there is a one-to-one correspondence between the quaternion and the rotation in space. If the first and second quadrants ($0 \leq \theta \leq \pi$) are arbitrarily chosen, then θ can be solved for. The rotation vector is then easily determined from the vector part of the quaternion.

B.3.7 Vector-Coordinate Transformations Using Quaternions

If $\vec{v} = [v_x \quad v_y \quad v_z]^T$ is a vector defined in TOD coordinates, $\vec{w} = [w_x \quad w_y \quad w_z]^T$ is the same vector expressed in spacecraft body coordinates, and $\bar{q} = \left[q^{\langle 0 \rangle} \quad q^{\langle 1 \rangle} \quad q^{\langle 2 \rangle} \quad q^{\langle 3 \rangle}\right]^T$ is the spacecraft attitude quaternion, the vector-coordinate transformation from TOD to spacecraft body coordinates can be expressed as

$$\begin{bmatrix} 0 \\ w_x \\ w_y \\ w_z \end{bmatrix} = \begin{bmatrix} q^{\langle 0 \rangle} \\ -q^{\langle 1 \rangle} \\ -q^{\langle 2 \rangle} \\ -q^{\langle 3 \rangle} \end{bmatrix} * \begin{bmatrix} 0 \\ v_x \\ v_y \\ v_z \end{bmatrix} * \begin{bmatrix} q^{\langle 0 \rangle} \\ q^{\langle 1 \rangle} \\ q^{\langle 2 \rangle} \\ q^{\langle 3 \rangle} \end{bmatrix}$$

This expression in compact form is

$$\begin{bmatrix} 0 \\ --- \\ \vec{w} \end{bmatrix} = (\bar{q}^{\,c}) * \begin{bmatrix} 0 \\ --- \\ \vec{v} \end{bmatrix} * \bar{q}$$

The inverse transformation from spacecraft body to TOD coordinates is

$$\begin{bmatrix} 0 \\ --- \\ \vec{v} \end{bmatrix} = \bar{q} * \begin{bmatrix} 0 \\ --- \\ \vec{w} \end{bmatrix} * \bar{q}^{\,c}$$

Appendix C
Coordinate Systems

C.1 TOD System

The TOD (geocentric equatorial true equinox of date) coordinate system (denoted X, Y, and Z) is a pseudo-inertial[3] right-handed Cartesian system with its origin situated at the center of the Earth. The X–Y plane is coincident with the Earth's equatorial plane and the Z axis passes through the North Pole. The X axis points in the direction of the vernal equinox (first point of Aries) on the date in question. This coordinate system is illustrated in figure C.1. Vectors expressed in this system are given the subscript TOD. This coordinate system is the basis for the translation model.

C.2 Spacecraft Body System

The spacecraft body coordinate system (denoted x, y, and z) is a right-handed Cartesian coordinate system whose origin is defined as the instantaneous, actual CG point of the spacecraft. The x axis is parallel to the long axis of the spacecraft, the positive direction being in the direction of the small receiver tank. The y axis is defined to be parallel to the solar panel connecting struts, and the z axis is in the direction opposite to the parabolic antenna. This coordinate system is not fixed with respect to the spacecraft rigid body but moves with the CG location. This coordinate system is the basis for the rotation model because all attitudinal motion of the spacecraft will occur about the CG. This system is illustrated in figure C.2. Vectors expressed in this system are given the subscript S/C.

C.3 Alternative Spacecraft Body System

The alternative spacecraft body coordinate system (denoted x', y', and z') is a right-handed coordinate system similar to the spacecraft body system discussed previously. The x', y', and z' axes point in the same directions, respectively, as the x, y, and z axes, but the origin of this coordinate system is located at the intersection of the plane containing the back thrusters and the line perpendicular to this plane that passes through the nominal spacecraft CG. Note that this system, unlike the x, y, z system, is fixed with respect to the spacecraft rigid body. It is thus convenient to use it to specify the locations of thrusters, tanks, and other components that are fixed with respect to the spacecraft rigid body. This system is illustrated in figure C.2.

C.4 Spacecraft Orbit Plane System

The spacecraft orbit plane (SCO) system is used in the initialization routine that converts a set of user-specified orbital elements into an equivalent position and velocity vector. This system is briefly mentioned in section 2.2 and defined as an Earth-centered, right-handed Cartesian coordinate system that is fixed with respect to the perigee of the spacecraft orbit. The x–y plane of this system is coincident with the spacecraft orbit plane, with the x axis passing through perigee of the orbit (if the

[3] Pseudo-inertial refers to the fact that this coordinate system does move very slowly with respect to inertial space because of the precession and nutation of the Earth's axis. However, over the proposed life of the COLD–SAT spacecraft, this movement is so slight as to be negligible. Therefore, for these purposes the TOD system can be considered to be an inertial frame.

orbit is circular, the orientation of the x axis is arbitrary). The z axis is in the direction of the spacecraft angular momentum vector. Vectors expressed in this system are given the subscript SCO.

C.5 Earth Magnetic Field System

The Earth magnetic field coordinate system (denoted X',Y',Z') is a right-handed Cartesian coordinate system that is fixed with respect to the rotating Earth. The z axis of this system is defined as passing through the Earth's north magnetic pole, and the x–y plane contains the magnetic equator, with the x axis passing through the meridian of longitude in which the north magnetic pole lies. Vectors expressed in this system are denoted with the subscript M. This system is used in computing the magnetic torque.

The transformation from the true-of-date (TOD) system to the magnetic (M) system consists of two successive Euler rotations. Starting with the TOD system, the first rotation is about the Z axis (i.e., the Earth's axis) by an angle δ, where δ is the angle between the vernal equinox (X axis) and a vector from the Earth's center through the point on the Earth's surface where the magnetic equator intersects the meridian of longitude containing the north magnetic pole. This intermediate system is denoted M'. The angle δ is defined as follows:

$$\delta = \alpha - \text{GHA}$$

where α is the longitude west of Greenwich of the north magnetic pole and GHA is the Greenwich hour angle, the angle measured westward from the Greenwich meridian to the vernal equinox. The Euler rotation matrix for this first rotation is

$$[\text{TOD} \rightarrow M'] = \begin{bmatrix} \cos\delta & -\sin\delta & 0 \\ \sin\delta & \cos\delta & 0 \\ 0 & 0 & 1 \end{bmatrix}$$

For the second Euler rotation the M' system is rotated about its y axis by angle β to form the M system, where β is defined as 90° minus the latitude of the north magnetic pole. This second transformation can be expressed as

$$[M' \rightarrow M] = \begin{bmatrix} \cos\beta & 0 & -\sin\beta \\ 0 & 1 & 0 \\ \sin\beta & 0 & \cos\beta \end{bmatrix}$$

Therefore, the complete transformation from TOD coordinates to magnetic coordinates is given by the following matrix:

$$[\text{TOD} \rightarrow M] = \begin{bmatrix} \cos\beta\cos\delta & -\cos\beta\sin\delta & -\sin\beta \\ \sin\delta & \cos\delta & 0 \\ \sin\beta\cos\delta & -\sin\beta\sin\delta & \cos\beta \end{bmatrix}$$

The values of α and β vary somewhat over time as the Earth's magnetic poles move but are generally known for a given date. The GHA is a simple function of the date and time:

$$\text{GHA} = \text{GHA}_0 + R_{\text{Earth}} t$$

where

GHA_0 Greenwich hour angle at start of simulation (found in Astronomical Almanac)

R_{Earth} Earth rotation rate, deg/sec

t simulation time, sec

C.6 Ecliptic Coordinate System

The ecliptic coordinate system is a heliocentric, right-handed Cartesian coordinate system whose x–y plane is coincident with the plane of the ecliptic, whose x axis points in the direction of the first point of Aries, and whose z axis is in the direction of the angular momentum vector of the Earth as it revolves about the Sun. Vectors expressed in this system are given the subscript e. This system is used in computing the desired spacecraft attitude for certain attitude options.

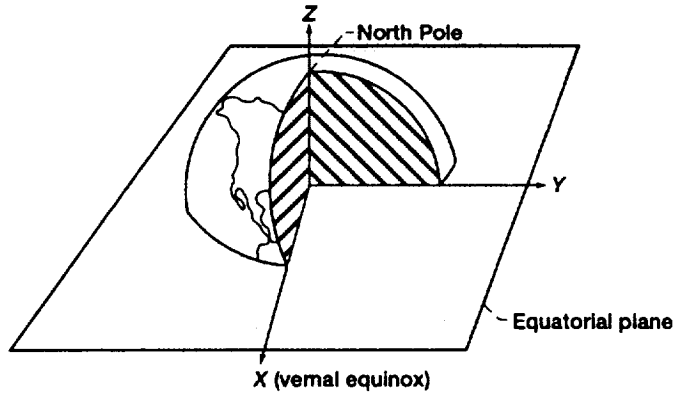

Figure C.1.—TOD coordinate system.

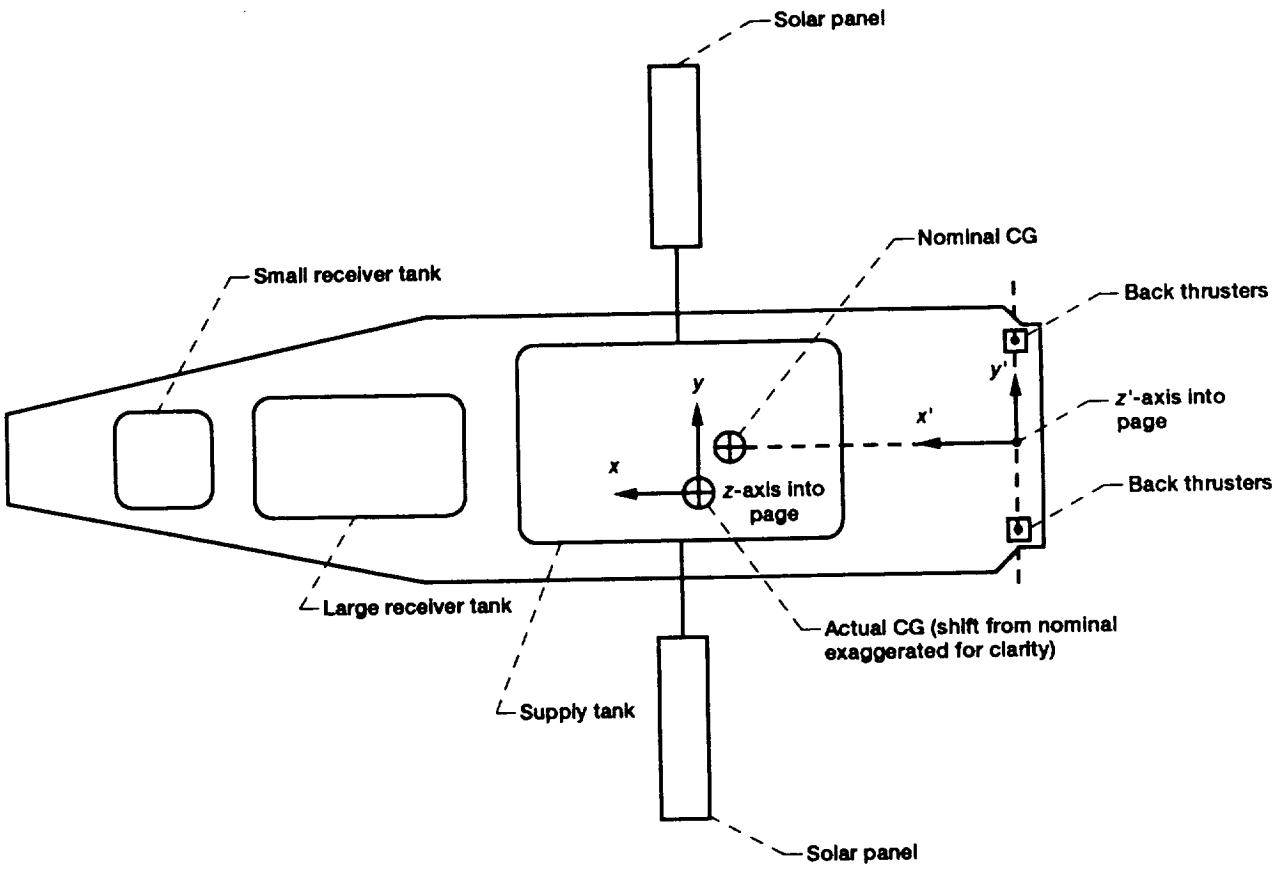

Figure C.2. —Spacecraft body coordinate system.

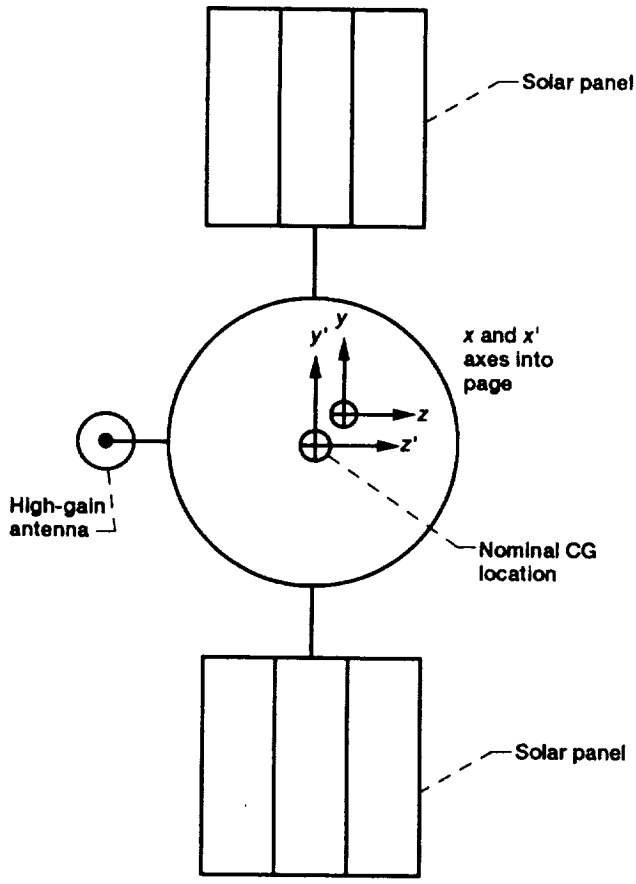

Figure C.3. —Alternative spacecraft body coordinate system.

Appendix D
Implementation of Model

D.1 Overview

The COLD–SAT dynamic model is implemented by using the EASY5 engineering analysis system. EASY5 is an analysis and design tool for simulation and control systems that is published by Boeing Computer Services. It incorporates the following features:

(1) The convenient block-diagram-based system modeling approach subdivides the model into separate components that can be developed and tested independently.

(2) The transient solution of systems is described by linear or nonlinear ordinary differential equations in time. One of several fixed-step or variable-step numerical integration schemes is used, including the Runge-Kutta, modified stiff-gear, Adams-Bashforth predictor/Adams-Moulton corrector, and Euler methods. The variable-step Adams-Bashforth/Adams-Moulton method was used for all COLD–SAT dynamic model simulations, for it yielded excellent stability and accuracy while consuming the least CPU time.

(3) "Standard component" libraries are available that contain a rich assortment of common control system elements, including basic first- and second-order transfer functions, nonlinear effects, basic control laws, and tabular function generators. Furthermore, user-specified Fortran and Macro components can be created to model additional effects by inclusion of the appropriate Fortran code. "Fortran components" were used to model the vast majority of COLD–SAT dynamic model subsystems.

(4) Linear control system analysis and design tools, such as root locus, frequency response, and linear-model generation, can be performed on both linear and nonlinear models. (Nonlinear models are automatically linearized about a given operating point.)

(5) High-resolution graphical display and hard copy of analysis may be output.

(6) Model code can call external subroutines. This approach, which permits modular program development, was extensively employed for the COLD–SAT dynamic model.

All of these capabilities are integrated into a single package that runs on a variety of platforms, including the Apollo Domain workstations, the VAX/VMS minicomputer, and the Cray X/MP supercomputer. Figure D.1 is a pictorial overview of the EASY5 system. For additional information, see reference 8.

D.2 Subroutines

The COLD–SAT dynamic model utilizes several external subroutines and functions. Some were developed specifically for this model, but others are general-purpose routines.

D.2.1 COLD–SAT Model-Specific Subroutines

SCATT (ATTUD)	computes desired spacecraft attitude direction-cosine matrix for given attitude option, axis alignment, optional rotation, and time (section 2.6). ATTUD is called by SCATT.
SLOSHP	computes equivalent mechanical slosh-model parameters for liquid hydrogen, by using an SMD slosh model, from tank dimensions, fill level, and local acceleration (section 4.1)
TTLACC	computes microgravity acceleration for given point in the spacecraft (section 5.0)
IRCSTGL	function that returns nonzero value when any RCS thruster is fired. This value is used in the microgravity acceleration plotting routine (section 5.4).

D.2.2 General Astronomical Routines

ATMJ (FUNC1, FUNC, and SIMPK)	function that returns atmospheric density at given point in spacecraft orbit by using Jacchia's 1970 model (ref. 2). FUNC1, FUNC, and SIMPK are called by ATMJ.
JDATE	computes Julian date with respect to year 2000 from given month, day, year, and Greenwich mean time
ORBEL	computes classical elliptized orbital elements from position and velocity vectors
SGHA	computes Greenwich hour angle for given date and GMT
SPHGGT	computes gravity-gradient torque by using spherical Earth model (section 3.2.1.1)
STVEC2	computes position and velocity vectors from given orbital elements (section 2.2)
SUNVEC	computes position of Sun in TOD coordinates on given Julian date, as well as vector normal to ecliptic (section 2.6.2)
SUNVIS	determines fraction of Sun's disk that is visible for given point in spacecraft orbit (section 3.2.1.4)

D.2.3 General Vector, Matrix, and Other Mathematical Routines

AROT	computes matrix that performs Euler rotation of angle θ about given axis
MPROD1	computes product of 3 × 3 matrix and a three-element vector: $\vec{v}_2 = \mathbf{A}\vec{v}_1$

MPROD2 computes product of transpose of 3 × 3 matrix and a three-element vector: $\vec{v}_2 = (\mathbf{A}^T)\vec{v}_1$

MTMPY1 computes product of two matrices: $\mathbf{C}_{n\times p} = \mathbf{A}_{n\times m}\mathbf{B}_{m\times p}$

MTMPY2 computes product of two matrices: $\mathbf{C}_{n\times p} = \mathbf{A}_{n\times m}(\mathbf{B}_{p\times m})^T$

MTMPY3 computes product of two matrices: $\mathbf{C}_{n\times p} = (\mathbf{A}_{m\times n})^T\mathbf{B}_{m\times p}$

SP2REC converts vector in spherical coordinates to Cartesian coordinates, provided that ϕ component (longitudinal component) of vector is zero

VCRS computes crossproduct of two vectors in three dimensions: $\vec{w} = \vec{v} \times \vec{u}$

VDOT computes dot product of two vectors: $x = \vec{v} \cdot \vec{u}$

VTSCAL computes product of vector and scalar: $\vec{w} = a\vec{v}$

XUNIT computes magnitude of given vector, as well as unit vector in same direction as given vector

HYPOT computes hypotenuse of right triangle: $z = \sqrt{x^2 + y^2}$

D.2.4 Quaternion Routines

DCMTOQ converts direction-cosine (attitude) matrix into equivalent attitude quaternion (section 2.6.8)

Q2RPY extracts rotation angles about spacecraft x, y, and z axes from quaternion specifying rotation from some reference attitude (sections 3.5 and 4.2.1)

QCVQ converts vector from coordinate system A to coordinate system B by using quaternion (appendix B, section B.3.7)

QVQC converts vector from coordinate system B to coordinate system A by using quaternion (appendix B, section B.3.7)

QMULT2 computes product of two quaternions: $\bar{p} = \bar{q}_1 * \bar{q}_2^{\,c}$ (appendix B, section B.3.3)

QMULT3 computes product of two quaternions: $\bar{p} = \bar{q}_1^{\,c} * \bar{q}_2$ (appendix B, section B.3.3)

D.3 Code Listing

D.3.1 EASY5 Model

The COLD–SAT dynamic model was developed and debugged on an Apollo workstation by using the EASY5/W program. EASY5/W is a graphical preprocessor to EASY5 that allows the user to create and connect both standard and user-defined components in a manner similar to a computer-assisted design (CAD) system. Once a valid model is created in EASY5/W, a batch-format EASY5 model-generation source file is created from the graphical model. This file can be compiled and run on the Apollo or ported to another machine (with the proper connectivity), such as the Cray, for faster execution. The output files can then be sent back to the Apollo or to a personal computer for graphical postprocessing (see figure D.1).

Figure D.2 is the EASY5/W Apollo workstation block diagram of the entire model.

D.3.2 Subroutines

In order to modularize the code as much as possible, much of the code used to implement the model was written in the form of standard Fortran 77 subroutines external to EASY5. These subroutines are called by the main model.

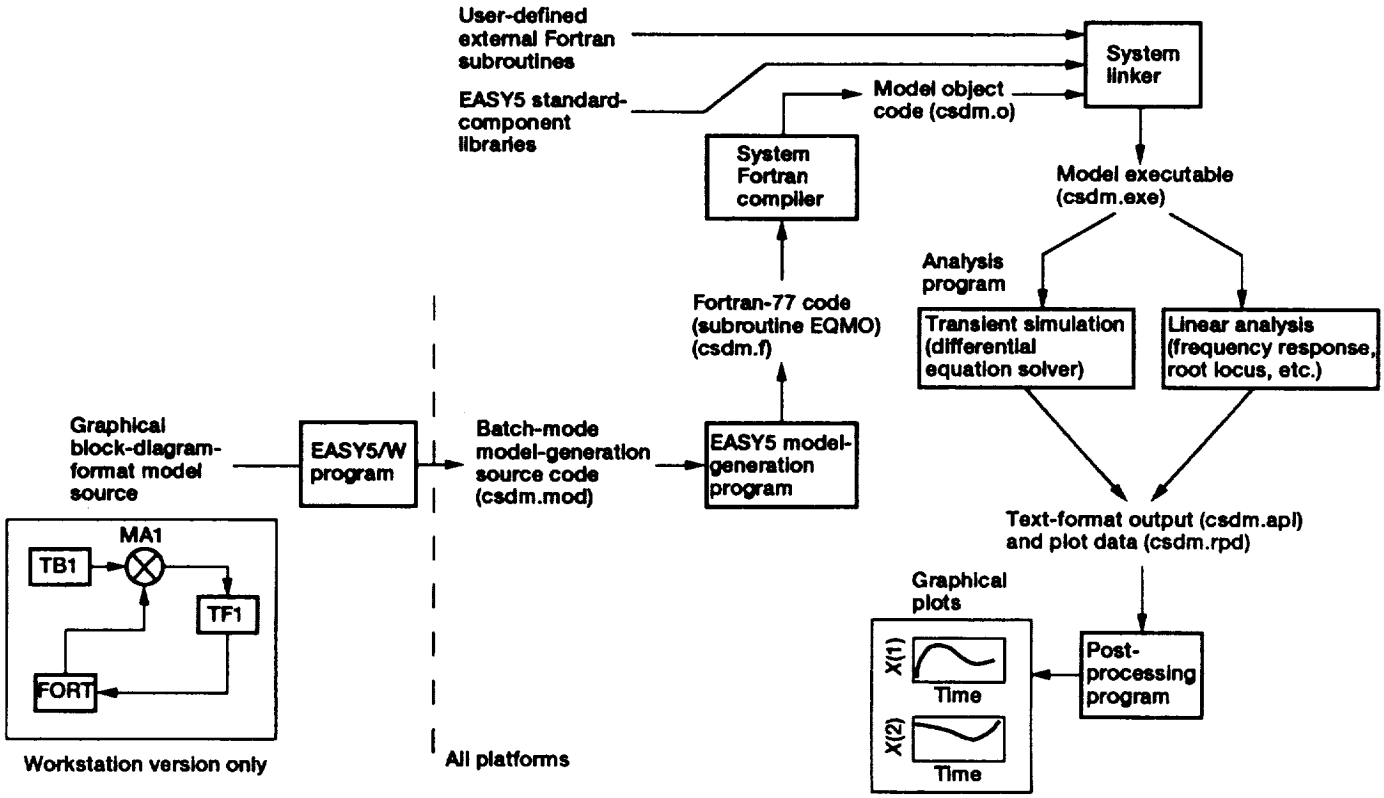

Figure D.1.—EASY5 modeling system.

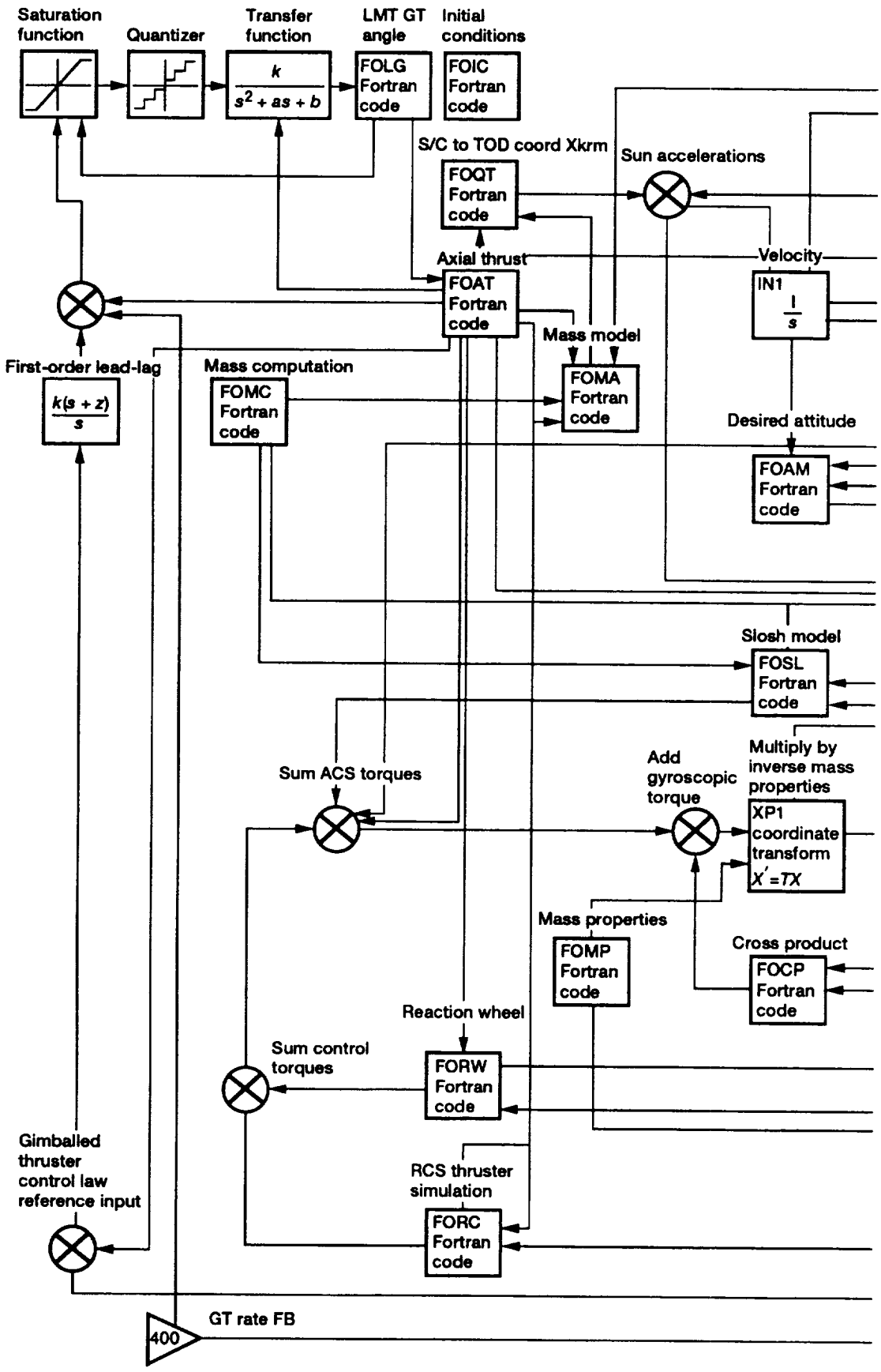

Figure D.2.—Apollo workstation block

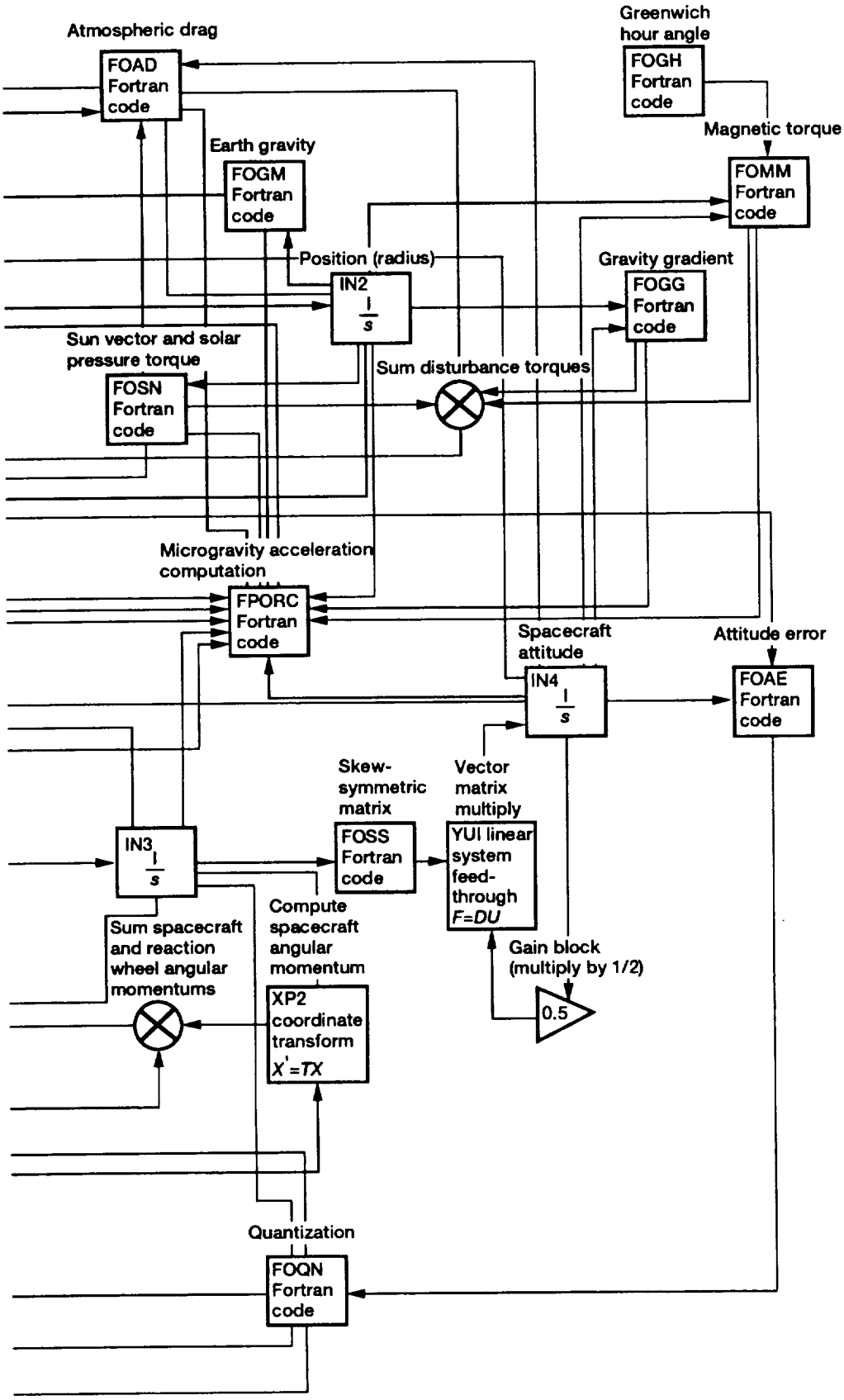

diagram of COLD–SAT dynamic model.

Appendix E
Acronyms and Abbreviations

A	ampere (a unit of electric current)
AU	astronomical unit
ACS	attitude control system
CG	center of gravity of spacecraft
CPU	central processing unit
COLD–SAT	Cryogenic On-orbit Liquid Depot—Storage, Acquisition, and Transfer
μg	unit of acceleration (32.16×10^{-6} ft/sec^2)
GHA	Greenwich hour angle
GMT	Greenwich mean time
H	henry (a unit of inductance)
lbf	pound force
lbm	pound mass
MID	maximum instantaneous deviation
m	meter (a unit of length)
N	newton (a unit of force)
N_2H_4	hydrazine
P–I	proportional-integral (control law)
psia	pounds per square inch absolute
RCS	reaction control system
RMSD	root-mean-square deviation
S/C	spacecraft (also refers to primary (x,y,z) spacecraft coordinate system)
slug	32.175 lbm
SCO	spacecraft orbit system

SMD	spring-mass-dashpot (slosh) model
TOD	true-of-date coordinate system
TOL	tolerance
V	volt (a unit of electric potential)

References

1. Centaur Vehicle Simulation Data Book (G-Configuration), Report No. GDC–SSC–85–005, General Dynamics Space Systems Division, prepared under NASA Contract NAS3–22901, May 1985.

2. New Static Models of the Thermosphere and Exosphere With Empirical Temperature Profiles, Smithsonian Astrophysical Observatory Special Report 313, NASA CR–112684, 1970.

3. The Astronomical Almanac for the Year 1987, Nautical Almanac Office, U.S. Naval Observatory, U.S. Government Printing Office.

4. Niva, G.D.: The Use of Quaternions With an All-Attitude IMU, Guidance and Control, 1982. R.D. Culp, et al., eds., Univelt, 1982, pp. 269–283.

5. Solar Cell Array Design Handbook, H.S. Rauschenbach, Van Nostrand Reinhold, 1980.

6. Abramson, H.N.: The Dynamic Behavior of Liquids in Moving Containers, NASA SP–105, 1966.

7. Concus, P.; Crane, G.E.; and Satterlee, H.M.: Small Amplitude Lateral Sloshing in a Cylindrical Tank With a Hemispherical Bottom Under Low Gravitational Conditions, (LMSC–A852007, Lockheed Missiles and Space Co., NASA Contract NAS3–7119, NASA CR–54700, 1967.

8. EASY5 Engineering Analysis Reference Manual 20491–0503–R1, Boeing Computer Services Company, Seattle, WA 98124.

REPORT DOCUMENTATION PAGE

Form Approved
OMB No. 0704-0188

1. AGENCY USE ONLY (Leave blank)	2. REPORT DATE	3. REPORT TYPE AND DATES COVERED
	December 1992	Technical Memorandum

4. TITLE AND SUBTITLE

COLD–SAT Dynamic Model

5. FUNDING NUMBERS

WU–506–42–73

6. AUTHOR(S)

Neil S. Adams and Gary Bollenbacher

7. PERFORMING ORGANIZATION NAME(S) AND ADDRESS(ES)

National Aeronautics and Space Administration
Lewis Research Center
Cleveland, Ohio 44135–3191

8. PERFORMING ORGANIZATION REPORT NUMBER

E–6483

9. SPONSORING/MONITORING AGENCY NAMES(S) AND ADDRESS(ES)

National Aeronautics and Space Administration
Washington, D.C. 20546–0001

10. SPONSORING/MONITORING AGENCY REPORT NUMBER

NASA TM–105185

11. SUPPLEMENTARY NOTES

Neil S. Adams, Analex Corporation, 3001 Aerospace Parkway, Brook Park, Ohio 44142; Gary Bollenbacher, NASA Lewis Research Center. Responsible person, Gary Bollenbacher, (216) 433–2276.

12a. DISTRIBUTION/AVAILABILITY STATEMENT

Unclassified - Unlimited
Subject Category 18

12b. DISTRIBUTION CODE

13. ABSTRACT *(Maximum 200 words)*

This report discusses the development and underlying mathematics of a rigid-body computer model of a proposed cryogenic on-orbit liquid depot storage, acquisition, and transfer spacecraft (COLD–SAT). This model, referred to in this report as the COLD–SAT dynamic model, consists of both a trajectory model and an attitudinal model. All disturbance forces and torques expected to be significant for the actual COLD–SAT spacecraft are modeled to the required degree of accuracy. Control and experiment thrusters are modeled, as well as fluid slosh. The model also computes microgravity disturbance accelerations at any specified point in the spacecraft. The model was developed by using the Boeing EASY5 dynamic analysis package and will run on Apollo, Cray, and other computing platforms.

14. SUBJECT TERMS	15. NUMBER OF PAGES
COLD–SAT; Spacecraft; Attitude control; Microgravity; Simulation; Slosh; EASY5; Rigid body; Quaternion	106
	16. PRICE CODE: A06

17. SECURITY CLASSIFICATION OF REPORT	18. SECURITY CLASSIFICATION OF THIS PAGE	19. SECURITY CLASSIFICATION OF ABSTRACT	20. LIMITATION OF ABSTRACT
Unclassified	Unclassified	Unclassified	